JIMMA UNIVERSITY

SCHOOL OF GRADUATE STUDIES

JIMMA INSTITUTE OF TECHNOLOGY

FACULTY OF CIVIL AND ENVIRONMENTAL ENGINEERING

STRUCTURAL ENGINEERING STREAM

Finite Element Analysis of Reinforced Concrete Beam Column Connection Subjected to Lateral loading

A Research Submitted to the School of Graduate Studies of Jimma University in Partial Fulfillment of the Requirements for the Degree of Masters of Science in Civil Engineering (Structural Engineering).

By: Gemechu Abdissa

February, 2019

Jimma, Ethiopia

JIMMA UNIVERSITY

SCHOOL OF GRADUATE STUDIES

JIMMA INSTITUTE OF TECHNOLOGY

FACULTY OF CIVIL AND ENVIRONMENTAL ENGINEERING

STRUCTURAL ENGINEERING STREAM

Finite Element Analysis of Reinforced Concrete Beam Column Connection Subjected to Lateral loading

A Research Submitted to the School of Graduate Studies of Jimma University in Partial Fulfillment of the Requirements for the Degree of Masters of Science in Civil Engineering (Structural Engineering).

By: Gemechu Abdissa

Advisor: Engr Elmer C.Agon

Co-advisor: Engr. Solomon Biratu

February, 2019

Jimma, Ethiopia

DECLARATION

I declare that the work in this thesis was carried out in accordance with the requirements of the University's regulations and that it has not been submitted for any other academic reward to any University or Institution. I certify that ,to the best of my knowledge, my thesis does not infringe upon anyone's copy right nor violate any proprietary right, and that any ideas, techniques, quotations and any other material from the work of other people included in my thesis published or otherwise, are fully acknowledged in accordance with the standard referencing practices.

Student

<u>Gemechu Abdissa</u>   _____   _____

   Name   Signature   Date

This thesis has been submitted for examination with my approval as a University advisor

Advisor

<u>Engr. Elmer C. Agon</u>   _____   _____

   Name   Signature   Date

Co-advisor

<u>Engr. Solomon Biratu</u>   _____   _____

   Name   Signature   Date

Dedicated to

My beloved family

ACKNOWLEDGEMENT

ABSTRACT

The beam column connection is the most critical zone in a reinforced concrete frame. The strength of connection affects the overall behavior and performance of RC framed structures subjected to lateral load and axial loads. Beam column connection may be subjected to large seismic lateral loading and severe ground shaking during earth quakes. The study of critical parameters that affects the overall joint performances and response of the structure is important.

Recent developments in computer technology have made possible the use of Finite element method for 3D modeling and analysis of reinforced concrete structures. Nonlinear finite element analysis of reinforced concrete beam column connections subjected to lateral loading was performed in order to investigate joint shear failure mode in terms of joint shear capacity, deformations and cracking pattern using ABAQUS software. A 3D solid shape model using 3D stress hexahedral element type (C3D8R) was implemented to simulate concrete behavior. Wire shape model with truss shape elements (T3D2) was used to simulate reinforcement's behavior. The concrete and reinforcement bars were coupled using the embedded modeling technique. In order to define nonlinear behavior of concrete material, the concrete damage plasticity (CDP) was applied to the numerical model as a distributed plasticity over the whole geometry. The study was to investigate the most influential parameters affecting joint shear failure due to column axial load, beam longitudinal reinforcement ratio, joint panel geometry and concrete compressive strength.

The Finite Element Model (FEM) was verified against experimental tests of two non-ductile exterior and interior RC beam column connection subjected to lateral loading. The model showed good comparison with test results in terms of load-displacement relation, cracking pattern and joint shear failure modes. At yielding of reinforcement and initiation of concrete crushing, the increase in concrete compressive strength influences the overall joint shear stress-strain behavior. Other parameters such as column axial load, beam longitudinal reinforcement ratio, and joint panel geometry did not show a distinct and significant effect that can predict the failure. The FEA clarified that the main influential parameter for predicting joint shear failure was concrete compressive strength.

Keywords: RC beam column connections   Finite Element Model   Shear strength

Joint shear failure   Crack patterns   Concrete Damage Plasticity

TABLE OF CONTENTS

Contents   **Page**

LIST OF FIGURES

LIST OF TABLES

ACRONYMS

AASHTO American Association State Highway and Transportation Officials

ASTM   American Society for Testing and Materials

ACI   American Concrete Institute

BCC   Beam Column Connection

CDP   Concrete Damage Plasticity

ECBCC   Exterior Conventional Beam Column Connection

EWBCC Exterior Wide Beam Column Connection

f'c   Concrete Compressive strength

f't   Concrete Tensile strength

FE   Finite Element

FEA   Finite Element Analysis

FEM   Finite Element Method

ICBCC   Interior Conventional Beam Column Connection

IWBCC   Interior Wide Beam Column Connection

JU   Jimma University

JiT   Jimma Institute of Technology

MRF   Moment Resisting Frames

RC   Reinforced Concrete

SRS   Steel Reinforced Concrete

NZS   New Zealand Association of Standards

LIST OF SYMBOLS

σ — Cauchy stress

d — Scalar stiffness degradation variable

ε — Strain tensor

ε^{pl} — Plastic strain

$\widetilde{\varepsilon}_t^{ck}$ — Cracking strain

$\varepsilon_{ot}{}^{el}$ — Elastic strain of undamaged material

ε_t — Elastic strain

D_o^{el} — The initial (undamaged) elastic stiffness of the material

$\bar{q}$ — Von Mises equivalent effective stress

$\bar{p}$ — Effective hydrostatic stress

β — Dilation angle measured in $p - q$ plane

γ_{ACI} — joint shear strength factor

b_j — effective joint shear width

h_c — column depth

b_b — beam width

b_c — column width

m — the slope to define the effective width of joint transverse to the direction of shear

v_j — joint shear stress

υ_j — shear strain

f_{jy} — yield stress of horizontal joint transverse reinforcement

f_{by} — yield stress of longitudinal reinforcement

$A_s{}^*$ — greater area of top or bottom reinforcement passing through the joint.

G_f — fracture energy of concrete

w — crack width

d_c — compression damage

d_t — tensile damage

E_c — Modulus of elasticity

σ_x — beam average axial stress

σ_y — column average axial stress

σ_t — joint principal tensile stress

ε_x — beam average axial strain

ε_y — column average axial strain

ε_t — joint principal tensile stress

Δ_y — Lateral deflection at the yield onset of the flexural reinforcement

Δ_u — Lateral deflection corresponding to 75% of the peak recorded strength.

CHAPTER ONE

INTRODUCTION

1.1 Background of the study

Beam column connections are one of important structural elements in concrete structures. It is also a critical seismic element because its behavior under severe earth quake motions has a significant effect on failure mode and strength and deformation capacity of the building structures. When the building is subjected to the earth quake, beam column connection is prone to joint shear failure due to high shear stress which appears in the joint panel as result of opposite sign moments on opposite side of the joint core. The joint shear failure is a brittle type of failure which can strongly affect ductility of the RC frames. The early occurrence of this failure causes the building frames collapse without reaching their ultimate capacity.

Beam column connections have been identified as potentially one of the weaker components when RC Moment Resisting Frame (MRF) is subjected to seismic lateral loading. Since the mid-1960s, numerous experimental tests and numerical studies have been conducted to investigate the performance of RC beam column connections subjected to lateral loading. When only the flexural strength of well detailed longitudinal beams limits over all response, RC BCCs typically display ductile behavior (with the joint panel region essentially remaining elastic). The failure mode wherein the beam forms hinges is usually considered to be the most desirable for maintaining good global energy dissipation without severe degradation of capacity at connections.

Many Finite element analysis and experimental investigations have been done so far to understand beam column connection failure and resistant mechanisms. The analyses were either 2D or 3D spatial discretization with bond-slip or bond-lock bond behaviors models. Nonlinear finite element analysis on the RC beam column connection shear failure under cyclic lateral loading and monotonic loading have been conducted to investigate shear failure modes and post peak behaviors such as cyclic deterioration and shear resistance mechanisms in terms of shear capacity, deformation and crack pattern.

In various countries like United States, New Zealand, Japan, Republic of Korea and others, many researchers have tried several approaches to improve understanding of RC joint shear behavior. Influence parameters on joint shear behavior have been examined using collected experimental test results and analytical procedures. However, there is no consensus about the effect of some

parameters on joint shear strength (Park and Mosalam, 2012). Thus, some design considerations for joint shear strength (and/or joint shear deformation), in addition, there is no generally accepted joint shear stress vs. joint shear strain prediction model that can be describe the complete joint shear behavior of diverse types of RC beam column connections.

1.2 Statement of the problem

Researchers have observed four types of failures that can take place in BCC. These modes of failure can be classified as shear failure in the joint, slippage of the beam main reinforcement bars, yielding of the beam main reinforcement (beam hinging) and yielding of the column longitudinal bars (column hinging). Shear failure of BCC was the main cause in failure of several moment-resisting frame structures during recent earthquakes (Kiran and Genesio, 2014).

The strength of beam column joints have long been recognized as a significant factor that affects the overall behavior of RC moment resisting frames subjected to large lateral loading. The reversal of forces in opposite direction in BCC during earth quake may cause distress which often results in failure when not designed and detailed in proper manner. The behavior of the joints when subjected to large forces and severe ground shaking during the earth quake determines the response of the whole structure. The assumption of joint being rigid fails to consider the effect of high shear force developed within the joint. The shear failure developed within the rigid joint is always brittle in nature which is not acceptable in seismic design of frames subjected to seismic loads.

1.3 Objectives of the study

1.3.1 General Objective

The main objective of this study was to investigate the most influential parameters affecting RC beam column joint shear failure subjected to lateral loading.

1.3.2 Specific Objectives

❖ To specify the shear strength and behavior of joints to control the overall response of RC beam-column connections subjected to lateral loads.

❖ To investigate the patterns of crack and load displacement behavior in the nonlinear analysis of RC beam-column connections.

❖ To analyze joint shear stress vs. joint shear strain prediction model that can describe the complete joint shear behavior.

❖ To develop improved finite element models for the study of the nonlinear behavior of RC beam column joints under lateral loading.

1.4 Research Questions

1. What are the influential parameters that affect the joint shear strength and the deformation capacity of RC beam-column connections?

2. What are the causes of cracks of joints in the nonlinear analysis of RC beam-column connections subjected to seismic loading?

3. How can joint shear failure influences shear strength, ductility and stability of overall frames of the structures?

4. How improved finite element models can be developed to govern the behavior of the connection that affects the global failure mechanism?

1.5 Significance of the study

Due to complexity of reinforced concrete beam-column connection behavior, experimental investigations have not provided definitive answers as to the impact of local nonlinear material inelastic response on the development of global mechanisms that determine connection behavior. The FEA using ABAQUS facilitates the design and analysis of RC beam column connections for researchers and designers. Through FEA, the effect of compressive strength of concrete, the failure mode of joint, the crack pattern, effect of longitudinal reinforcement, effect of column width and beam depth, and effect of axial column load ratio can be obtained. Therefore, with the proposed FEA, it was possible for engineers to achieve a reasonable solution for beam-column connection behavior and propose specific design standards.

1.6 Scope of the study

The suggested modeling technique in this paper has been conducted by means of the commercial FEA program ABAQUS and calibrated by modeling and analyzing experimentally tested exterior and interior beam-column connections in which the governing failure mode during simulated seismic actions on the specimens was the joint shear failure type. The study presented herein has endeavored to propose a suitable numerical model that describes the nonlinear shear behavior of reinforced concrete beam–column connections including poorly designed and detailed interior and exterior joints. The comparison between numerical and experimental results indicated the ability of the proposed method in simulating the governing joint shear behavior pre and post peak failure phases.

3

CHAPTER 2

REVIEW OF RELATED LITERATURE

This chapter deals with the previous research works related to the behavior of beam column joint subjected to seismic loads. It deals with the experimental study and finite element modeling on the effect and behavior of axial and lateral loads on column, shapes and sizes of beam and column, beam longitudinal reinforcement, anchorage of beam and column longitudinal reinforcement, joint geometry and concrete compressive strength on joint shear failure in terms of joint shear capacity, deformations and cracking pattern as reported by various authors.

2.1 Theoretical Reviews

Beam column connections are one of the structural elements in concrete structures. They are the main reason of structural collapse due to construction difficulty and its manual design particularly, when subjected to seismic loads.

In present day, behaviors of beam column connections have been modeled by Finite element analysis. Many researchers simulated the behavior of BCC using favorite finite element soft wares such as ABAQUS, ANSYS, DIANA and VECTOR2. A series of numerical investigations have been done on beam column connections using FEM analysis. (Niroomandi et al. (2014)) performed numerical investigation of affecting parameters on the shear failure of non-ductile exterior joints. According to their numerical results, two important parameters influencing the joint shear behavior were joint aspect ratio and beam longitudinal reinforcement ratio.

An extensive data base of the RC BCC test specimens for exterior, interior and knee joints exhibiting joint failure when subjected to reversed cyclic lateral loading was prepared by (Jaehong and LaFave, 2007). They collected the data of experimental sub-assemblies from all over the world. They suggested that the most influential parameters for predicting joint shear failure in terms of joint shear strength and deformation capacity was concrete compressive strength.

The structural performance and cyclic behavior of RC beam column joints were studied by computational simulations with ABAQUS (Kuang and Kam, 2012). Five wide beam column joint specimens with the same column sizes but different beam widths beam depths were simulated. The study focused on the effects of beam depths on the lateral load transfer paths. It was shown that the beam width has significant on the load transfer paths in wide beams and corresponding joint cores. The simulated result also indicated that joint shear stress in wide beam column connections is higher than that of conventional ones.

A method to predict the ductile capacity of RC beam column joints failing in shear after the development of plastic hinges at both ends of adjacent beams was proposed by (Lee et al. (2009)). The proposed method includes the effect of longitudinal axial strain of a beam in the plastic hinge region of the beam on the joint longitudinal strain and the strength deterioration of the joint. The provision of joint transverse reinforcement for ductility was conducted by (Prabu and Kandasmy, 2015) using ANSYS linear elastic FEA in order to ensure the shear strength and deformations.

(Fadwa et al. (2014)) carried out experimental research to compare behavior of two RC wide beam column connections and two RC conventional beam column connections subjected to quasi static cyclic loading in terms of hysteresis response and total energy dissipating capacity. The specimens were full scale connections and they were composed of two sets of interior and exterior joints. The indicated that the hysteresis response of the wide beams was likely exhibited remarkable enhancement compared to the conventional beams and the total energy dissipating capacity of a wide beam column connection was higher than the conventional joint.

A nonlinear FEA of non-seismically detailed RC beam column connection under reversed cyclic loading was conducted by (Supayiriyakit et al. (2008)). The nonlinear FEA was applied to simulate to the tested specimens of mid-rise RC frame buildings designed according to the non-seismic provisions of the American concrete building code (ACI). The analysis employed the smeared crack approach for modeling beam, column and joint, and employed the discrete crack approach for modeling the interface between beam and joint face. They showed that the specimens representing small and medium column tributary area failed in brittle joint shear while the specimen representing large column tributary area failed by ductile flexure though no ductile reinforcement details were provided.

A finite element model was developed to quantitatively investigate the effect of the geometric parameters on the behavior of the RC wide beam column connection by (Etemandi, 2017). The impact of geometry of the wide beam on the mechanical properties, types and patterns of crack, length of the plastic hinge through the steel reinforcements and plastic dissipation energy of the joint was investigated. The analysis indicated that increasing the width and depth of the beam caused the plastic hinge length reduced. It was also showed that tensile stress through the beam axis, compressive stress through column axis and shear stresses are responsible for the initiation of flexural cracks, narrow flexural cracks and inclined cracks, respectively.

The shear stresses and deformations of monotonically loaded exterior and corner beam column joints were studied by (Patil and Manekari, 2013). The analysis was conducted by varying the stiffness's of beam and column at the joints. They compared the maximum and minimum

stresses and load displacement behavior of exterior and corner joints and concluded that the graphs plotted were different.

The seismic behavior of RC exterior WBCC was investigated through computational simulations of ABAQUS by (Luk and Kuang, 2012). The study mainly focused on the load transfer paths and different performance of joints with conventional and wide beams subjected to quasi static cyclic loads. It was found that lesser crack opening occurs in WBCC; hence less pinched hysteresis loops were observed. The results also indicated that the beam width has significant on the load transfer paths and joint shear stress in wide beam column connections was higher than the conventional ones.

(Behnam et al. (2018)) presented FEA of RC WBCC using theoretical context of the Concrete Damage Plasticity model. They simulated the four full scales EWBCC that were tested under reversed cyclic loading conditions. The parametric study was conducted to explore the effects of several parameters including the column axial load, column and beam dimensions, beam bar anchorage ratios and spandrel beam reinforcement on EBCCs.

Non-linear FEA of RC BCC without joint reinforcement was also performed to investigate joint shear failure in terms of shear capacity, deformation capacity and type of crack pattern by (Najafgholipour et al. (2017)). The finite element model was verified against experimental results of two non-ductile (one exterior and one interior) BCC vulnerable to shear failure and showed the capability of FEM to predict the failure.

2.2 Material Properties

2.2.1 Concrete properties

Concrete stress-strain behavior is different in tension and compression under uniaxial and biaxial loading. The concrete in tension and compression is modeled separately. The concrete uniaxial stress-strain behavior for compression was modeled using advanced Hognestad type parabola (Hognestad, 1951). There were three phases to represent the uniaxial stress-strain behavior of concrete in compression.

Phase 1: This stage is linear-elastic phase. It is continuous up to 40% of the maximum compressive stress level $\sigma_{co} = 0.4 f_c'$.

Phase 2: This stage is the hardening phase. At this phase the stress increases gradually until it reaches a strain level of 0.0035. It describes the ascending branch of the stress strain relationship reaching the peak stress, σ_{cu} at corresponding strain level $\varepsilon_o = 2 f_c'/E_c$.

Phase 3: This stage is post peak softening phase. It represents the initiation and progression of compressive damage in the concrete material until the ultimate compressive strain ε_u attained. The stress-strain compatibility at stress level of $\sigma_{co} = 0.4f_c'$. Fig.2.1 shows typical concrete uniaxial compressive stress-strain behavior used in the model.
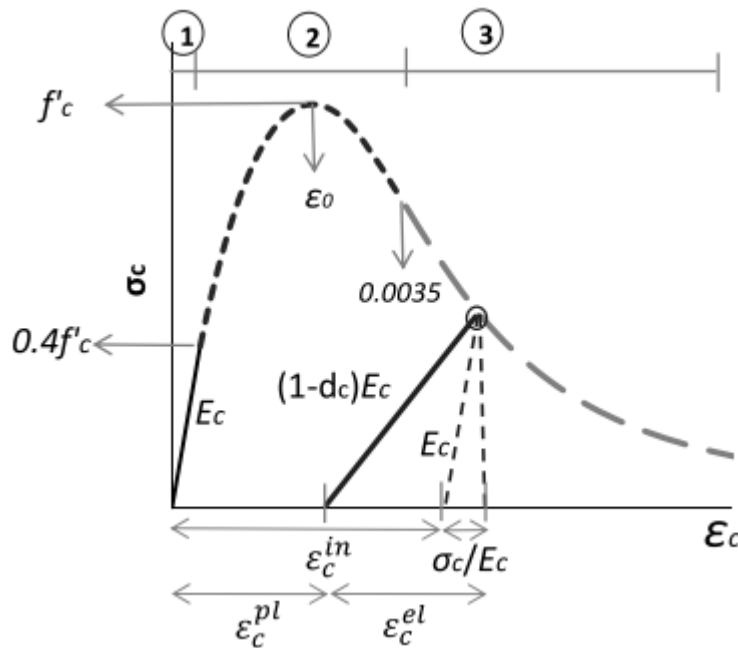
Fig.2.1 Concrete compressive uniaxial stress-strain (ABAQUS manual, 2008)

Concrete tensile uniaxial stress-strain behavior consists of two stages.

Stage 1: Linear elastic behavior phase which goes linearly up to concrete tensile strength σ_{to}.

Stage 2: Initiation of crack and its propagation in concrete material under tension phase. After this point the concrete cracks and stress decreases gradually to zero. In this stage is the concrete behavior is modeled by softening procedure which can be modeled using linear, bilinear or nonlinear stress-strain relationships (Belarbi and Thomas, 1994). In this study linear behavior is used. Fig.2.2 shows tensile softening assumptions to be used in the model.
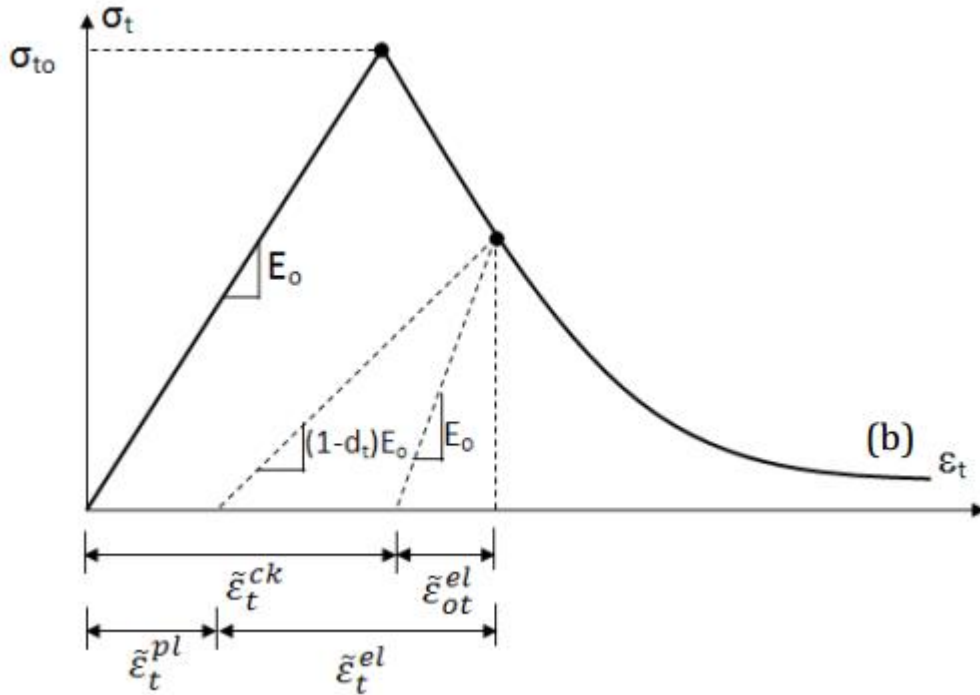
Fig.2.2 Concrete uniaxial tensile stress-strain behavior (ABAQUS manual, 2008)

The ultimate tensile strength of concrete was estimated by (Genikomsu and Polak, 2015)

$$f'_t = 0.33\sqrt{f'_c} \text{ (Mpa)} \ldots\ldots\ldots (2.1)$$

$$E_C = 4730\sqrt{f'_c} \text{ (Mpa)} \ldots\ldots\ldots (2.2)$$

Concrete compression and tensile damage is defined during softening procedure in concrete damage plasticity. Damage in compression occurs just after reaching the maximum uniaxial compressive strength corresponding to strain level ε_o. Damage in tension occurs after the maximum tensile stress, σ_{to} reached. The degradation of elastic stiffness in softening region is characterized by two damage variables, dt and dc which are assumed to be functions of plastic strain corresponding to tensile and compressive damage, which were discussed in Concrete damage plasticity shows default settings of ABAQUS that represents stiffness recovering at the transition from tension to compression side and damage cumulating at the transition from compression to tension side.

2.2.2 Reinforcement steel properties

The uniaxial stress-strain relationship for reinforcement in the concrete is assumed as the elasto-plastic with strain hardening. In present nonlinear finite element analysis the reinforcement is modeled in elasto-plastic range. The elastic behavior is modeled with conventional Young's modulus of elasticity and Poisson's ratio. The plastic behavior is also modeled by including yield stress and corresponding plastic strain. Properties of plastic phase are defined to the model by using bilinear behavior (Summer and Aktas, 2017). Fig.2.3 shows the elasto-plastic behavior of reinforcement steel with strain hardening using bilinear model.
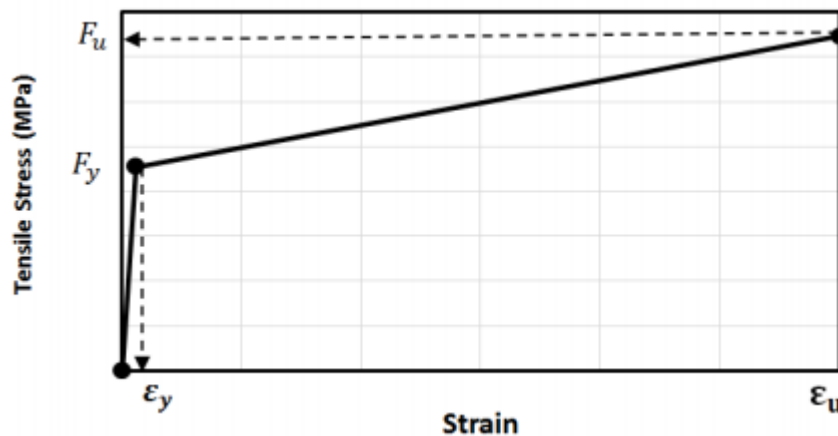
Fig.2.3 Typical steel uniaxial stress-strain for steel reinforcement (Mandel et al. (1986))

2.3 Concrete Damage Plasticity (CDP)

Concrete constitutes a wide range of materials whose properties are quantitatively and qualitatively different for compression and tension tests. Recently, modeling of failure and fracture has become one of the fundamental issues in structural mechanics particularly in concrete structures. A scalar variable is used to model failure (in both tension and compression) to describe crack patterns (Jankowiak et al. (2003)). CDP is the governing concrete material plasticity model over the whole geometry of the specimens. The model is the plasticity based model which is developed using concepts of continuum damage mechanics and the application of scalar damaged elasticity in combination with isotropic tensile and compressive plasticity to properly represent the inelastic behavior (Lubliner et al. (1989)).

2.3.1 Assumptions of CDP.

According to assumptions of CDP model, the two main failure mechanisms of the concrete material are tensile cracking and compressive crushing.

2.3.1.2 Additive strain rate decomposition (Kim and LaFave, 2007)

$$\dot{\varepsilon} = \dot{\varepsilon}^{el} + \dot{\varepsilon}^{pl} \quad \text{…………..} \quad (2.3)$$

Where $\dot{\varepsilon}$ -total strain rate, $\dot{\varepsilon}^{el}$- elastic strain, and $\dot{\varepsilon}^{pl}$- plastic strain

2.3.1.3 Stress-strain relations

In CDP model, the stiffness degradation is modeled by defining the relationship between effective stresses and stresses. Stress strain model provided in CDP model is based on a simple model which provides coupling between damage and plasticity using scalar damage and effective stress (Kotsovou and Mouzakis, 2012).

$$d = (1 - d)D_o^{el} : (\varepsilon - \varepsilon^{pl}) = D^{el} : (\varepsilon - \varepsilon^{pl}) \quad \text{…………………} \quad (2.4)$$

Where σ - Cauchy stress

d - Scalar stiffness degradation variable which have a value in the range of undamaged to fully damage

ε- Strain tensor

ε^{pl}- Plastic strain

D_o^{el}- The initial (undamaged) elastic stiffness of the material

$D^{el} = (1 - d)D_o^{el}$ – Degraded elastic stiffness tensor

The effective stress tensor is defined as:

$$\bar{\sigma} = D_o^{el} : (\varepsilon - \varepsilon^{pl}) \quad \text{…………...............……..} \quad (2.5)$$

Where ε^{pl} is the plastic strain

2.3.1.4 Hardening Variables

In the formulation, it is necessary to propose the evaluation of the scalar degradation variable.

$$d = d(\bar{\sigma}, \tilde{\varepsilon}^{pl}) \quad \ldots\ldots\ldots\ldots\ldots\ (2.6)$$

Governed by set of effective stress tensor $\bar{\sigma}$ and hardening (softening) variables $\tilde{\varepsilon}^{pl}$. In CDP model, the stiffness degradation is initially isotropic and defined by degradation variables d_c, in compression zone and d_t, in tension zone. Finally, the Cauchy stress tensor is related to the effective stress tensor $\tilde{\sigma}$ through the scalar degradation variable $(1-d)$.

$$d = (1-d)\tilde{\sigma} \quad \ldots\ldots\ldots\ldots\ldots\ (2.7)$$

Damage states in tension and compression are characterized independently by two hardening variables, $\tilde{\varepsilon}^{pl}{}_{t}$ and $\tilde{\varepsilon}^{pl}{}_{c}$, which are referred to equivalent plastic strains in tension and compression, respectively. The evaluation of hardening variables is given by the following expression.

$$\tilde{\varepsilon}^{pl} = \begin{bmatrix} \tilde{\varepsilon}^{pl}{}_{c} \\ \tilde{\varepsilon}^{pl}{}_{t} \end{bmatrix} \quad \text{and} \quad \dot{\tilde{\varepsilon}}^{pl} = h(\bar{\sigma}, \tilde{\varepsilon}^{pl}).\dot{\varepsilon}^{pl} \ldots\ldots\ldots\ldots\ldots..(2.8)$$

2.3.1.5 Yield Criterion

Cracking (tension) and crushing (compression) in concrete are represented by increasing values of the hardening (softening) variables. These variables control the evolution of the yield surface and the degradation of the elastic stiffness. The yield function represents a surface in effective stress space which determines the states of failure or damage. The yield surface function requires a loading surface definition and takes the following form in effective stress form proposed by (Lubliner et al. (1989)).

$$F = \frac{1}{1-\alpha}\left(\bar{q} - 3\cdot\alpha\cdot\bar{p} + \theta\left(\tilde{\varepsilon}^{pl}\right)\langle\bar{\sigma}_{max}\rangle - \gamma\langle-\bar{\sigma}_{max}\rangle\right) - \bar{\sigma}_c\left(\tilde{\varepsilon}_c^{pl}\right). \quad\text{-----------------}\ (2.9)$$

Where $\bar{q}$ – Von Mises equivalent effective stress

$\qquad \bar{p}$ – Effective hydrostatic stress

$\qquad \alpha, \theta$ and γ are dimensionless variables defined below with modifications (Lee and Fenves, 1998).

$$\alpha = \frac{(f_{b0}/f_c)-1}{2(f_{b0}/f_c)-1} \quad ; 0 \leqslant \alpha \leqslant 0.5 \quad \text{------------------} \quad (2.10)$$

α − the ratio of biaxial compressive strength and uniaxial compressive strength.

$$\theta(\tilde{\varepsilon}^{pl}) = \frac{\overline{\sigma}_c(\tilde{\varepsilon}_c^{pl})}{\overline{\sigma}_t(\tilde{\varepsilon}_t^{pl})}(1-\alpha)-(1+\alpha) \quad \text{------------------} \quad (2.11)$$

$$\gamma = \frac{3(1-\rho)}{2\rho+3} \quad \text{------------------} \quad (2.12)$$

The coefficient ρ is the ratio of the coefficient of the hydrostatic effective stress in tensile meridian to that on the compressive meridian when the maximum principal stress is negative. This coefficient defines the shape of the yield surface in the deviatory plane. The CDP model suggests to assume default value of $\rho = \frac{2}{3}$ based on tri-axial stress test results.
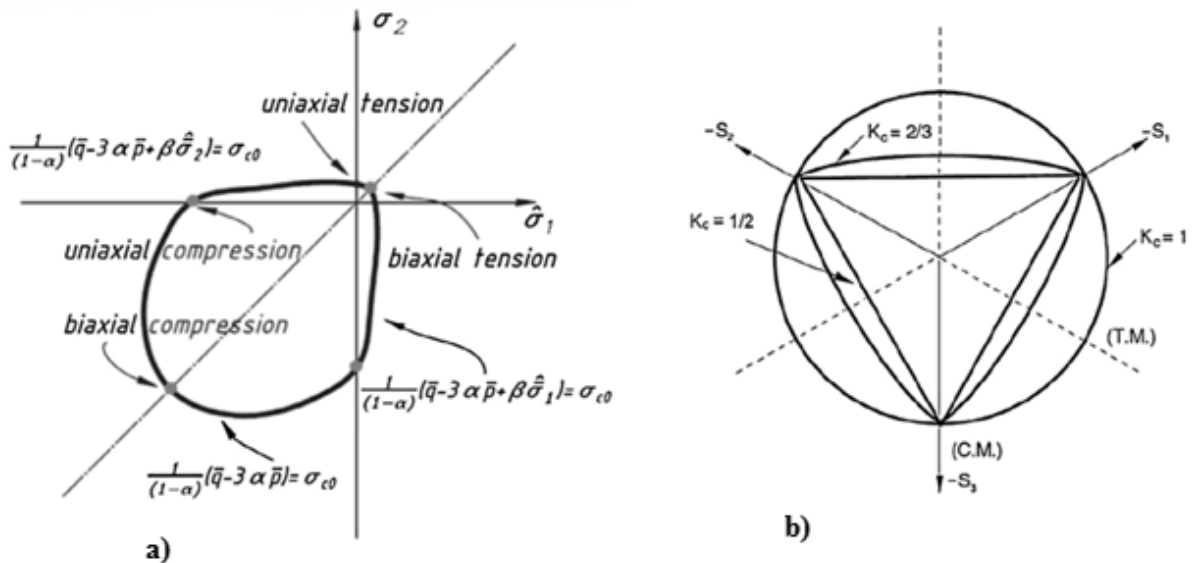
Fig.2.4 Yield surface a) Yield surface in plane stress   b) Yield stress in a deviatoric plane

2.3.1.6 Flow rule

The concrete stress-strain relationships and the yield surface are connected using flow rule. In this model for the flow potential G, the Drucker-Prager hyperbolic function is accepted in the form:

$$G = \sqrt{(f_c - m.f_t.tan\beta)^2 + \overline{q}^2} - \overline{p}.tan\beta - \sigma \quad \text{------------------} \quad (2.13)$$

Where f_t and f_c are uniaxial tensile and compressive strengths of concrete, respectively.

β – Dilation angle measured in $p - q$ plane.

2.3.1.7 Viscoplastic regularization

The materials that exhibit softening behavior and stiffness reduction may lead to convergence difficulties. To overcome these difficulties, viscoplastic regularization of the constitutive material model was used. The CDP model can be regularized using Devaunt-Lions approach. In the CDP model with viscous parameter, plastic strain tensor is derived using additional viscosity parameters known as relaxation time. The default value of viscoplastic regularization in ABAQUS model is zero. Damage variables are formulated and given below.
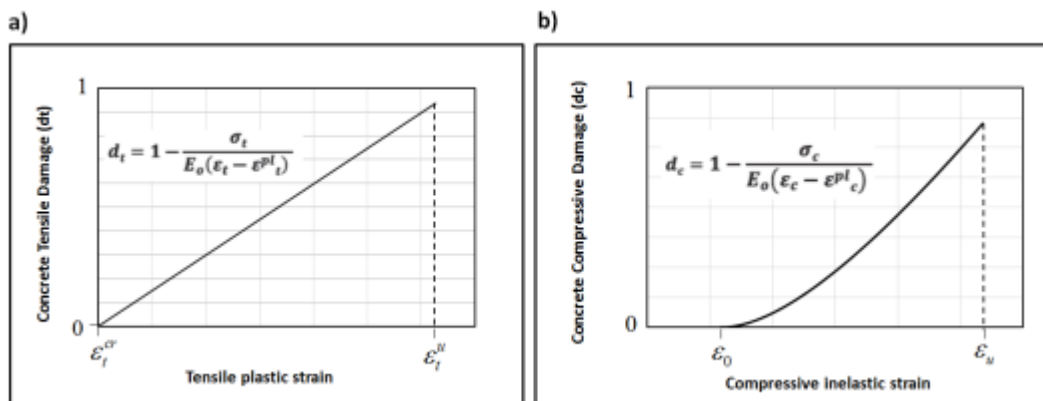
Fig.2.5 Concrete damage parameters in CDP model (Najafgholipour et al. (2017))

a) Uniaxial compressive damage   b) Uniaxial tensile damage

2.3.1.8 Tension stiffening effect

Most finite elements studies of RC structures do not consider bond-slip reinforcing steel and the inherent interaction between reinforcement and RC members. The post failure behavior for direct straining is modeled with tension stiffening in CDP model which helps to define the strain-softening behavior for cracked concrete (Najafgholipour et al. (2017)). Inorder to define bond slip interaction, the tension stiffening given by the following function (Lubliner et al. (1989)) is applied in the finite element model.

$$\widetilde{\varepsilon}_t^{\,ck} = \varepsilon_t - \varepsilon_{ot}^{\,el} \ \dots\dots\dots\dots\ (2.14)$$

$$\varepsilon_{ot}^{\,el} = {\sigma_t}/{E} \ \ \dots\dots\dots\dots\ (2.15)$$

Where $\widetilde{\varepsilon}_t{}^{ck}$ - Cracking strain

$\varepsilon_{ot}{}^{el}$ - Elastic strain of undamaged material

ε_t - Elastic strain
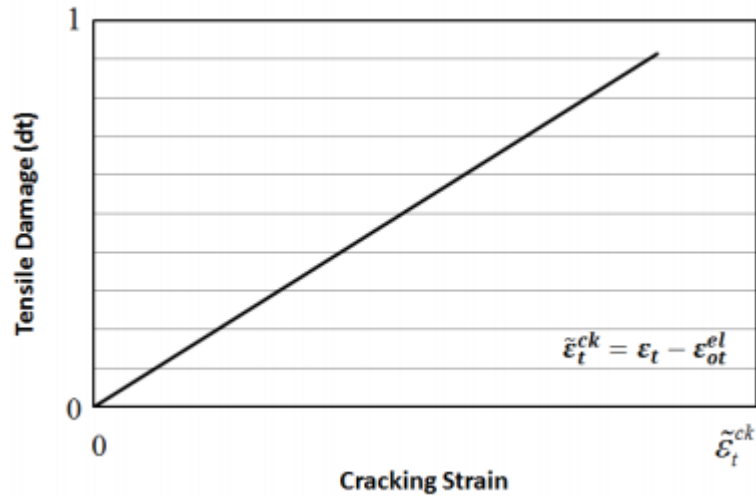
Fig.2.6 Tension stiffening in terms of tensile damage cracking strain relationship

2.4 Design of beam column connections (joints)

Beam column joints in RC frames designed for inelastic response to severe seismic attack subjected mostly to horizontal and vertical shears than the adjacent beams and columns. When the building is subjected to the earth quake, beam column connection is prone to joint shear failure due to high shear stress which appears in the joint panel as result of opposite sign moments on opposite side of the joint core. The joint shear failure is a brittle type of failure which can strongly affect ductility of the RC frames. The early occurrence of this failure causes the building frames collapse without reaching their ultimate capacity. The figure 2.7 is the typical RC frame joints with their adjacent beams and columns.
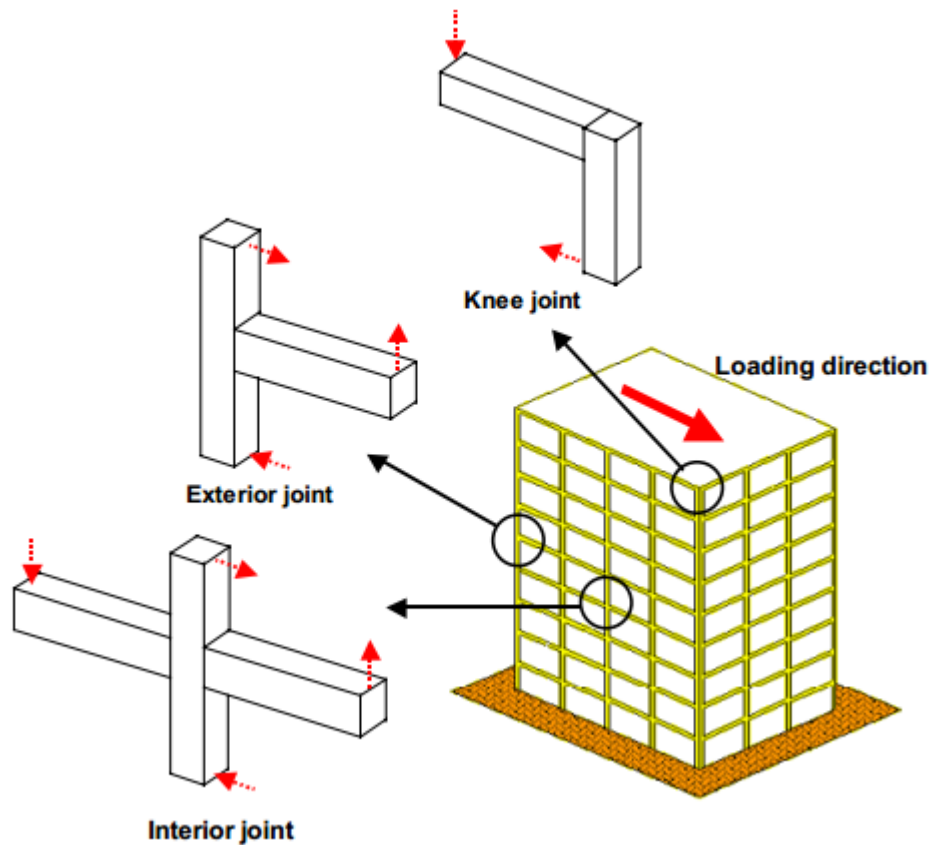
Fig.2.7 Terminology of RC beam column connections (Kim and LaFave, 2009)

2.4.1 Interior Joint

An interior joint has beams framing in to all four sides of the joint. In order to be classified as an interior joint, the beam should cover at least ¾ width of the column, and the total depth of the shallowest beam shouldn't be less than ¾ depth of the deepest beam (Patil and Manekari, 2013).

2.4.2 Exterior Joint

.An exterior joint has at least two beams framing in to opposite sides of the joint. In order to be classified as an exterior joint, widths of the beams on the two opposite faces of the joint should cover at least ¾ of the width of the column, and the depths of these two beams should not be less than ¾ the total depth of the deepest beam framing in to the joint (Patil and Manekari, 2013).

2.5 Types of frame loading system

The behavior of building is studied with different types of loads (Patil and Manekari, 2013).

a) Static loading: slow loading in structures to test components to determine strength limits and flexibility/rigidity of structures.

b) Quasi-static loading: Very slowly applied loading in one direction (monotonic).

15

c) Quasi-static reversed cyclic loading: Very slowly applied loading in both direction (cyclic).

d) Dynamic (random) loading: Shake at the base or any other elevation of the structure similar to that of earth quakes.

2.6 Joint Loads and resulting forces

a) Building Frame Under Earthquake Loading   b) Earthquake Loading of a Typical Joint
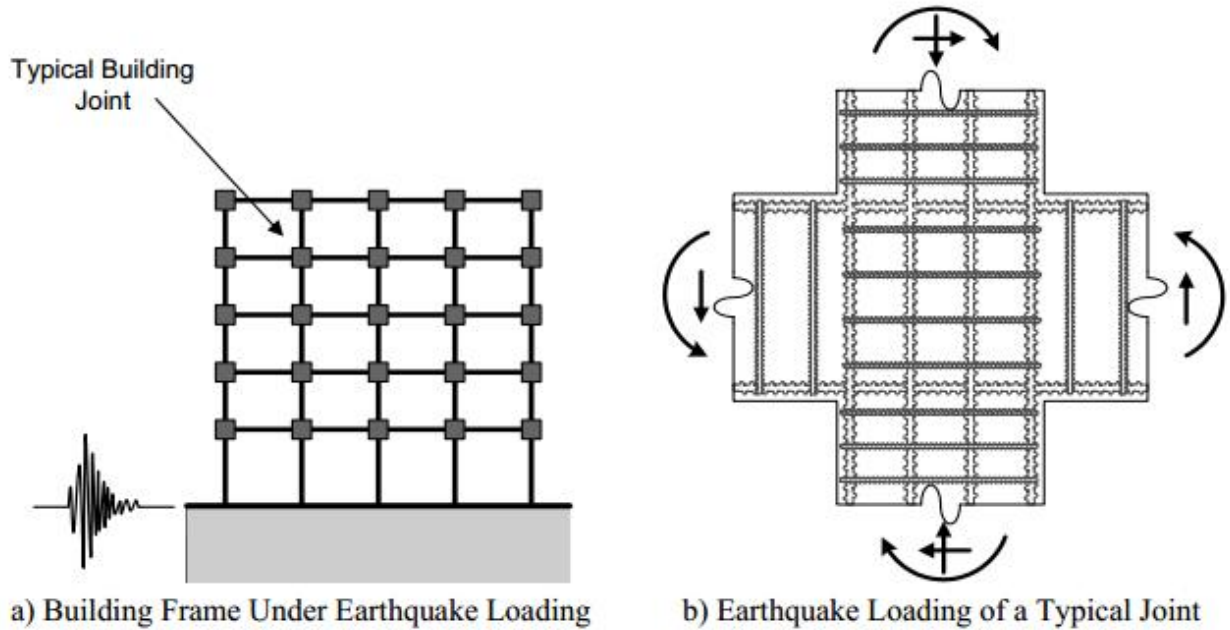
Fig. 2.8 Beam column joint loads under earth quake loading (Laura et al. (2003))
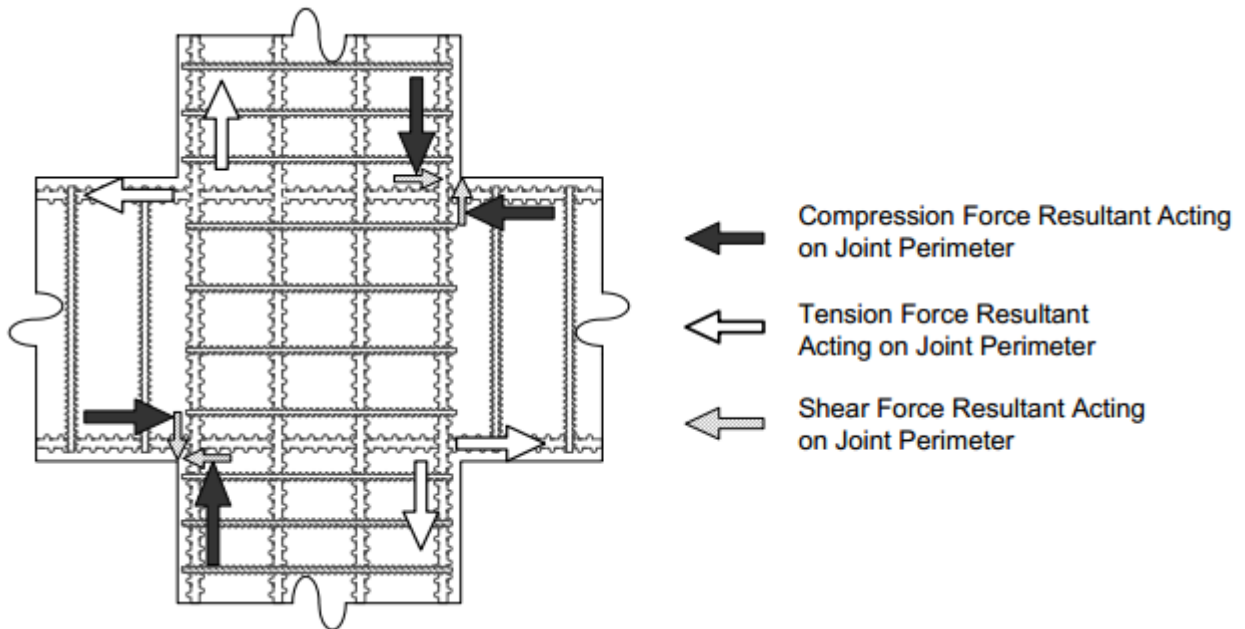
Fig.2.9 Idealized load distribution at the perimeter of the joint (Laura et al. (2003))
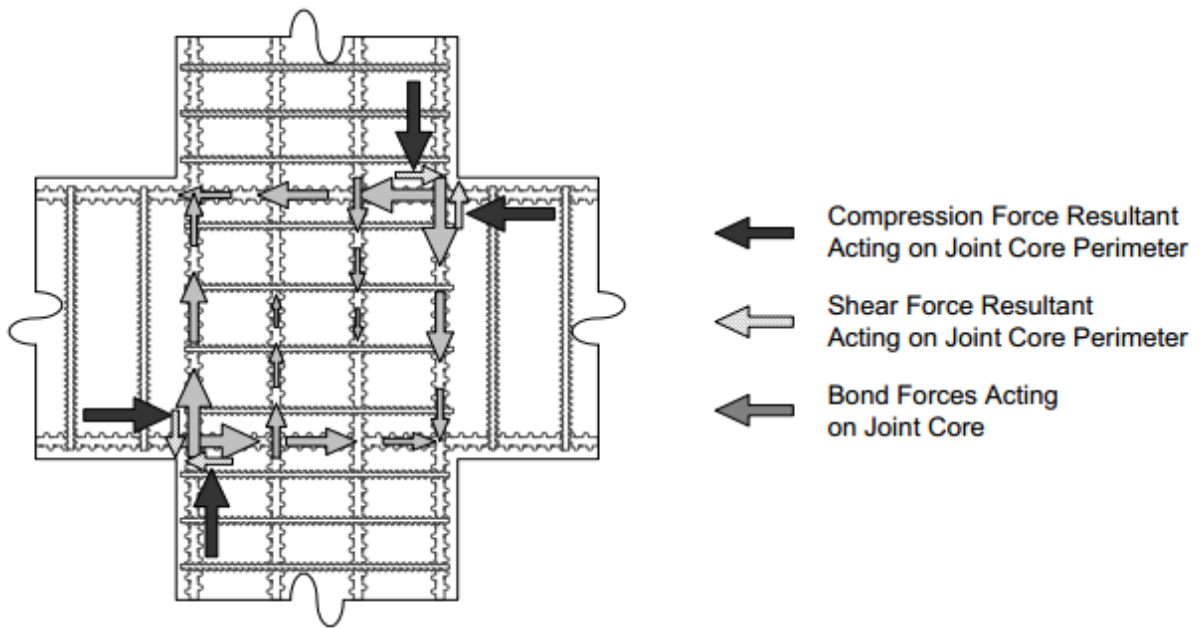
Fig.2.10 Idealized loading of the Joint core (Laura and Lowes, 2005)
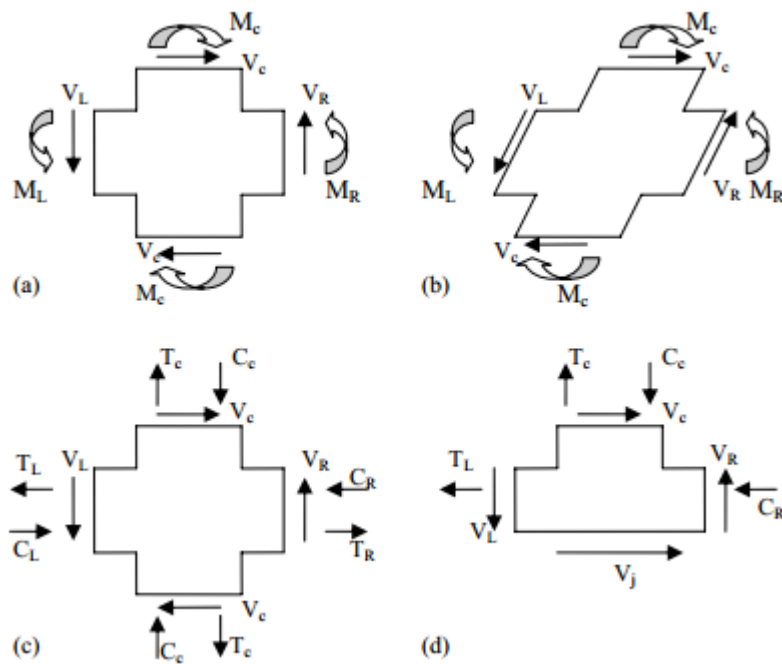
Fig.2.11 Joint free body diagrams (Lowes, 2005)

(Lowes et al. (2003)) proposed two dimensional idealization of an interior beam column joint. The model includes bar slip components to simulate stiffness and strength loss associated with bond strength association for beam and column longitudinal reinforcement embedded in the joint core, shear panel components to simulate strength and stiffness loss associated with shear failure of the joint core, one shear panel to simulate strength and stiffness loss associated with shear

failure of the joint core and four interface shear components to simulate loss of shear transfer capacity at the joint under severe loading as shown in Fig.2.12
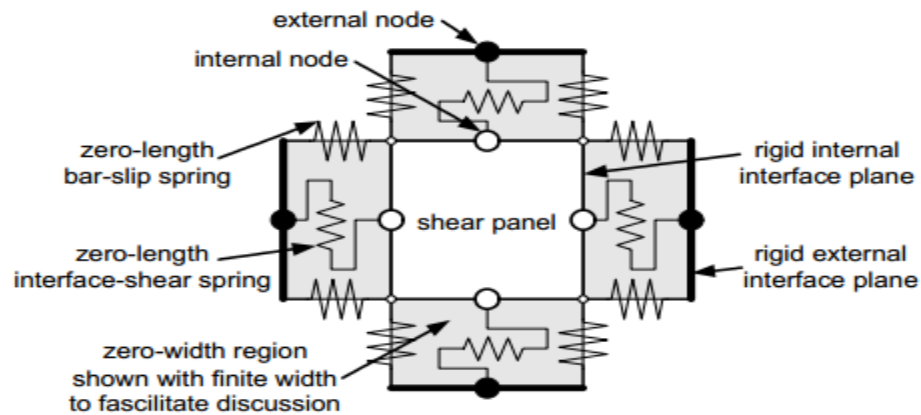
Fig.2.12 Components of typical beam column joints model (Lowes, 2005)

2.7 Investigations of joint shear failure parameters

2.7.1 Joint aspect ratio

Several previous researchers showed that the behavior of unreinforced RC joints is mostly affected by the joint aspect ratio, which is defined as the ratio of beam to column cross sectional heights and it mainly affects shear strength of the unreinforced exterior joints (Park and Mosalam, 2012). (Kim and LaFave, 2007) had reported that the increase of joint aspect ratio (h_b/h_c) had little influence on the shear strengths and shear strains. (Wong and Kuang, 2008) had conducted tests on unreinforced exterior joints having three joint aspect ratios. The test showed that the shear strength is inversely proportional to joint aspect ratios.

2.7.2 Beam longitudinal reinforcement ratio

Beam longitudinal reinforcement ratio is one of the parameters affecting join shear strength. (Niroomandi, 2014) performed numerical analysis and reported that increasing the beam longitudinal reinforcement ratio changes the failure type from a ductile failure (beam flexural failure) to a brittle one (joint shear failure). (Anderson et al. (2008)) claimed that joint shear strength is not a single number and beyond a certain threshold, join shear failure can occur at joint shear demand related to the beam reinforcement strength and the specimen geometry. (Wong, 2005) tested unreinforced exterior joints with two different longitudinal ratios. The result shows that the specimens having high beam longitudinal reinforcement ratio showed joint shear

failure prior to beam reinforcement yielding while the specimens having low longitudinal reinforcement ratio experienced joint shear failure with beam reinforcement yielding.

2.7.3 Column axial load

The effect of column axial load on shear strength of beam column joints has been investigated by many researchers. (Haach et al. (2008)) evaluated the influence of the column axial load on the behavior of monotonically loaded exterior beam column joints through numerical simulations. They observed that there were significant values of strain in the stirrups inside the joint region in specimens with low column axial loads compared to specimens with high column axial loads. (Li and Kulkarni, 2009) investigated the effect of axial load on seismic response of wide beam column connection and found that the axial load improved the capacity of the joint up to a load of $0.25fc'Ag$,after which any further increases reduced the strength and the stiffness. (Masi, 2014) tested two identical WBCC under different axial load. Test results showed that the axial load value is able to modify the damage evolution and, in turn, affect the deformation capacity of the joints. The joint with higher axial load was subjected to delay vertical cracking at the beam-column interface in compared to the joint tested under low axial load.

2.7.4 Code Recommendations

In various countries like United States, New Zealand, Japan, Republic of Korea, etc., many researchers have tried several approaches to improve understanding of RC joint shear behavior. Key influence parameters on joint shear behavior have been examined using collective experimental test results and analytical procedures. There is still no consensus about the effect of some parameters on joint shear strength/joint shear deformation. Thus some design considerations for joint shear strength have not yet been fully codified due to insufficient conclusive information. In addition, there is no generally accepted joint shear stress-strain prediction model that can describe the complete joint shear behavior of diverse types of RC beam column connections (Kim and LaFave, 2009).

2.7.4.1 ACI 352R-02 and ACI 318-05

For modern RC beam column connections (maintaining proper confinement within a joint panel), ACI-ASCE committee 352 ("Joints and connections in monolithic structures") has defined a nominal joint shear strength; that is:

$$V_n = \gamma_{ACI} \sqrt{(f'_c b_j h_c)} \quad \dots\dots\dots\dots\dots\dots\dots\dots (2.15)$$

Where γ_{ACI} −joint shear strength factor

f'_c −specified concrete compressive strength

b_j −effective joint shear width

h_c −column depth

Effective joint shear width is determined as the smallest of the three values

$$b_j = smallest(\frac{b_b+b_c}{2}, b_b + \sum \frac{mh_c}{2}, b_c) \quad .... \text{(2.16)}$$

Where b_b −beam width

h_c −column width

m −the slope to define the effective width of joint transverse to the direction of shear

ACI Committee 318 ('Building code requirements for structural concrete (ACI 318-05) and commentary (ACI 318R-05))") has generally accepted a similar joint shear design philosophy so that of ACI 352R-02 except for a few points.

$$b_j = smaller(b_b + b_c, b_b + 2x) \quad .... \text{(2.17)}$$

Where x the smaller of the distances from the beam is face to the column face

2.7.4.2 NZS 3101:1995

New Zealand, NZS 3101:1995 ("Concrete structures standard") has suggested the design joint shear strength as:

$$V_j = v_j b_j h_c \quad .... \text{(2.18)}$$

Where v_j −joint shear stress, $v_j = \left. f'_c f_{jy} A_{jh} \middle/ 6\alpha f_{by} A_s{}^* \right.$

b_j −effective joint shear width α −parameter considering column axial load

h_c −column depth

f_{jy} −yield stress of horizontal joint transverse reinforcement

f_{by} −yield stress of longitudinal reinforcement

$A_s{}^*$ −greater area of top or bottom reinforcement passing through the joint.

2.8 Finite Element Method

2.8.1 Introduction

The Finite element analysis (FEA) is a numerical technique for solving problems of Engineering and Mathematical physics. It is useful for problems with complicated geometries, loading, and material properties where analytical solutions cannot be obtained. The modern development of Finite element method was begun in 1941 with the work of Hrennikoff in the field of structural Engineering (Logan, 2012). In FEA method, all solutions obtained are approximate (Bhavikatti, 2005). The FEA originated as a method of stress analysis in the design of aircrafts. Civil Engineers use this method extensively for the analysis of beams, space frames, plates, shells, folded plates, foundations, rock mechanics problems and seepage analysis of fluid through porous media. The fast improvements in computer software technologies have boosted commercial finite element analysis packages to analyze complex structures. Some of the popular brands of these packages are ABAQUS, STAAD-PRO, ANSYS, NASTRAN, NISA AND GT-STRUDEL.

2.8.2 Areas of application of FEM

a. Structural/ stress analysis

> - Static/dynamic
> - Linear/Nonlinear

b. Solid Mechanics analysis

c. Heat transfer analysis

d. Electromagnetic potential distribution analysis

e. Biomechanical Engineering

f. Mechanical/aerospace/civil/automotive Engineering (Logan, 2012).

2.8.3 Advantages of Finite element method

The advantages of Finite element method are the ability to:

- ❖ Model irregularly shaped bodies quite easily
- ❖ Handle general load conditions without difficulty
- ❖ Model bodies composed of several different materials because element equations are evaluated individually.

21

❖ Handle unlimited numbers and kinds of boundary conditions.
 ❖ Vary the size the elements to make it possible to use small elements where necessary (Logan, 2012).

2.8.4 Procedures of formulating Finite element problems

In many Engineering problems if unknowns are found the behavior of the entire structure can be predicted. The basic unknowns or the field variables which are encountered in the engineering problems are displacements in solid mechanics. In a continuum, these unknowns are infinite. The finite element procedure reduces such unknowns to a finite numbers by dividing the solution region in to small parts called elements (discretization) and by expressing unknown field variables in terms of assumed approximating function (Interpolating functions/shape functions) within each element. The approximating functions are defined in terms of field variables of specified points called nodes/ nodal points. Thus, in FEA the unknowns are the field variables of the nodal points (Bhavikatti, 2005). The procedures may take the following steps.

a. Divide structure in to pieces (Elements with nodes)

b. Describe the behavior of the physical quantities on each element.

c. Connect (assemble) the elements at the nodes to form an approximate system of equations for the whole structure

d. Solve the system of equations involving unknown quantities at the nodes (e.g., displacements)

2.8.5 Types of Finite Elements

a) 1-D (Line) Element   b) 2-D (Plane) Element)

(Spring, beam, truss, pipe, etc.)   (Membrane, plate, shell, etc.)
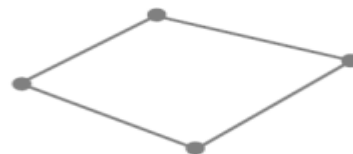
c) 3-D (Solid) Element
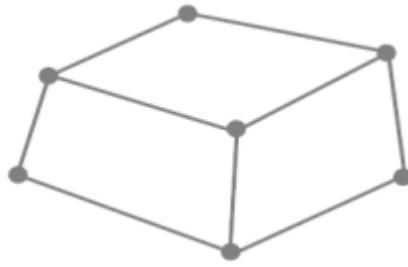
(3-D fields-temperature, displacement, stress, flow velocity)

d) Axisymmetric elements

These are known as ring type elements. These elements area useful for the analysis of axis-symmetric problems such as analysis of cylindrical storage tanks, shafts, and rocket nozzles. These elements can be constructed from one or two dimensional elements (Bhavikatti, 2005). .
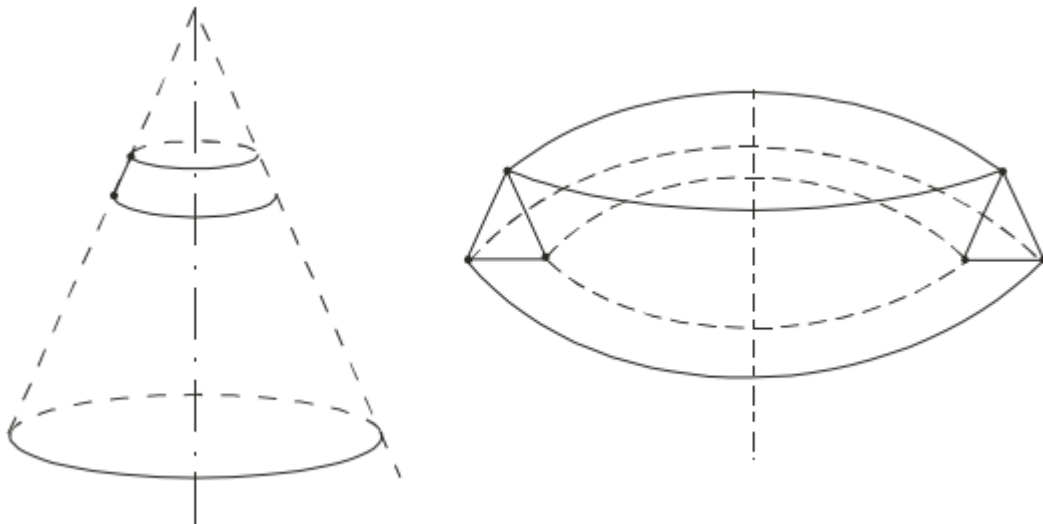
Fig.2.13 Elements and Nodes

2.8.6 Steps of FEA

The following are the general steps involved in finite element analysis

Step 1. Divide the body in to an equivalent system of finite elements with associated nodes and choose the most appropriate element type.

Step 2. Choose a displacement function within each element

Step 3. Relate the stress to the strains through the stress-strain law generally called the constitutive law.
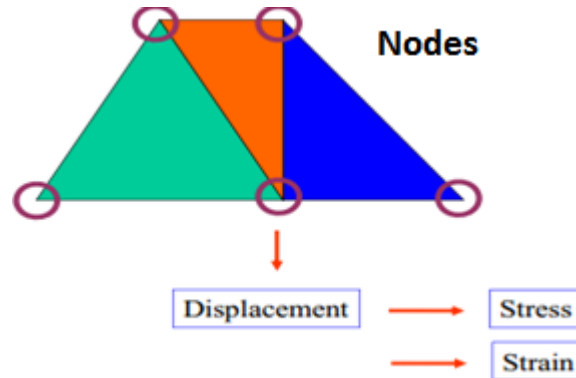
Step 4. Derive the element stiffness matrix and equations. Use the direct equilibrium method, a work or energy method, or a method of weighted residuals to relate the nodal forces to nodal displacements.

Step 5. Assemble the element equations to obtain the global or total equations and introduce boundary conditions

Step 6. Solve for unknowns degrees of freedom (or generalized displacements).

Step 7. Solve for the element stress and strains.

Step 8.Interpret and analyze the results for use in the design /analysis process (Logan, 2012).

2.8.7 Nonlinear FEA

A nonlinear structural problem is one in which the structure's stiffness changes as it deforms. All physical structures exhibit nonlinear behavior. Linear analysis is a convenient approximation that is often adequate for design purposes. It is obviously inadequate for many structural simulations including manufacturing process, such as forging or stamping; crash analyses; and analyses of rubber components, such as tires or engine mounts (ABAQUS 6.13, interactive).
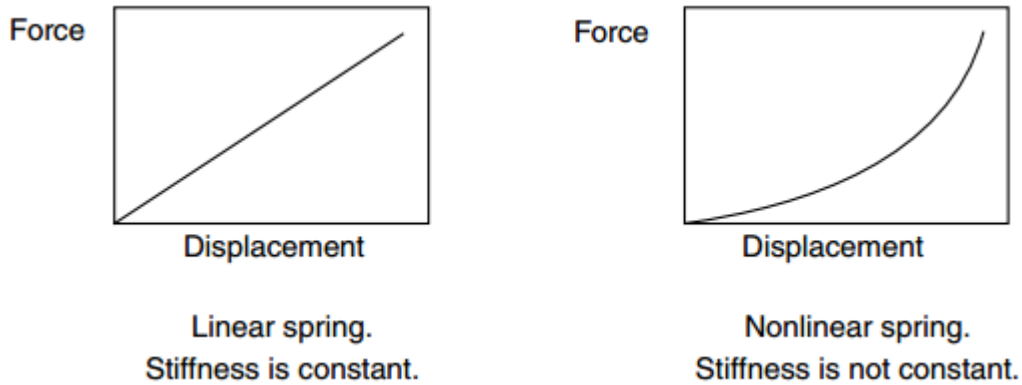
Fig.2.14 Linear and Nonlinear spring characteristics (ABAQUS 6.13, interactive)

Various nonlinear problems in nonlinear finite element analysis are grouped in to the following three categories based on the sources of nonlinearities (Bhavikatti, 2005).

a. Material nonlinearity

b. Boundary nonlinearity

c. Geometric nonlinearity

a. Material nonlinearity

The stress-strain relation for the material i.e. the constitutive law may not be linear and may be some times time dependent too. As shown below the concrete and steel stress-strain curve beyond yielding is nonlinear. Hence Young's modulus of elasticity depends up on the deformation. Apart from these basic relations, there are time dependent complex constitutive relations like plasticity, creep which make the problem nonlinear (Bhavikatti, 2005).

b. Boundary nonlinearity

Boundary nonlinearity occurs if the boundary conditions sudden change or when contact occurs during the analysis/simulation (ABAQUS 6.13, interactive). In boundary nonlinearity, the modifications to the external restraints resulting from deformation process such as lift-off, or smooth or frictional contact are taken in to account within analysis.

c. Geometry nonlinearity

Geometry nonlinearity is related to changes in the geometry of the structure during the analysis. It occurs whenever the magnitude of the displacements affects the response of the structure. It may be caused by large deflections, or rotations, "snap through", and initial stresses or load

stiffening (ABAQUS 6.13, interactive). Large problems like the analysis of tension structures and post buckling studies of beams, plates and shells also fall under this category. In this type of problems, the actual displacement relations need to be considered rather than linear strain displacement relations (Bhavikatti, 2005).

2.8.8 Meshing in FEA

The basic idea of FEA is to make calculations at only limited (finite) number of points and then interpolate the results for the entire domain (surface or volume).Any continuous object has infinite degrees of freedom and it's just not possible to solve the problem in this format. Finite element method reduces the degrees of freedom from infinite to finite with the help of discretization or meshing (nodes and elements) (Lee, 2014). For analysis, the software needs all three dimensions defined. It cannot make calculations unless the geometry is defined completely (by meshing using nodes and elements). The geometry can be categorized as 1D, 2D, or 3D based on the dominant dimensions and then the type of element is selected accordingly. Meshing the model also discretizes the original continuous boundary condition. The loads and restraints are represented by discrete loads and supports applied to element loads.

2.9 ABAQUS

ABAQUS is a suite of powerful engineering simulation programs, based on the finite element method that can solve problems ranging from relatively simple linear analyses to the most challenging nonlinear simulations (ABAQUS 6.13 documentation, 2013). It is finite element software which provides a preprocessing and post processing environment for the analysis of models. It is used in a wide range of industries like automotive, aerospace etc. and also extensively used in academic and research institutions due to its capability to address nonlinear problems (Manjunath, 2009).

2.9.1 ABAQUS Basics

A complete ABAQUS analysis usually consists of three distinct stages linked together by files as shown in Fig. below.
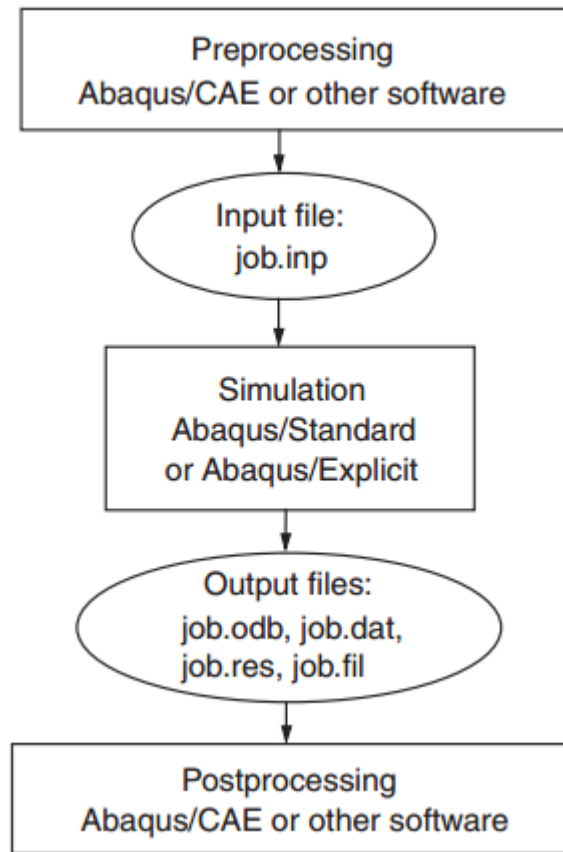
Fig.2.15 Stages of ABAQUS analysis (ABAQUS 6.13 documentation, 2013)

a. Preprocessing stage

Preprocessing is the initial phase of the Finite element analysis program. This phase includes various modules for creating a model, defining material properties, specifying boundary conditions, external loads and meshing the assembly of the model (Manjunath, 2009).

2.9.2 Modules of ABAQUS Analysis

| Part Module | → | Property Module | → | Assembly Module | → | Step Module | → | Interaction Module | → | Mesh Module | → | Job Module |
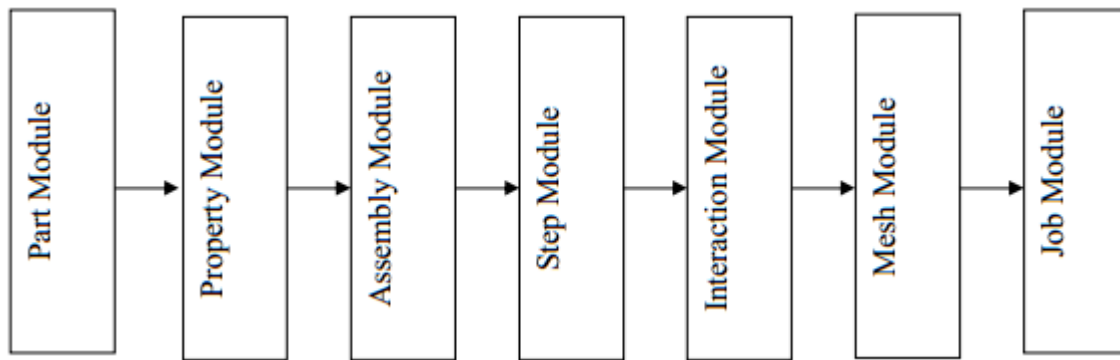
b. Simulation stage

The simulation, which normally runs as a background process, is the stage in which ABAQUS solves the numerical problem defined in the model. It is also a stage where outputs obtained are stored in binary files ready for post processing.

c. Post processing stage

Post processing stage is the stage where results generated in the analysis are visualized once the simulation completed.

2.10 Critique of the existing literature relevant to the study

Nonlinear stress-strain relationship of concrete, time dependent deformations such as creep and shrinkage, aggregate interlock, tension cracks, compression failure and the adhesion between concrete and reinforcing steel cause difficulties in the modeling of R/C members

The study of RC beam column joints presented herein has endeavored to propose suitable numerical and analytical models that describe the nonlinear behavior of RC BCC including the design and details of interior and exterior joints. The result of previous researches indicate that the primary mechanisms that determine the earthquake response of beam column joints are anchorage failure of frame member longitudinal reinforcement embedded in the joint, Inelastic shear response of the RC joint core and shear transfer failure at the joint column and joint beam interfaces . The study shows that:

> ❖ Most finite element studies of RC structures do not consider bond slip of reinforcing steel and the inherent interaction between reinforcement and concrete in RC members.

- ❖ The idea of joint transverse reinforcement in the shear panel joint zone and its design and detail rarely studied.

- ❖ From the analytical studies, the provision of cross diagonal reinforcement in beam region increased the ultimate load carrying capacity and ductility of joints in upward and downward loading conditions.

- ❖ Concrete damage plasticity (CDP) model is applied to the numerical procedure as a distributed plasticity over the whole geometry of the specimens to appropriately simulate material non linearity.

- ❖ The beam flexure type of failure took place in case of specimens with joint shear reinforcement while the joint shear failure occurred in case of specimens with no joint shear reinforcement.

In RC moment resisting frames structures, the functional requirement of a joint, which is the zone of intersection beams and columns, is to enable the adjoining members to develop and sustain their capacity. The demand on these finite size elements is always severe and more complex due to the possible two way actions in 3D frame structures. However the codes consider one direction of loading at a time and arrive at the design parameters for the joint (Uman and Jain, 2005).

In seismic conditions involving reversed cyclic loading, anchorage requirements assume great importance in deciding the sizes of the members. The relevant expressions suggested by three codes with regard to development length and flexural strength ratios are summarized in Table

Parameters	ACI 318M-02	NZS 3101:1995	EN 1998-1:2003
Development length for interior joints	$d_b/h_c \geq 1/20$	$\dfrac{d_b}{h_c} \leq 6\left[\dfrac{\alpha_t \alpha_p}{\alpha_s}\right]\alpha_f \dfrac{\sqrt{f'_c}}{\alpha_0 f_y}$	$\dfrac{d_b}{h_c} \leq \dfrac{7.5 f_{ctm}}{\gamma_{Rd} f_{yd}} \dfrac{1 + 0.8\, \nu_d}{1 + 0.75\, k_D \rho'/\rho_{max}}$
Development length for exterior joints	$L_{dh} = \dfrac{f_y d_b}{5.4\sqrt{f'_c}}$	$L_{dh} = 0.24\,\alpha_b \alpha_1 \alpha_2 \dfrac{f_y d_b}{\sqrt{f'_c}}$	$\dfrac{d_b}{h_c} \leq \dfrac{7.5 f_{ctm}}{\gamma_{Rd} f_{yd}}(1 + 0.8\, \nu_d)$
Flexural strength of columns	$\sum M_{n,c} \geq 1.2 \sum M_{n,b}$	$\sum_c M_n \geq 1.4 \sum_b \phi_o M_n$	$\sum M_{Rc} \geq 1.3 \sum M_{Rb}$

Table 2.1 Code revisions that influence the size of members (Uman and Jain, 2005)

When longitudinal beam bars near the column face are stressed beyond the yield stress, splitting cracks are initiated along the joint face. Longitudinal bar is to be provided with adequate development length at the joint taking the yield penetrations in to consideration. Therefore, the size of the beams and columns framing in to the joint depends on the bond requirements of the

bar. (Wong, 2005) tested unreinforced exterior joints with two different longitudinal ratios. The result shows that the specimens having high beam longitudinal reinforcement ratio showed joint shear failure prior to beam reinforcement yielding while the specimens having low longitudinal reinforcement ratio experienced joint shear failure with beam reinforcement yielding.

Behnam et al. (2018) simulated the four full scales EWBCC that were tested under reversed cyclic loading conditions. The parametric study was conducted to explore the effects of several parameters including the column axial load, column and beam dimensions, beam bar anchorage ratios and spandrel beam reinforcement on EBCCs. In their study they used beam column dimensions and anchorage ratios as independent parameters.

(Park and Mosalam, 2012) indicated that the join aspect ratio ((h_b/h_c) mainly affects shear strength of the unreinforced exterior joints. (Kim and LaFave, 2007) had reported that the increase of Joint aspect ratio (h_b/h_c) had little influence on the shear strengths and shear strains. However, (Metelli et al. (2015)) points out the importance to model the joint deformation by means of two unrelated contributions, which are the shear deformation the shear panel zone, and the added rotation at the interface sections between the joint and the structural members, due to the bar slip within the joint core.

Lee et al. (2009) conducted experimental and analytical investigations on strength deterioration of RCC BC joints and concluded that the deformability of RC joints failing in shear after plastic hinges developed at both ends of adjacent beams was due to the degradation of diagonally compressed concrete due to strain penetration. They indicated in the test that the deformability of the joint increased as the amount of beam bars decreased.

An extensive data base of the RC BCC test specimens for exterior, interior and knee joints exhibiting joint failure when subjected to reversed cyclic lateral loading was prepared by (Jaehong and LaFave 2007). They collected the data of experimental sub-assemblies from all over the world. They suggested that the most influential parameters for predicting joint shear failure in terms of joint shear strength and deformation capacity is concrete compressive strength.

CHAPTER THREE

MATERIALS AND RESEARCH METHODOLOGY

The fast improvements in computer software technologies have boosted commercial finite element analysis packages to analyze complex structures. Some of the popular brands of these packages are ABAQUS, STAAD-PRO, ANSYS, NASTRAN, NISA AND GT-STRUDEL. In order to meet the objectives of this research, nonlinear finite element analysis on the RC beam column connection subjected shear failure under cyclic lateral loading was modeled using ABAQUS 6.13-1 to investigate shear failure modes and post peak behaviors such as cyclic deterioration and shear resistance mechanisms in terms of shear capacity, deformation and crack pattern. In this research, the overall response of RC beam column interior and exterior connections subjected to lateral load and factors affecting joint shear failure are identified.

This chapter deals with the overall process and method of modeling, analysis and results of nonlinear finite element analysis using ABAQUS/Standard 6.13-1 software.

3.1 Research Design

Nonlinear finite element analysis of RC conventional exterior and interior beam column connections is performed using ABAQUS/Standard. Geometry and material nonlinearities are considered in order to properly simulate the behavior of the connections to analyze joint shear failure under lateral loading. In pre-processing stage, geometry, boundary conditions, element types, material properties and nonlinear analysis solutions were defined. Concrete Damage Plasticity (CDP) was selected and introduced to the numerical model. The main and essential elements of model based on classical plasticity theory, which were the "yield criteria", "flow rule" and "hardening rule" were all effectively considered in damage plasticity model. Numerical modeling of RC joint shear behavior calibrated by experimental results of other researchers was the main strategy of this study.
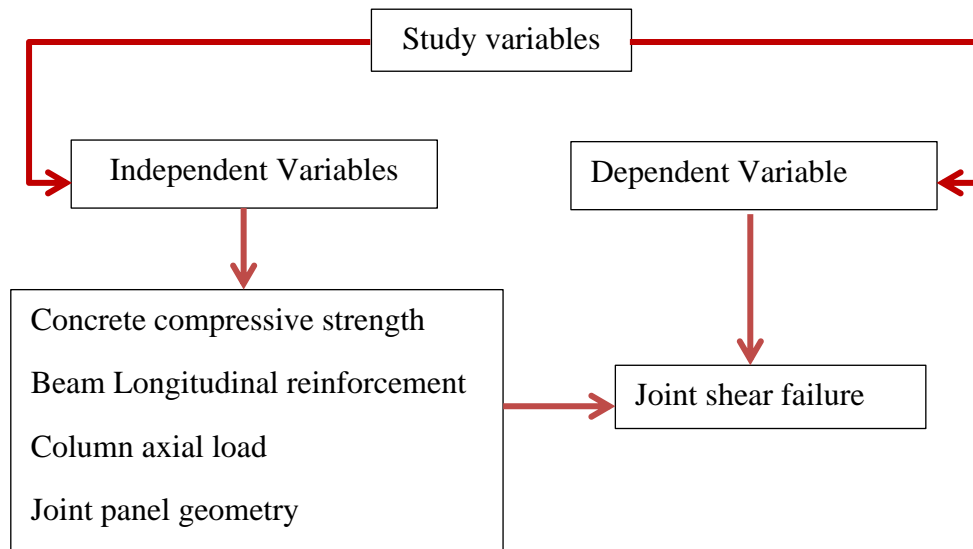
3.2 Study variables

Fig.3.1 Conceptual frameworks of study variables

3.3 Model geometry and size

Finite element modeling of RC conventional exterior and interior joint shear behavior calibrated by experimental results of other researcher was the main strategy of this study. To verify the model, two RC exterior and interior beam column joint configurations are modeled and simulated. To represent non-ductile detail of the joint, no transverse was considered within the joint panel in both exterior and interior joints. The numerical modeling is calibrated by experimental results of cyclic lateral loading test on exterior and interior done by (Fadwa et al. (2014)). The measured uniaxial concrete compressive strength of the test specimens, yield strength and ultimate tensile strength of reinforcement used in the tests were reported in table 3.1 and table 3.2.

3.4 Modeling and analysis

The material properties used to conduct the experiments are used to model the beam column joints so that the study parameters clearly define the joints. The configuration of numerical model is implemented in finite element code ABAQUS. The finite element model is validated with experimental results. Finite Element Analysis (FEA) of the connection specimens is performed in a nonlinear static analysis format and the analysis procedure considers both material and geometric nonlinearities. In a nonlinear analysis, the total specified loads acting on a finite element body will be divided into a number of load increments. At the end of each increment the structure is in approximate equilibrium and the stiffness matrix of structure will be modified in order to reflect nonlinear changes in structure's stiffness.

3.5 Test setups, boundary conditions, loading, dimensions, and details

The schematic test setups, reaction frames, specimen and loading system were the same for both exterior and interior. The beams and columns were pinned at their ends to simulate points of inflection. The pins at the end of the beams were supported by vertical steel links that restrained only vertical displacements at the beam ends. The column was pin supported at its base and deflected laterally at its tip. On-plane movement of the specimen was prevented by two braced I-sections connected to the reaction frame.

Each specimen was tested under constant axial load 230 KN, which is the total specified load acting on a finite element body and will be divided into a number of load increments, applied on the column and quasi static cyclic lateral loading at column's tip to simulate earthquake loading. The load was applied by means of three hydraulic actuators with 1000KN capacity and a stroke of ±150mm. The selected lateral load history consisted of two phases. The first phase was force-control and the second phase was displacement control. At early stage of the first phase of the loading, two cycles approximately 10% of the theoretical yield load of the beam was applied to check the test setup and ensure that all data acquisition channels were functioning properly.
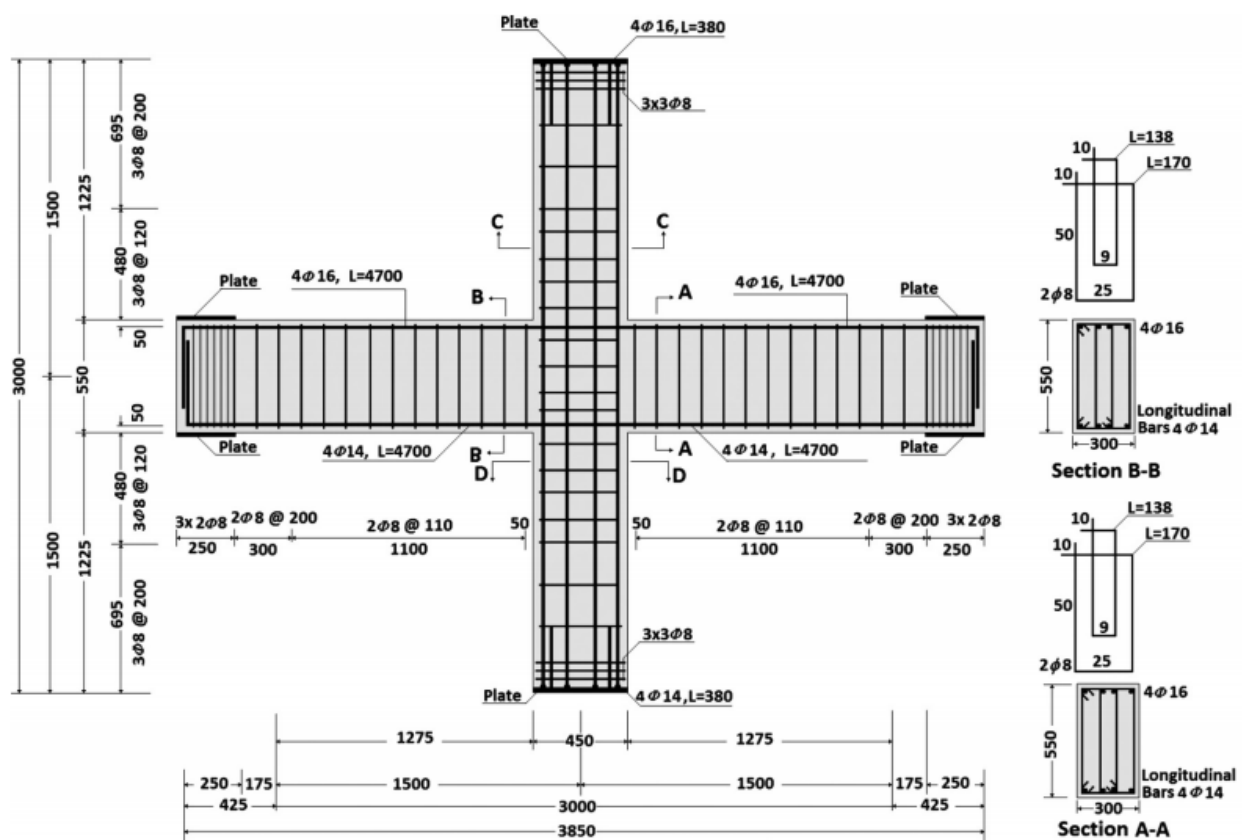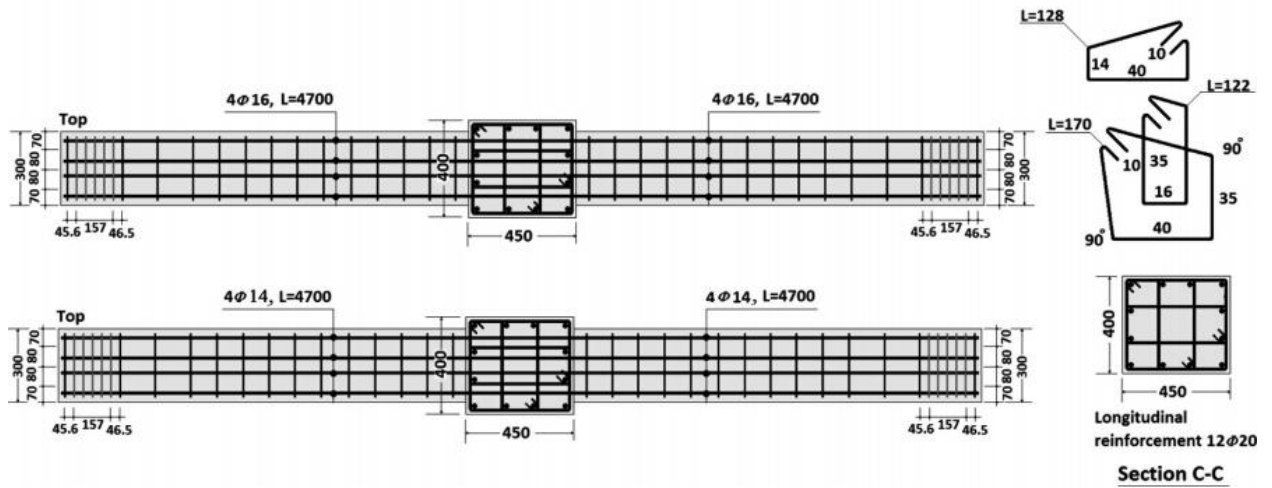
Fig.3.2 Dimensions and reinforcement details of ICBCC (Fadwa et al. (2014)
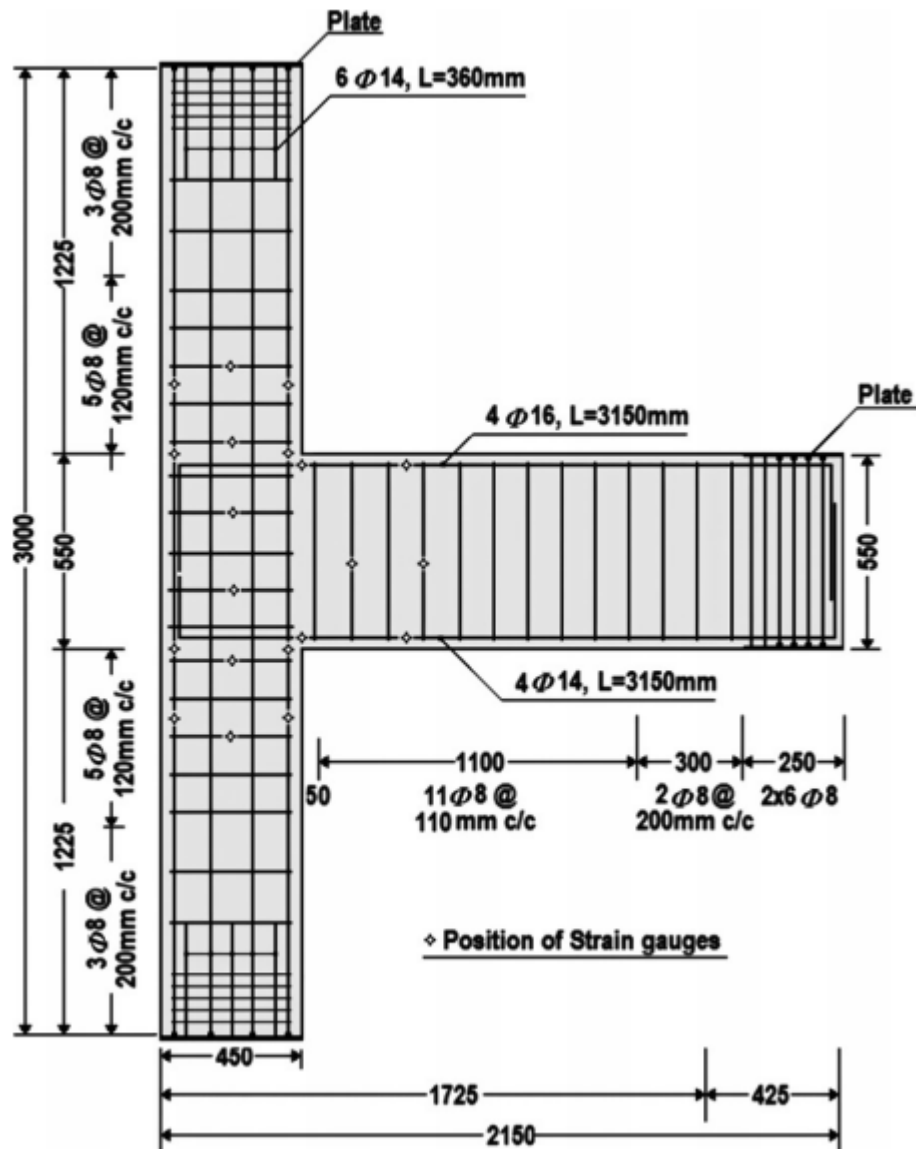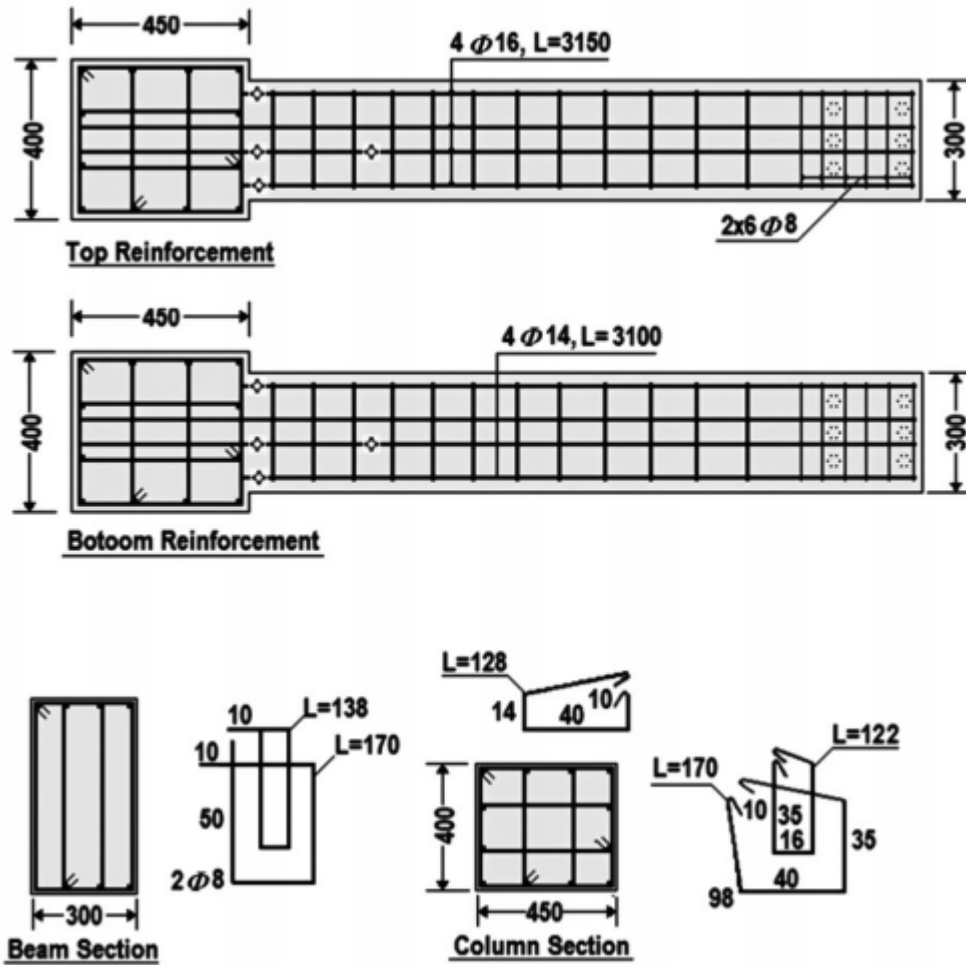
Fig.3.3 Dimensions and reinforcement details of ECBCC (Fadwa et al. (2014)
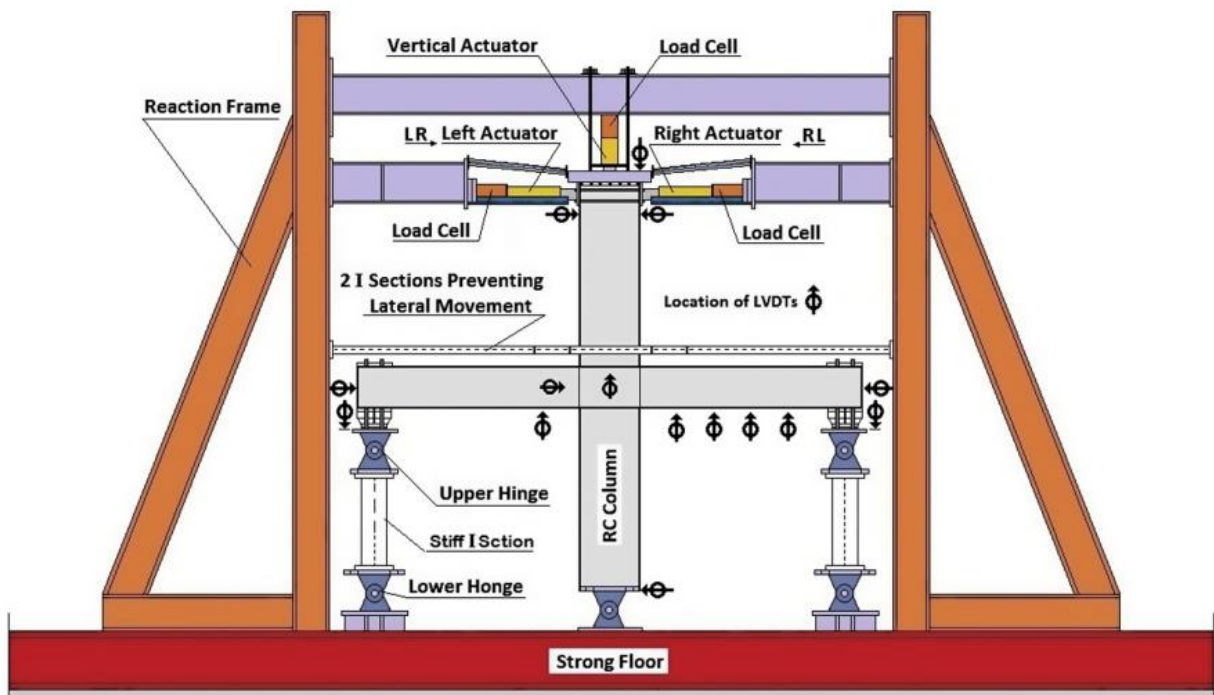
Fig.3.4 Schematic test setups for the interior and exterior test specimens
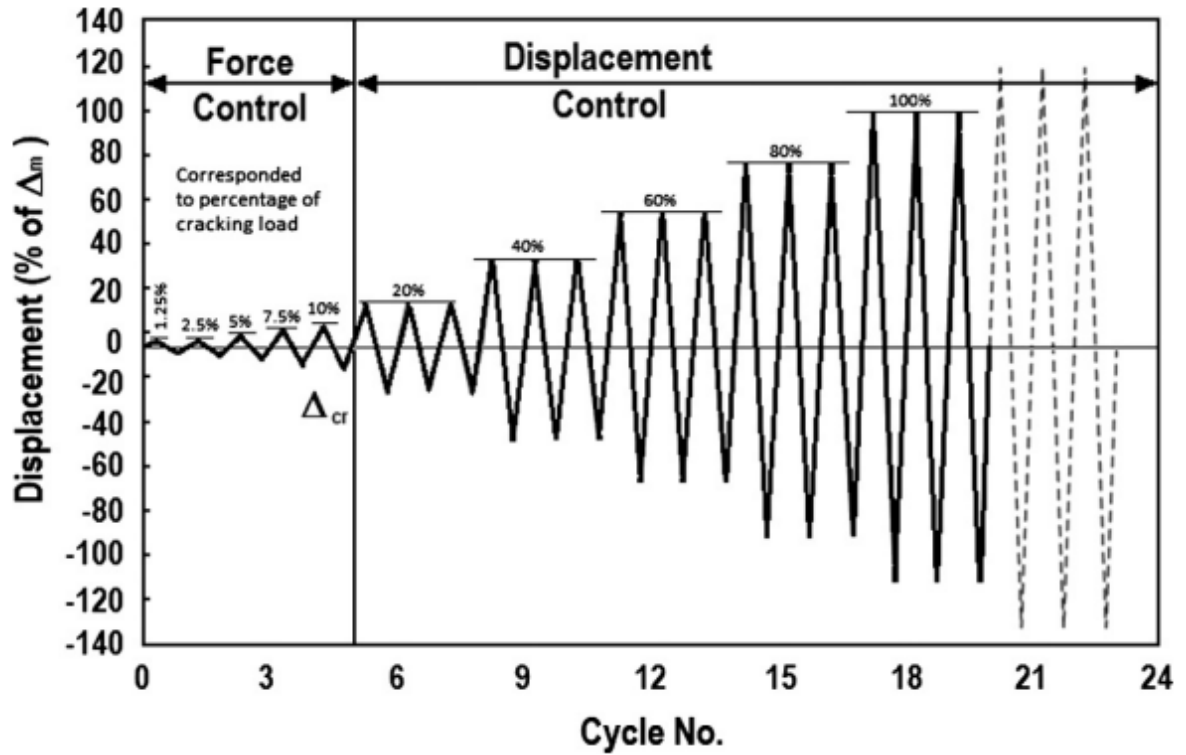
Fig.3.5 Cycle displacement schedule for the two tests

Connection	Geometry	b (mm)	h (mm)	Concrete cover (mm)
Interior	Beam	300	550	25
	Column	450	400	
Exterior	Beam	300	550	25
	Column	450	400	

Table.3.1 Geometry characteristics

36

3.6 Material properties of test specimens

Connection type	Concrete compressive strength $f_c{'}$ (Mpa)	Tensile strength Concrete f_{ct} (Mpa)	Reinforcement type: Longitudinal and stirrup		Bar dia in mm	Yield strength F_y (Mpa)	Modulus of Elasticity, E	Yield strain (for steel)
Interior	34.32	2.84	Beam	Top	16	497.64	202,405	0.00247
				Bottom	14	345.38	202,405	0.00171
			Column	Top	16	497.64	202,405	0.00247
				Bottom	14	345.38	202,405	0.00171
			Stirrup		8	345.38	195,733	0.00171
Exterior	34.32	2.84	Beam	Top	18	497.64	202,405	0.00247
				Bottom	14	345.38	202,405	0.00171
					16	345.38	202,405	0.00171
			Column	Top	14	345.38	202,405	0.00171
				Bottom	14	345.38	202,405	0.00171
			Stirrup		8	345.38	195,733	0.00171

Table 3.2 Material properties of test specimens

3.7 Finite element analysis

The static analysis in ABAQUS/Standard with viscosity regularization was performed. For solving this model using ABAQUS/Standard, a full Newton solver with default matrix storage was used. An automatic incremental with a small time step size and a large maximum number of increments were used to the convergence rate.

3.7.1 Element type and shape

Connection		Element type	Element shape	Geometrical order	Number of elements
Interior	Concrete	C3D8R	Hexahedral	Linear	19002
	Reinforcement	T3D2	Line	Linear	15850
Exterior	Concrete	C3D8R	Hexahedral	Linear	14298
	Reinforcement	T3D2	Line	Linear	12744

Table 3.3 Number and types of elements in Finite element model

A 3D solid shape model using 3D stress hexahedral element type (C3D8R) implemented to simulate concrete behavior. Wire shape model with truss elements (T3D2) is to simulate reinforcement's behavior. A uniform mesh size was chosen for concrete elements for the whole geometry and the same size for reinforcement mesh was adopted for steel bar. The size of elements is refined several times in order to obtain converged solution.

3.7.2 Modeling of material properties

Material		Density (tonn/mm3)	Youngs modulus of elasticity (Mpa)	Poisson's ratio
Concrete		2.54e-9	31848	0.2
Steel	Rebar	7.85e-9	202405	0.3
	Stirrup	7.85e-9	195733	0.3

Table 3.4 Modeling of material properties

a. Concrete compressive uniaxial stress-strain behavior

The concrete stress-strain behavior under compression was categorized and modeled in three phases.

Phase 1: This stage is linear-elastic phase. It is continuous up to about 40% of the maximum compressive stress level $\sigma_{co} = 0.4f_c'$.

$$\sigma_{c,1} = E_c\varepsilon_c, \quad \varepsilon_c \leqslant 0.4f_c'/E_c \quad \text{............. (3.1)}$$

Phase 2: This stage is the hardening phase. At this phase the stress increases gradually until it reaches a strain level of 0.0035. It describes the ascending branch of the stress strain relationship reaching the peak stress, σ_{cu} at corresponding strain level $\varepsilon_o = 2f_c'/E_c$ where η_c is material constant obtained from the relation of phase 1 and 2.

$$\sigma_{c,2} = \frac{\eta_c\frac{\varepsilon_c}{\varepsilon_0} - \left(\frac{\varepsilon_c}{\varepsilon_0}\right)^2}{1 + (\eta_c - 2)\frac{\varepsilon_c}{\varepsilon_0}}f_c', \quad 0.4f_c'/E_c \leqslant \varepsilon_c \leqslant 0.0035 \quad \text{.................... (3.2)}$$

Phase 3: This stage is post peak softening phase. It represents the initiation and progression of compressive damage in the concrete material until the ultimate compressive strain ε_u attained. The stress-strain compatibility at stress level of $\sigma_{co} = 0.4f_c'$. Using the stress-strain compatibility at strain level of $\varepsilon_{cu} = 0.0035$ for phase 1 and 2, gives the value of λ_c which represents constant crushing energy as material property. ABAQUS uses data in terms of

inelastic strain $\breve{\varepsilon}_c^{in} = \varepsilon_c - (\sigma_c/E_c)$ which is total strains minus elastic strains corresponding to undamaged material. Fig. shows concrete uniaxial compressive stress-strain behavior used in the model.

$$\sigma_{c,3} = \left(\frac{2 + \lambda_c f'_c \varepsilon_0}{2f'_c} - \lambda_c \varepsilon_0 + \frac{\lambda_c \varepsilon_c^2}{2\varepsilon_0}\right)^{-1}, \quad 0.0035 \leqslant \varepsilon_c \leqslant 0.03 \quad \text{...................} \quad (3.3)$$

$$d_c = 1 - \frac{\sigma_c}{E_o(\varepsilon_c - \varepsilon^{pl}_c)} \quad \text{..........} \quad (3.4)$$
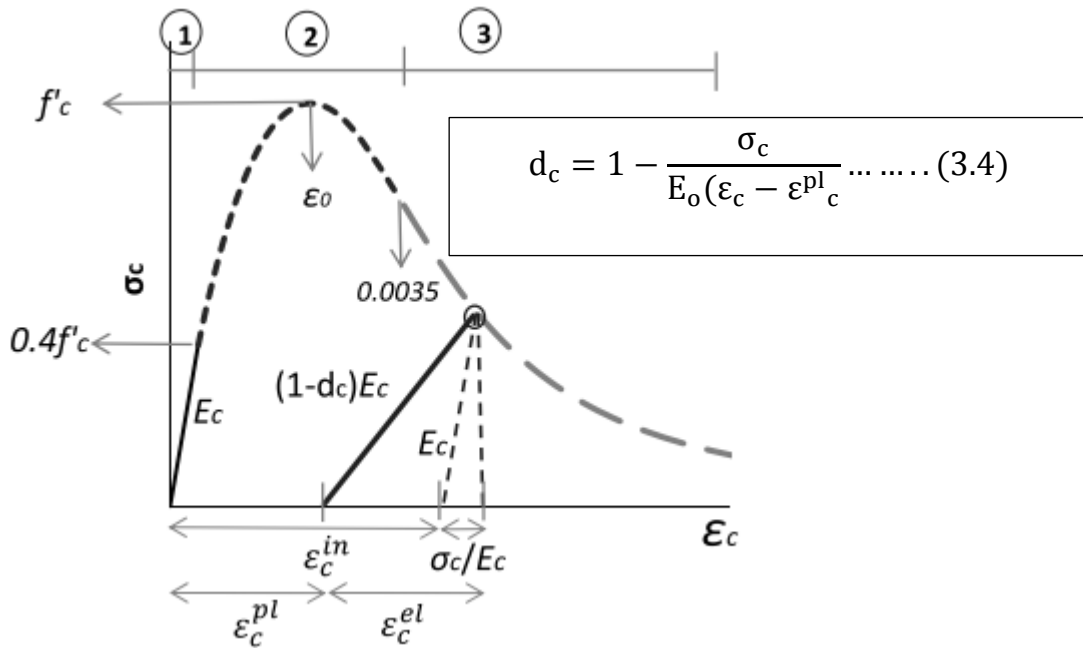
Fig.3.6 Concrete compression damage

Compression behavior	
Yield stress	Inelastic strain
12.837924	0
22.617245	0.000150766
29.407914	0.000368223
33.277769	0.000677529
34.32	0.001015435
34.292609	0.001076616
32.516269	0.001563476
28.010699	0.00213616
20.836026	0.002792779
19.792773	0.002877586

Table 3.5 Concrete compression damage

b. Concrete tensile uniaxial stress-strain behavior

$$d_t = 1 - \frac{\sigma_t}{E_o(\varepsilon_t - \varepsilon^{pl}{}_t)} \dots\dots\dots (3.5)$$

Fig.3.7 Concrete tension damage

Tensile behavior		0.30594173	0.14
		0.28039339	0.15
Yield stress	Displacement	0.25484505	0.16
2.65447422	0	0.2292967	0.17
2.24570071	0.01	0.20374836	0.18
1.8369272	0.02	0.17820001	0.19
1.42815369	0.03	0.15265167	0.2
1.01938018	0.04	0.12710332	0.21
0.61060667	0.05	0.10155498	0.22
0.53089484	0.051950024	0.07600663	0.23
0.51032849	0.06	0.05045829	0.24
0.48478014	0.07	0.02490995	0.25
0.4592318	0.08	0.38258677	0.11
0.43368346	0.09	0.35703842	0.12
0.40813511	0.1	0.33149008	0.13

Table 3.6 Concrete tension damage

d. Uniaxial tensile stress-crack width relationship for concrete

The concrete behavior in tension for normal weight concrete is characterized by a stress crack displacement response as shown in fig.3.2.10.

$$G_f = G_{f0}((f'_c + 8)/(f_{cmo}))^{0.7} \dots\dots\dots\dots \ (3.6)$$

Where G_f −fracture energy of concrete that represents the area under the tensile stress crack displacement curve (N/m)

f_t −maximum tensile strength

$G_{f0} = 0.03 N/mm$ −base fracture energy that depends on the maximum aggregate size

$f_{cmo} = 10 MPa$

Tension damage for post cracking behavior is obtained from tensile stress failure and fracture energy by specifying the tensile damage variable as a function of cracking displacement (w).
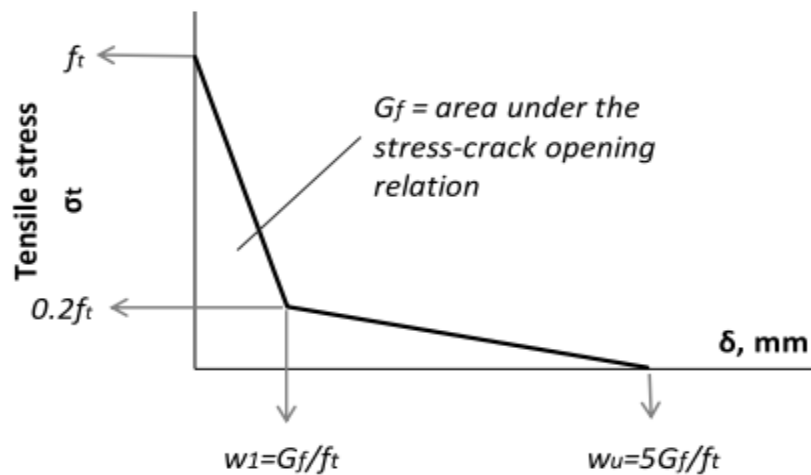

Fig.3.8 Uniaxial tensile stress-crack width relationship for concrete

w	F						
0	1.983447	0.069525	0.396689	0.13	0.310427	0.2	0.210578
0.01	1.75522	0.07	0.396012	0.14	0.296163	0.21	0.196314
0.02	1.526993	0.08	0.381748	0.15	0.281899	0.22	0.18205
0.03	1.298766	0.09	0.367484	0.16	0.267635	0.23	0.167786
0.04	1.070539	0.1	0.35322	0.17	0.253371	0.24	0.153521
0.05	0.842312	0.11	0.338956	0.18	0.239106	0.25	0.139257
		0.12	0.324692	0.19	0.224842		

Table 3.7 Uniaxial tensile stress-crack width relationship for concrete

d. Steel uniaxial stress-strain behavior

The plastic properties of the reinforcement were determined based on the bilinear strain hardening yield stress-strain plastic strain curve. The load buckling of the reinforcing bar and the Bauschinger effect was not considered in steel material properties.
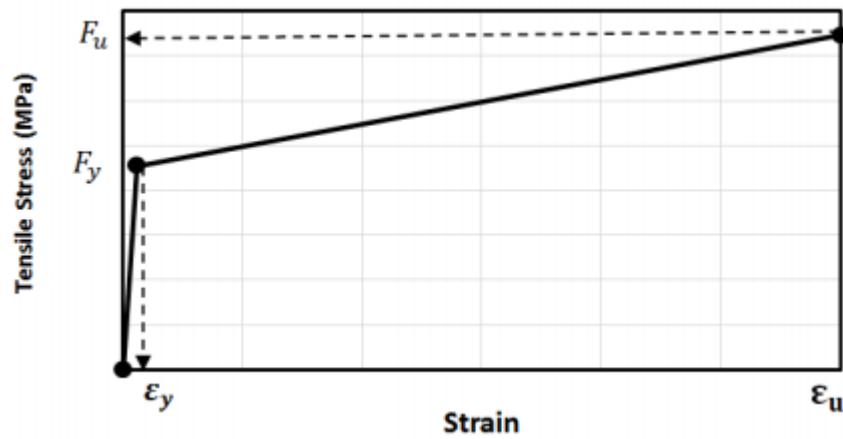

Fig.3.9 Reinforcement uniaxial stress-strain behavior

Yield stress	Plastic strain
320	0.1
460	0.235
730	0.51

Table 3.8 Reinforcement uniaxial stress-strain behavior

e. Concrete damage plasticity (CDP) input parameters

Plasticity parameter	Dilation angle	Eccentricity	Stress ratio	Shape factor	Viscosity Parameter
Value used in the model	38	1	1.12	0.6667	0.01

Compression damage (d_c)　　　　　　**Tensile damage (d_t)**

Compression damage	
Damage parameter	Inelastic strain
0	0
0	2.72917E-05
0	0.000150766
0	0.000368223
0	0.000677529
0	0.001015435
0.000798117	0.001076616
0.052556258	0.001563476
0.18383744	0.00213616
0.392889673	0.002792779
0.423287502	0.002877586

Tensile damage	
Damage parameter	Displacement
0	0
0.153994153	0.01
0.307988307	0.02
0.46198246	0.03
0.615976613	0.04
0.769970766	0.05
0.8	0.051950024
0.807747807	0.06
0.817372442	0.07
0.826997077	0.08
0.836621711	0.09
0.846246346	0.1
0.85587098	0.11
0.865495615	0.12

0.87512025	0.13
0.884744884	0.14
0.894369519	0.15
0.903994153	0.16
0.913618788	0.17
0.923243422	0.18
0.932868057	0.19
0.942492692	0.2
0.952117326	0.21
0.961741961	0.22
0.971366595	0.23
0.98099123	0.24
0.990615864	0.25

Table 3.9 Concrete damage plasticity (CDP) input parameters

CHAPTER 4

ANALYSIS, RESULT AND DISCUSSIONS

A nonlinear finite element analysis on exterior and interior RC beam column connections subjected joint shear failure under lateral loading was modeled using ABAQUS 6.13-1 to investigate the joint shear failure modes and post peak behaviors such as deformation behavior and shear resistance mechanisms in terms of shear capacity, deformation capacity and crack pattern. The overall response of RC beam column interior and exterior connections subjected to lateral load and the key influential factors affecting joint shear failure were identified.

4.1 Results of Finite element analysis

RC joint shear behavior was described as an envelope curve by connecting key points displaying the most distinctive stiffness changes. The first point indicates the initiation of diagonal cracking within a joint panel, the second point results from yielding of reinforcement, and the third point corresponds to maximum response. It is important that the stress-strain relation describes quite realistically not only the tensile cracking and fracture, but also the nonlinear tri-axial behavior under various stress/strain histories, for both tensile and compressive stress states.

In this study more realistic analysis models such as a transition hysteresis model for concrete stress-strain relationships especially in tension compression regions, an orthogonal fixed cracking model, and a hysteresis model for shear characteristics of cracked concrete, considering deterioration and fracture mechanics were not incorporated in nonlinear FEA. It should be mentioned that full cyclic lateral loading analysis was performed in experimental test; it consumed a tremendous amount of time. However, the hysteretic loops obtained from the analysis may occur due to different factors shear, bond deterioration, bauschinger effects in the reinforcement bar, etc. The behavior of reinforced concrete elements under cyclic loading such as the tangent stiffness for unloading and reloading, slip stiffness, residual strain and deterioration did not simulated due to complexity in the constitutive modeling of the concrete and reinforcement and the adoption of the embedded method to simulate the bond between concrete and reinforcement. Therefore, in this paper, only monotonic loading was presented.

Beam

Column

Bottom Rebar

Top Rebar
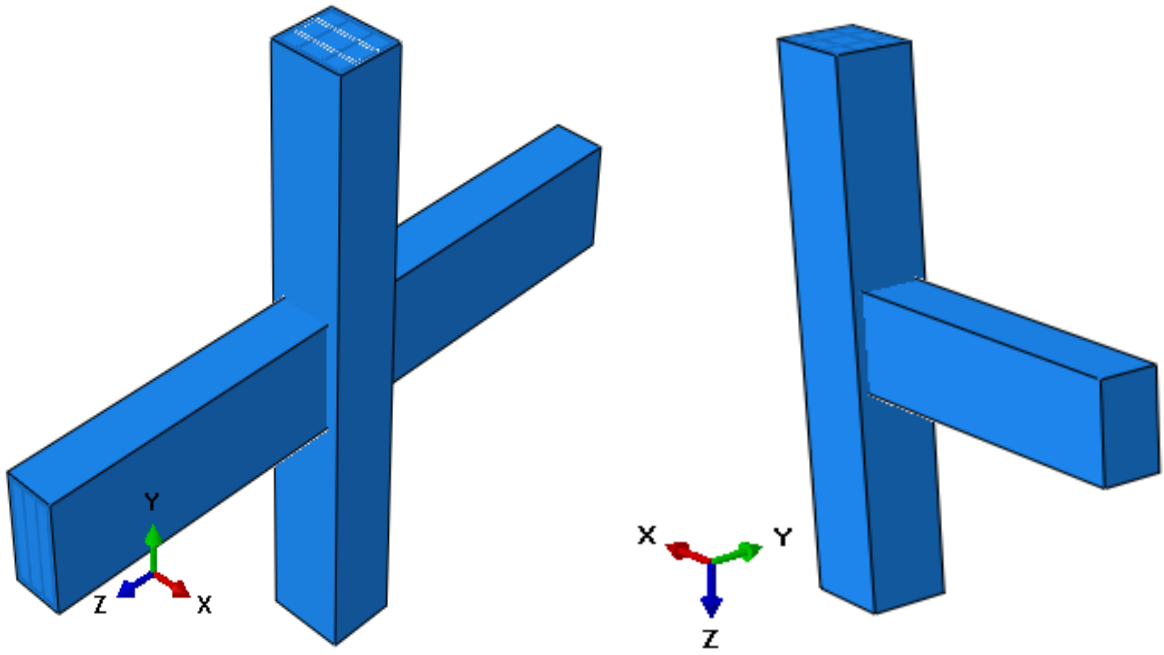
Column stirrup

Beam stirrup
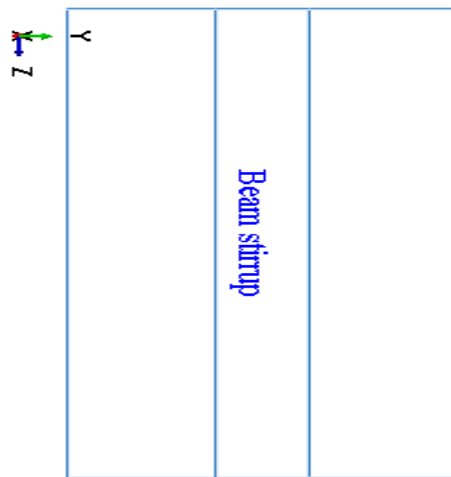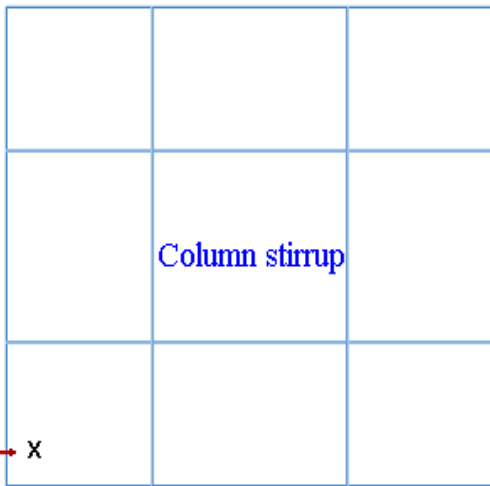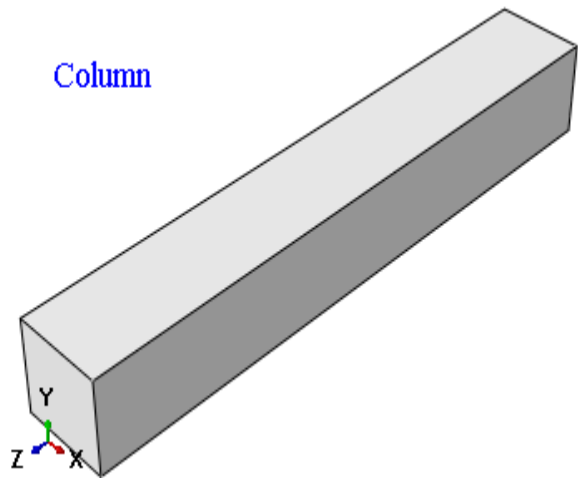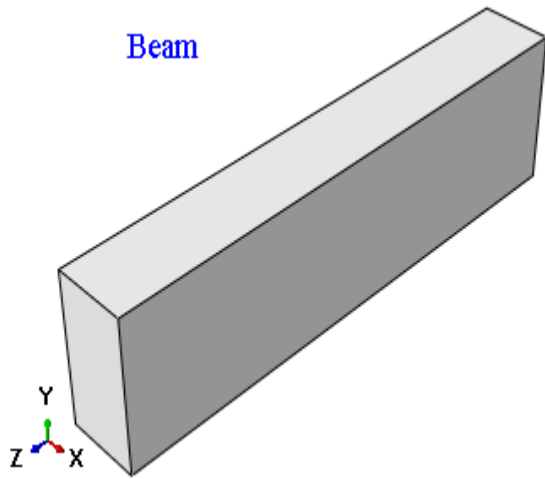
Fig.4.1.1 Geometric model
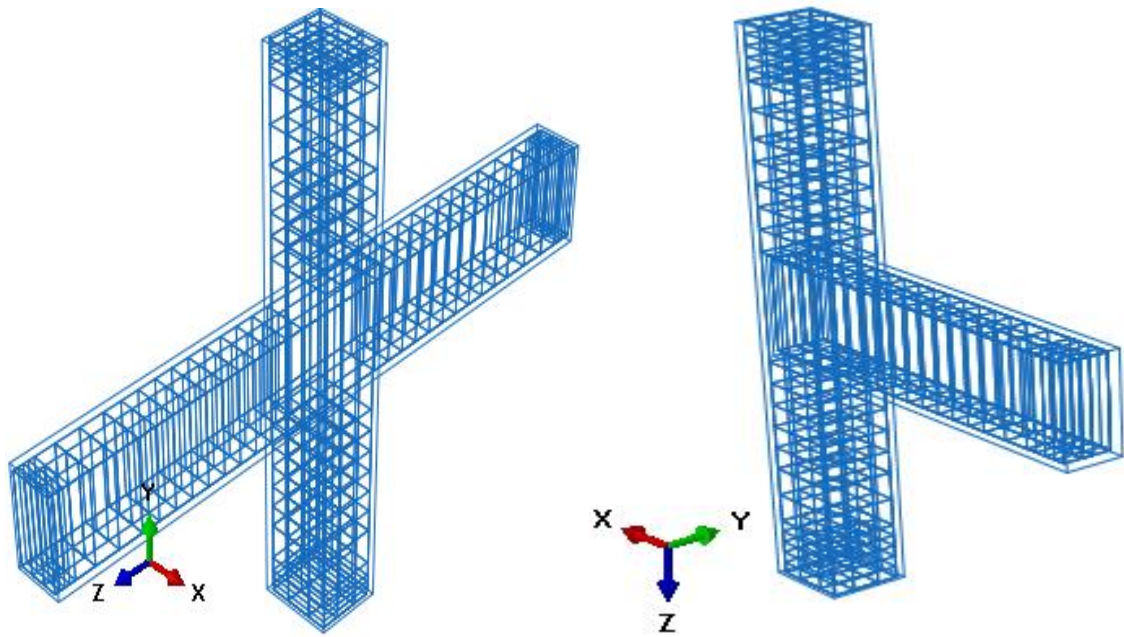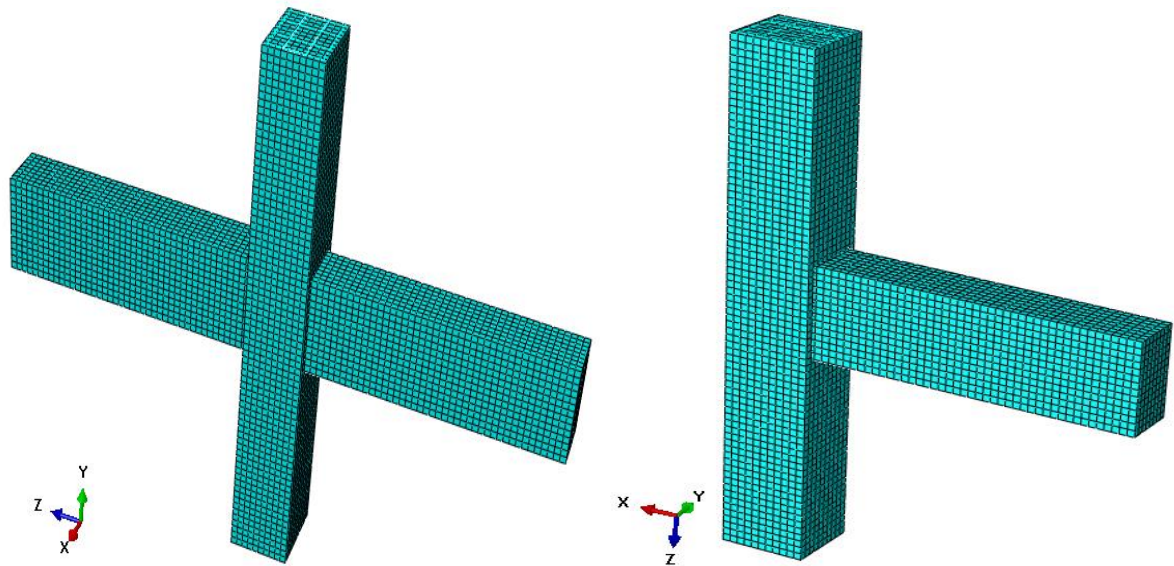

Fig.4.1.2 Reinforcement model details of interior and exterior connections

Fig.4.1.3 Mesh geometry of the model
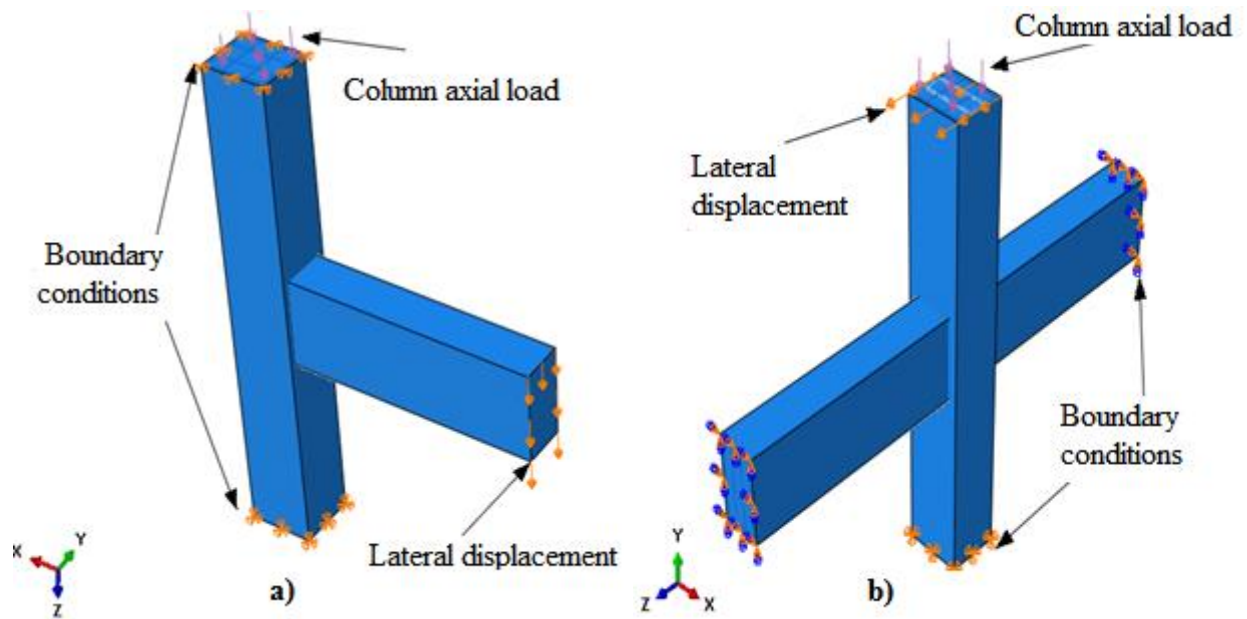
Fig.4.1.4 a. Simulated boundary condition and loading of the specimen of exterior connection

Fig.4.1.4 b. Simulated boundary condition and loading of the specimen of interior connection
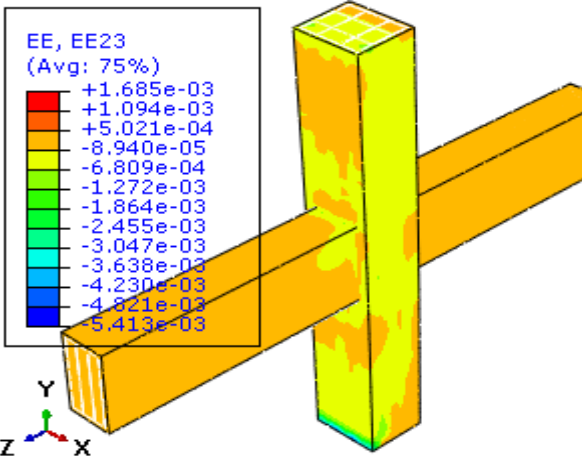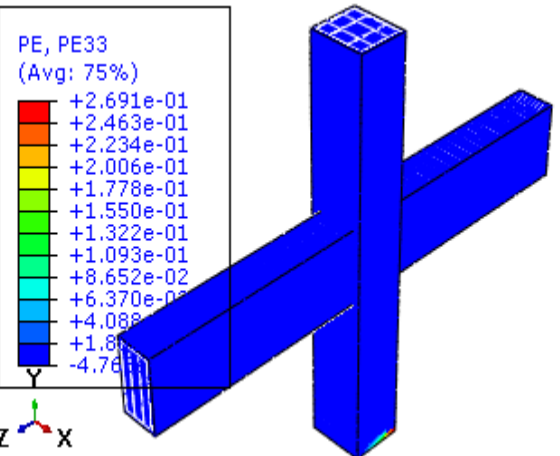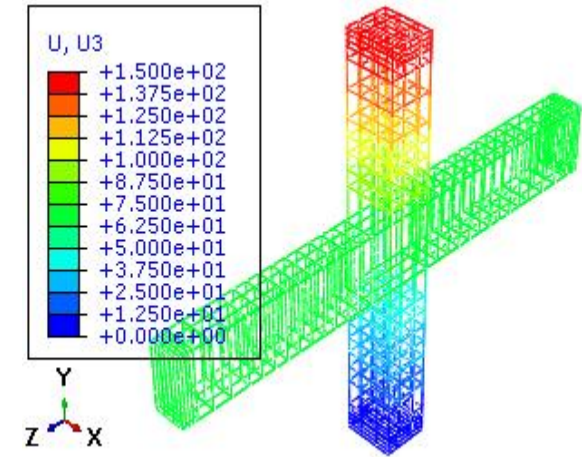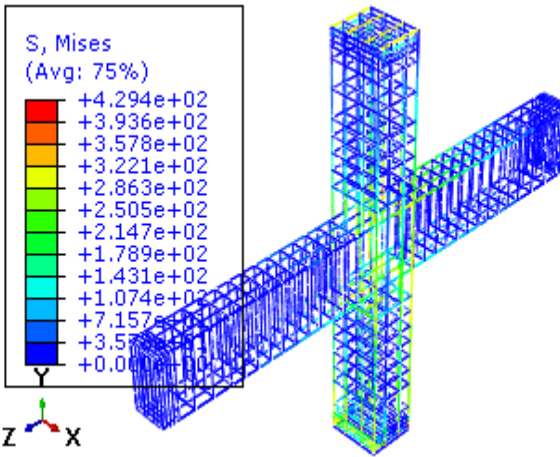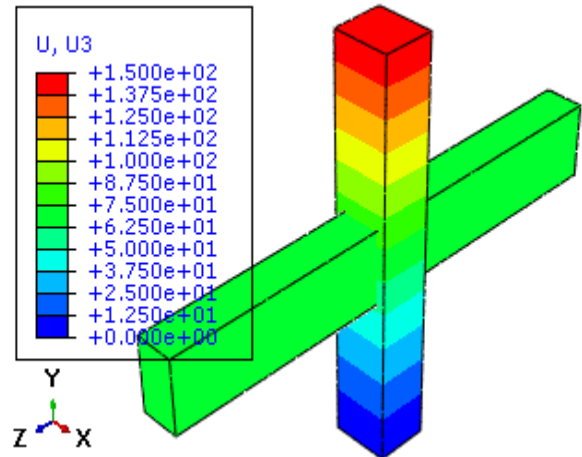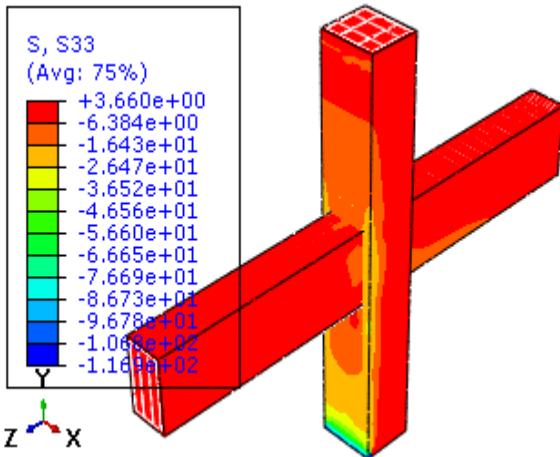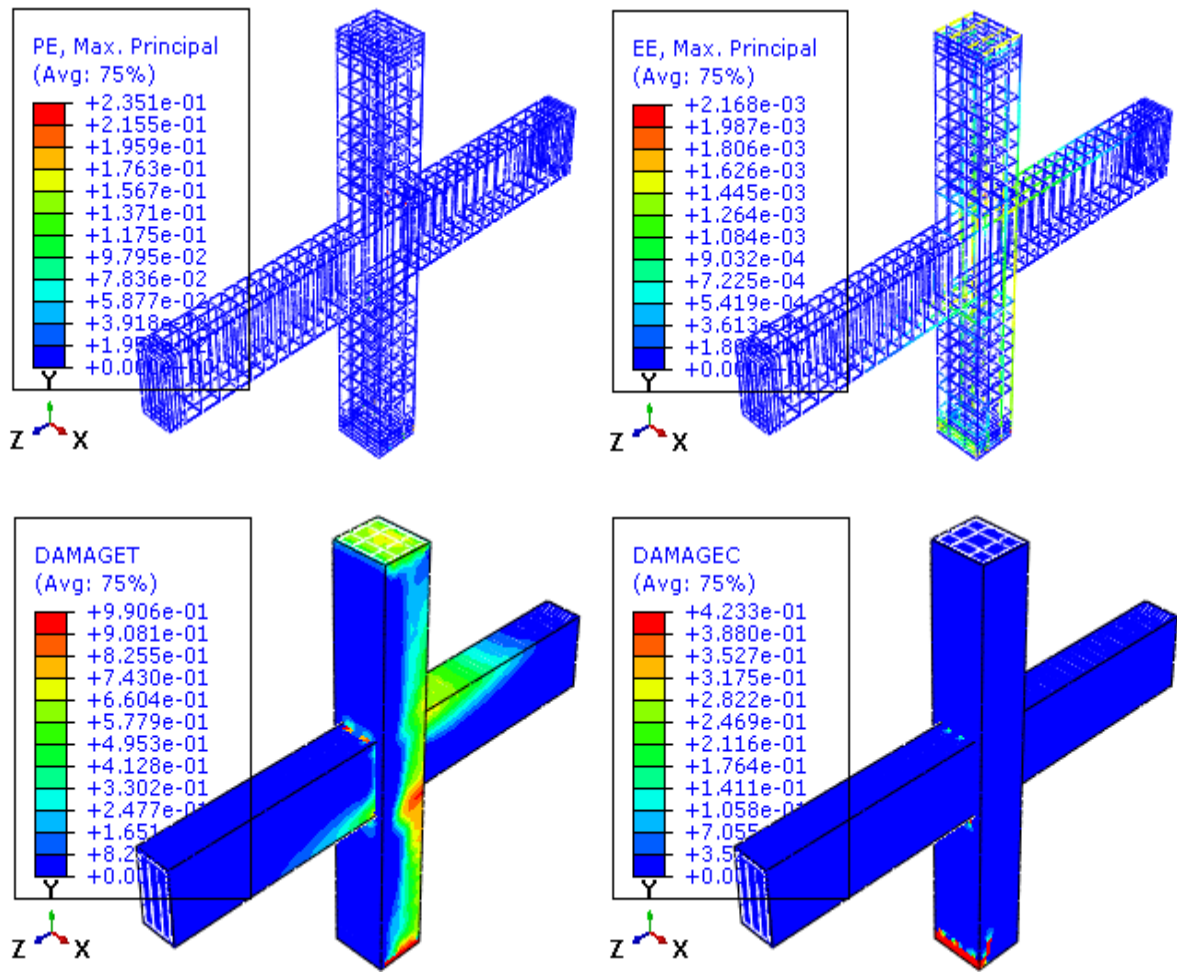
Fig. 4.1.5 FEA results of RC interior beam column connection for both steel and concrete
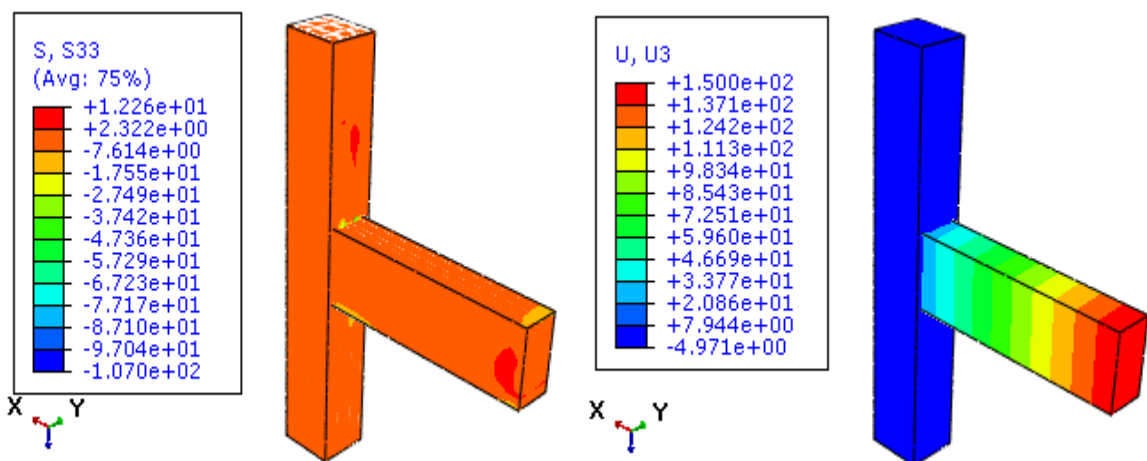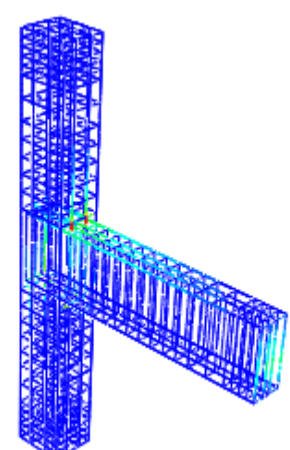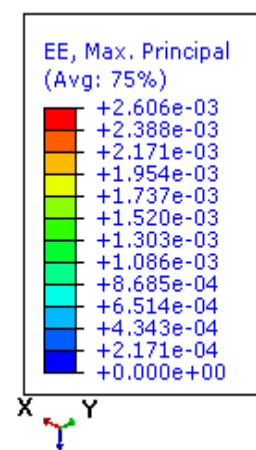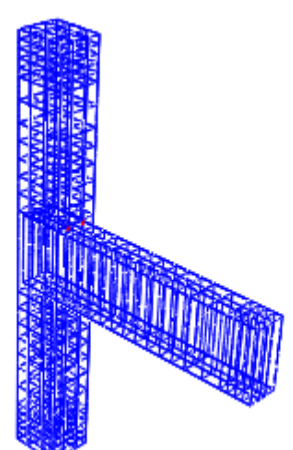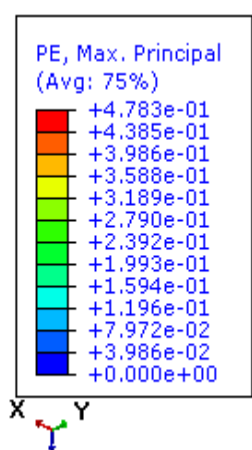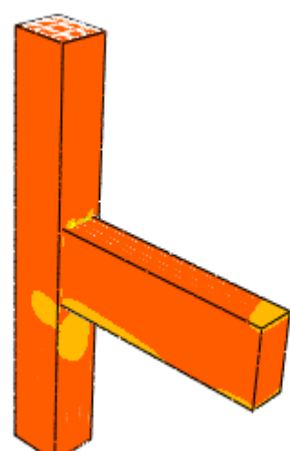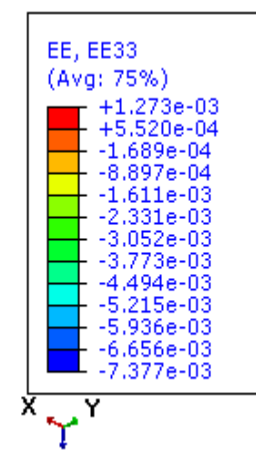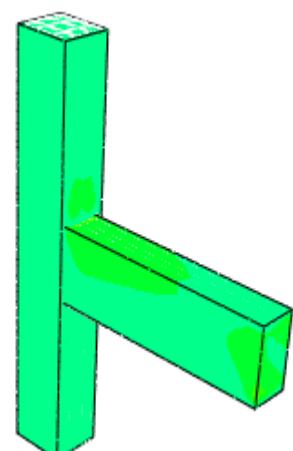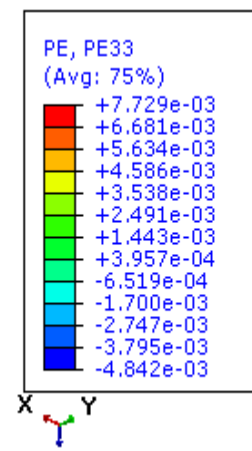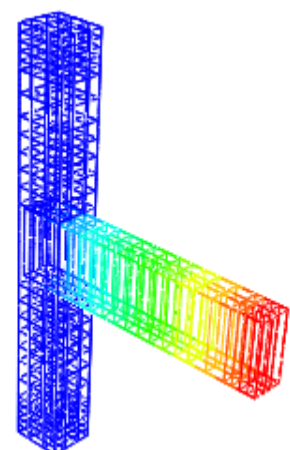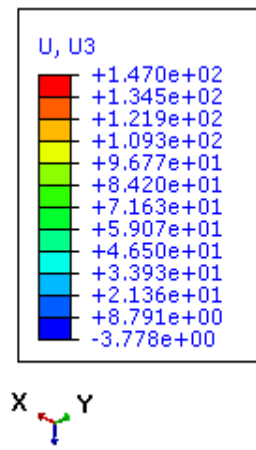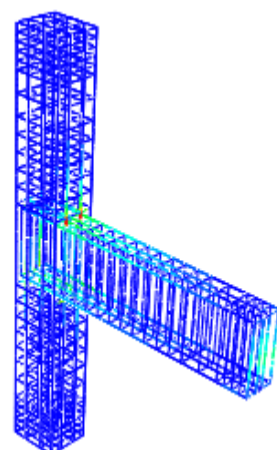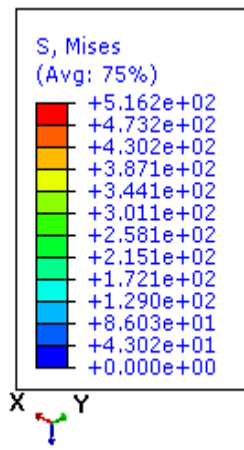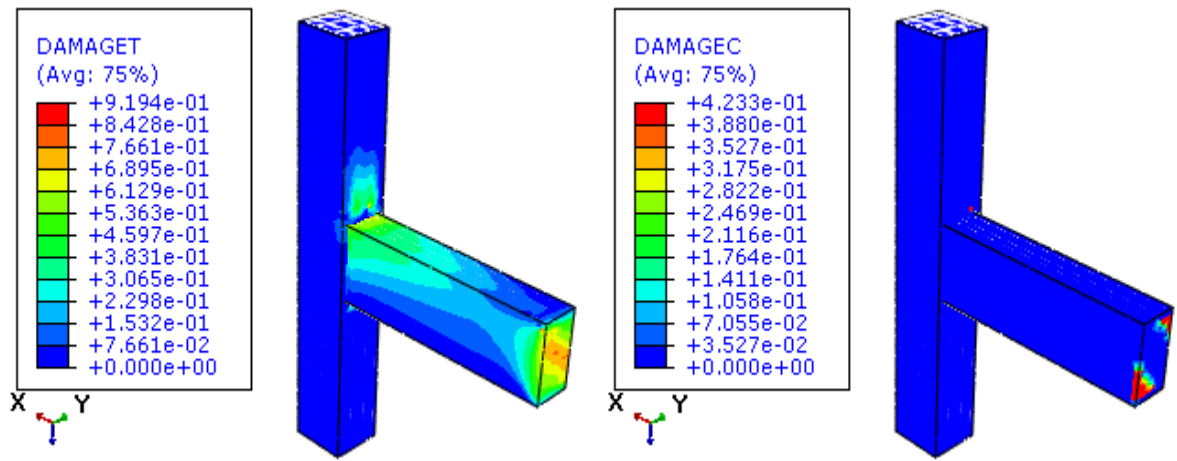
Fig. 4.1.6 FEA results of RC exterior beam column connection for both steel and concrete

4.2 Types and positions of the cracks

Crack initiation and propagation is an important parameter that should be carefully investigated while concrete structures are being studied. Different types of cracks were the main reasons of damages of RC beam column connections.
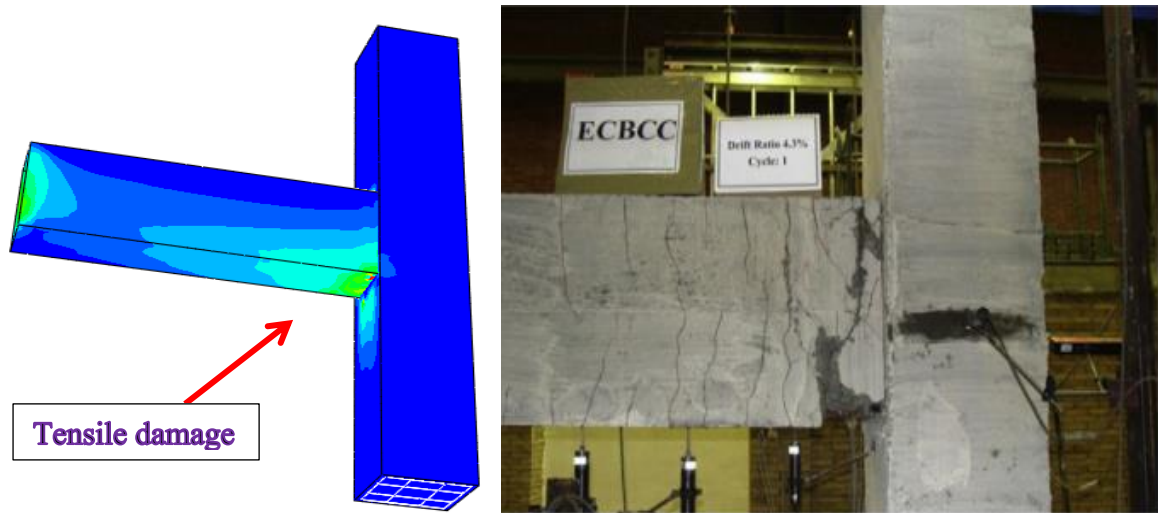
Fig.4.2.1 Tensile damage pattern at the maximum displacement for exterior connection
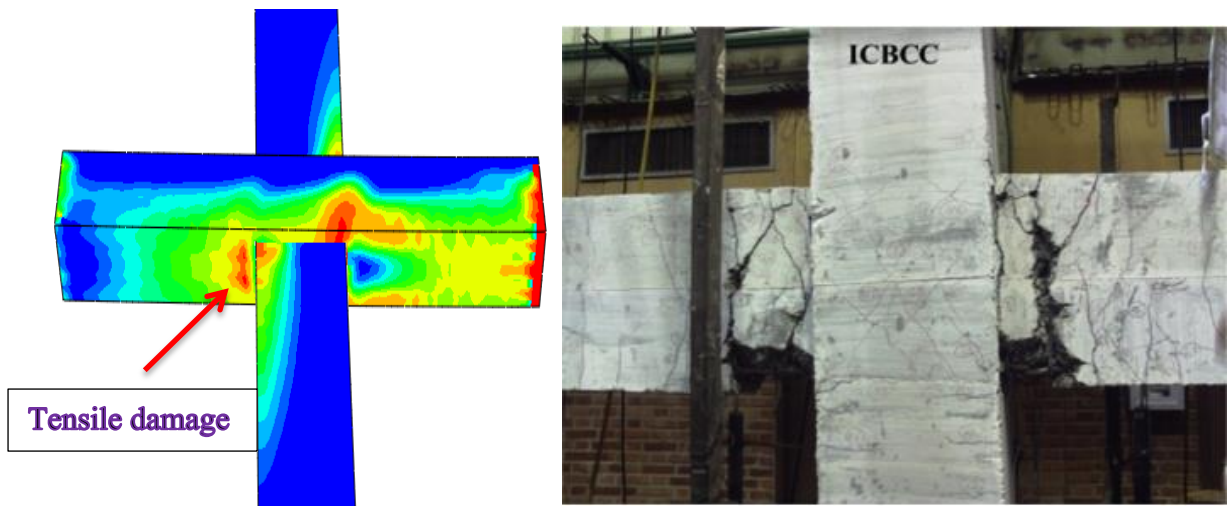
Fig.4.2.2 Tensile damage pattern at the maximum displacement for interior connection

It was also showed that tensile stress through the beam axis, compressive stress through column axis and shear stresses are responsible for the initiation of flexural cracks, narrow flexural cracks and inclined cracks, respectively. The following crack types were developed with corresponding stress components responsible for the initiation of the concrete cracks.

Crack type A: Crack initiated from the corner face of the column and/or beam

Crack type B: Crack distributed on the bottom and top surface through the length of column and/or beam

Crack type C: Crack developed at outer part of beam adjacent to column face

Crack type D: Narrow flexural cracks propagated at the face of the column
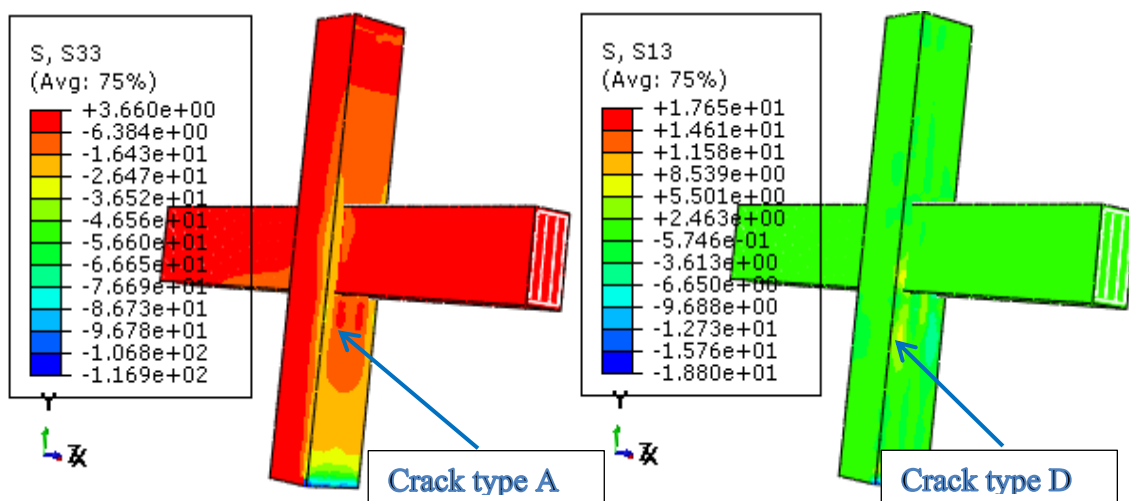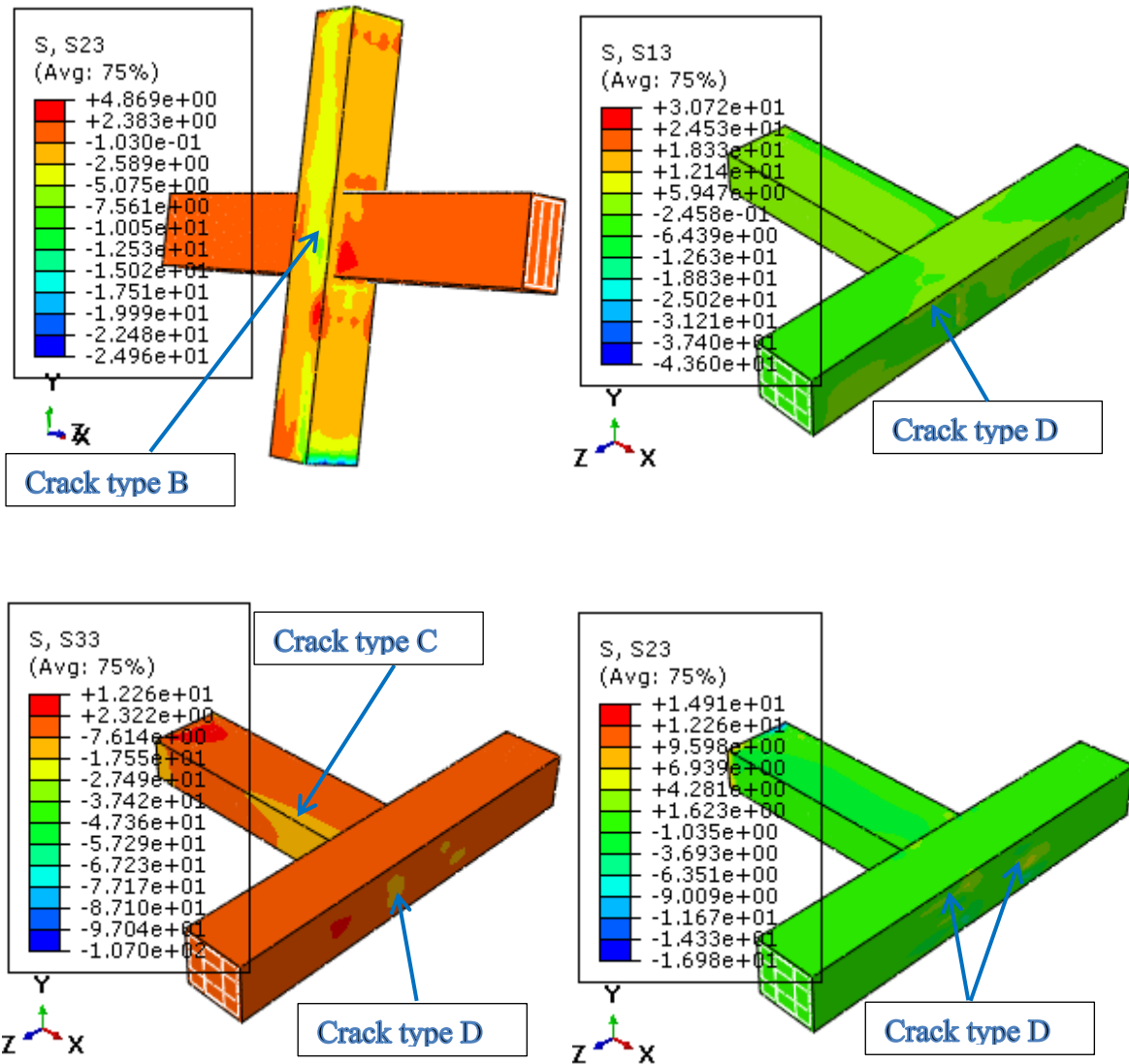
Fig.4.2.3 Types and positions of cracks for both interior and exterior connections

From Fig.4.2.3 Contour S33 represents principal stress through Z-axis for which negative values represent compressive stress and positive values represent tensile stress. For both exterior and interior beam column connections, tensile stresses were responsible for the initiation of crack type A while compressive stresses were responsible for crack type C. Contour S13 which represents shear stress along X-Z plane in which tensile shear stress was responsible for the development of crack type D and compressive shear stress was responsible for crack type B. Counter S23 represents shear stress along Y-Z plane in which compressive shear stress was responsible for crack type B for column while tensile shear stress was responsible for crack type B for beam in interior beam column connection. However, in exterior beam column connection, tensile shear stress was responsible for crack type D, and compressive shear stress was responsible for crack type B. According to the contours, compressive stress values of S33 are

very close to the compressive strength of concrete (34.32MPa) for both joints. However, tensile stress is larger than tensile strength of concrete (2.86Mpa) for exterior connection.

4.3 Discussion

4.3.1 Key points of the joint shear failure

The cyclic overall or local behaviors can be reasonably represented as envelope curves by linearly connecting points A, B and C, which display the most distinct stiffness changes as shown in Fig.4.3.1.1 and 4.3.1.2. The locations displaying distinct stiffness changes in Lateral load vs. Joint shear strain shows the overall and local behavior. Thus the formation of new damage around a joint panel also initiates distinct stiffness changes in overall behavior and joint shear stresses can be calculated using the lateral load values at points A, B, and C of overall behavior. Significant concrete cracking, reinforcement yielding, and/or concrete crushing represent the formation of new damage within the joint panel. The stiffness change (point A) is caused by the initiation of diagonal cracking within the joint panel. Additional stiffness change may be occurring at (point B) from the yielding of reinforcement before the initiation of concrete crushing (point C). In both types of connections and for all failure modes, after concrete crushing occurred within the joint panel (at point C), the joint shear resistance was usually reduced which limited the overall capacity and initiates lateral load decrease.
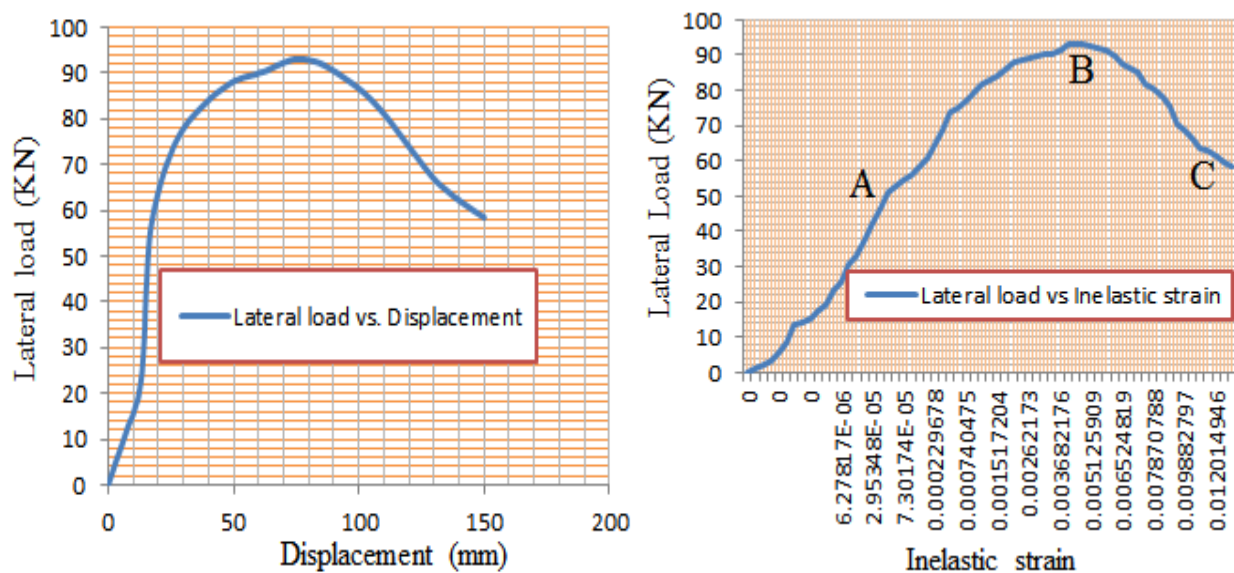
Fig.4.3.1.1 Lateral-displacement and Lateral load-strain relation for exterior connection
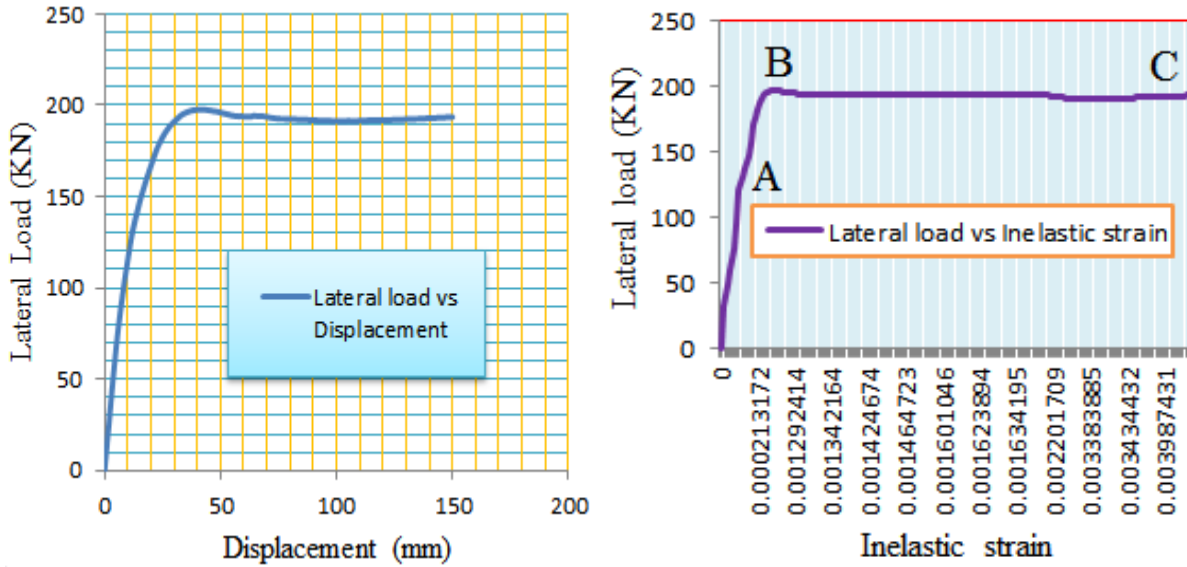
Fig.4.3.1.2 Lateral-displacement and Lateral load-strain relation for interior connection

For interior and exterior beam column connections, the columns are typically subjected to constant axial force during testing; column axial stress and strain can therefore be considered as constant values up to the cracking point.

Deformation of the joint panel in RC beam column connections determines the story deflection of overall frames. When overall response is governed by the joint shear, the contribution of the joint panel to the overall story deflection increases which indicates the joint shear deformation has a significant impact on over all story deflection and that overall ductile responses cannot necessarily guaranteed.

4.3.2 Initiation of diagonal cracking within the Joint panel (point A)

Joint shear stress (v_j) and shear strain (γ) can be obtained by applying three coordinate transformations if shear stress or shear strain is known.

$$v_j(\text{cracking}) = \sqrt{\sigma_x\sigma_y - \sigma_x\sigma_t - \sigma_y\sigma_t + \sigma_t{}^2}$$

$$v_j(\text{cracking}) = \sqrt{\varepsilon_x\varepsilon_y - \varepsilon_x\varepsilon_t - \varepsilon_y\varepsilon_t + \varepsilon_t{}^2}$$

Where σ_x − beam average axial stress ε_x −beam average axial strain

σ_y −column average axial stress ε_y −column average axial strain

σ_t −joint principal tensile stress ε_t −joint principal tensile stress

55

In the above equation tensile stress and strain are positive values whereas compressive stress and strain are negative values. The angle of inclination of the principal strains with respect to the x-axis is the same as the angle of inclination of the principal stresses to the x-axis. These principal stresses were assumed for the stress and strain of the concrete tensile strength because point A corresponds to initiation of diagonal cracking within the joint panel. For both interior and exterior connections, the columns are typically subjected to constant axial load. Therefore, column axial stress and strain can be considered as constant values up to the cracking point.
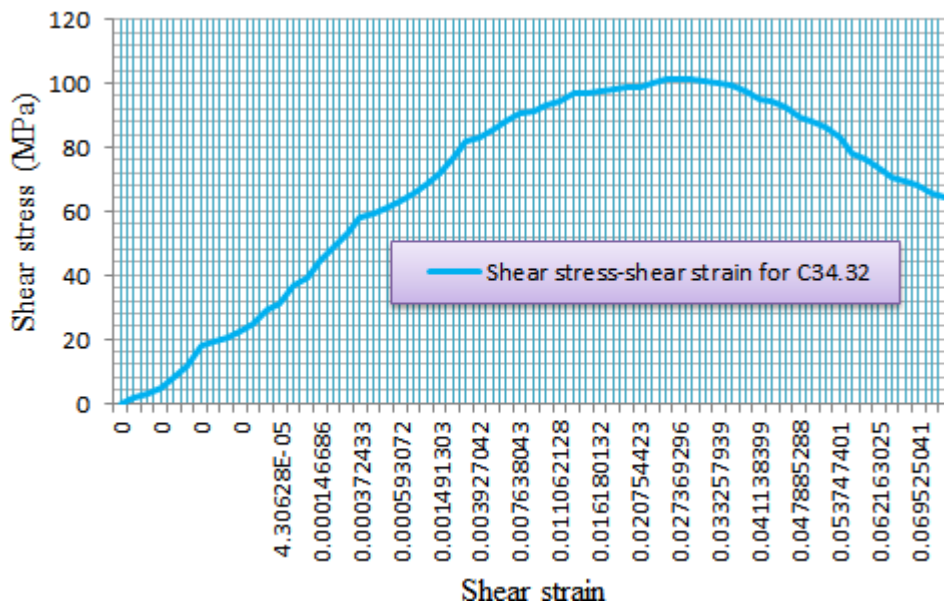
Fig.4.3.2.1 Shear stress-shear strain relation for exterior connection
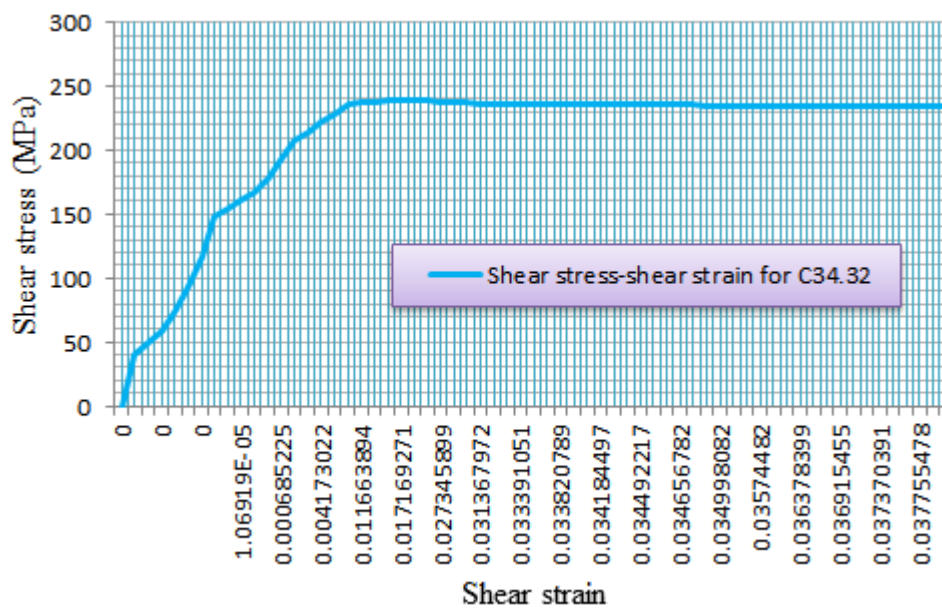
Fig.4.3.2.2 Shear stress-shear strain relation for interior connection

56

According to the CDP model, the concrete cracking is initiated when the maximum principal plastic strain is positive with the direction of the vector normal to the crack plane, parallel to the direction of maximum principal plastic strain. To find the beam and column axial stress at cracking, the joint shear stress was calculated for a given column shear by using force and moment equilibrium along with a free-body diagram at the mid-height of the joint panel. Then this joint shear stress can be compared to the joint shear stress calculated from cracking equations. Then, this joint shear stress was compared to the joint shear stress calculated from these equations; the column shear was continuously increased until the joint shear stress from equilibrium was equal to the joint shear stress from cracking equations. Finally, then, beam and column axial stress and strain could be determined

$$V_{jh} = A_s f_s - V_c = \text{Horizontal shear force}$$

$$V_j = C_c + C_s + T - V_{col}$$

(a) Loading condition

(b) Free-body diagram at the mid-height of interior connections
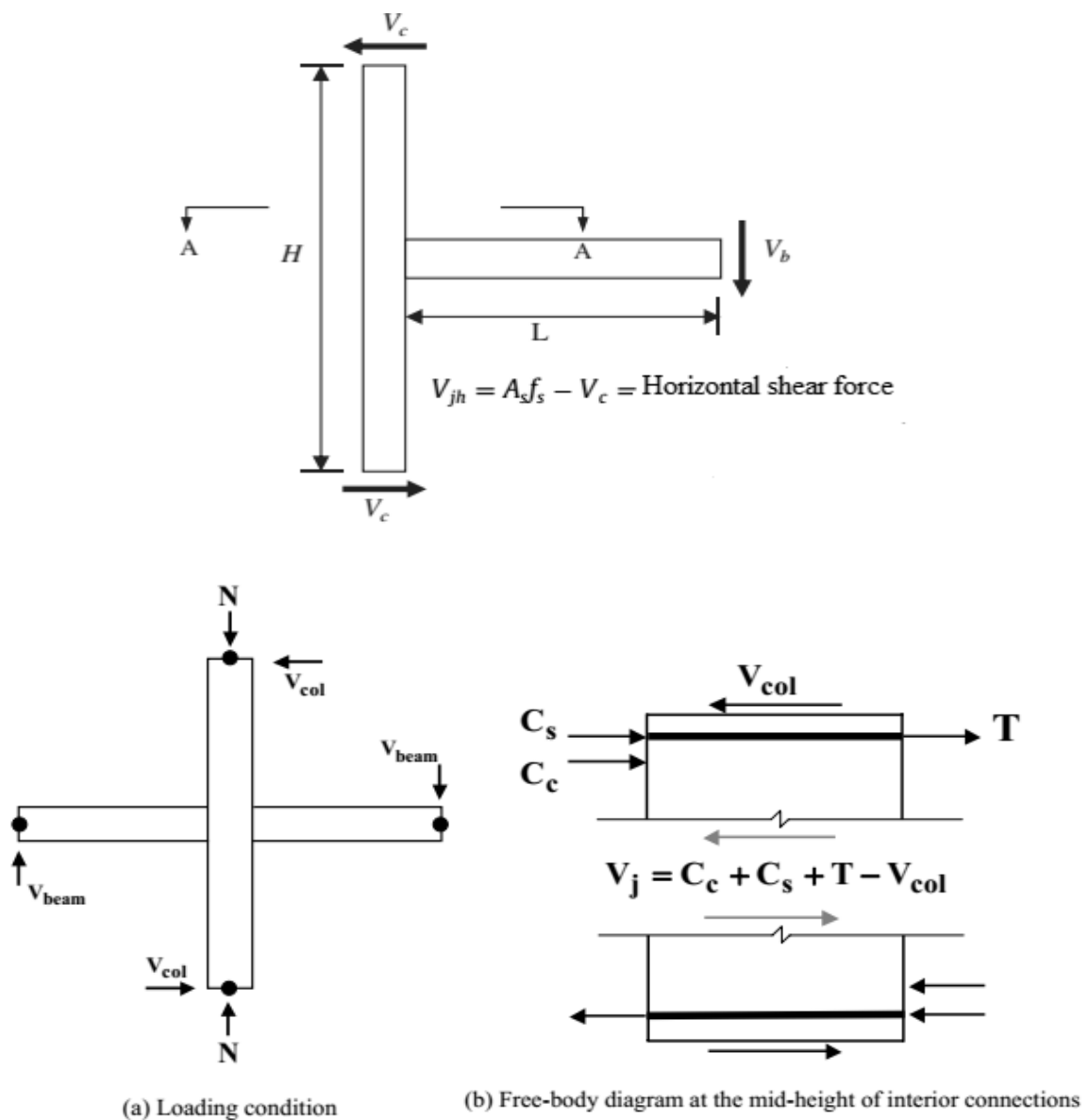
Fig.4.3.2.3 Loading condition and free-body diagram for interior and exterior connections

4.3.3 Assessment of influence parameters (at points B and C)

4.3.3.1 Influence of concrete compressive strength

An increase in concrete compressive strength initiated an improvement of the joint shear resistance that comes from force transfer to the joint panel by bearing (from beam and column compression zones), and also that coming from bond between reinforcement and surrounding concrete. Compressive strength is the most influential parameter for joint shear stress at point B and C. Joint shear stress had similar relations to the square root of compressive strength at identified key points for both interior and exterior connections. The correlation coefficient at point B is 0.876 and 0.969 at point C for exterior, and 0.824 at Point B and 0.832 at point C, for interior.
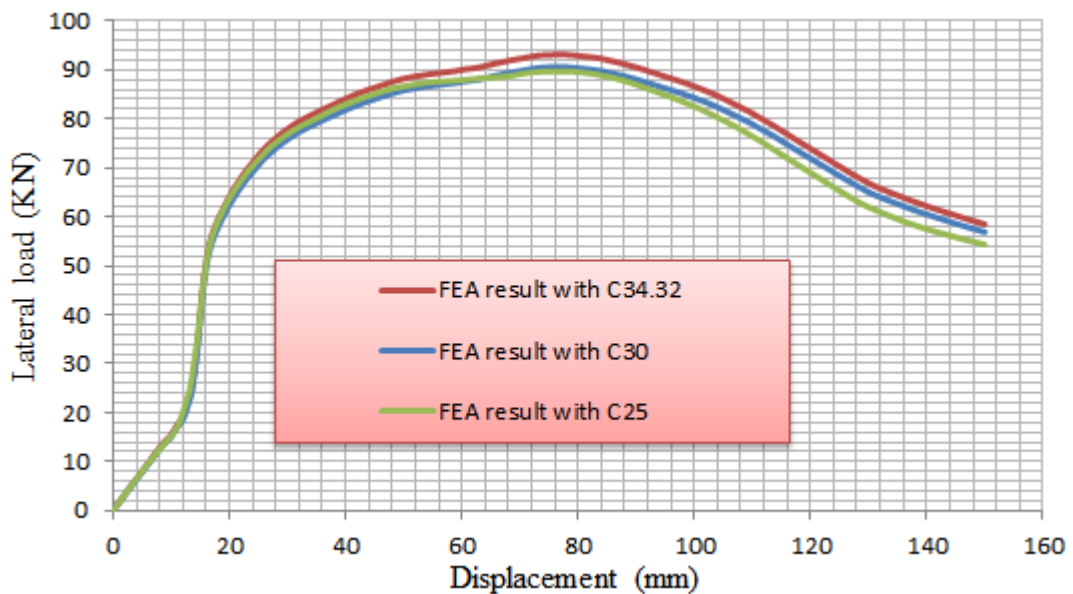
Fig. 4.3.3.1 Influence of concrete compressive strength for exterior connection
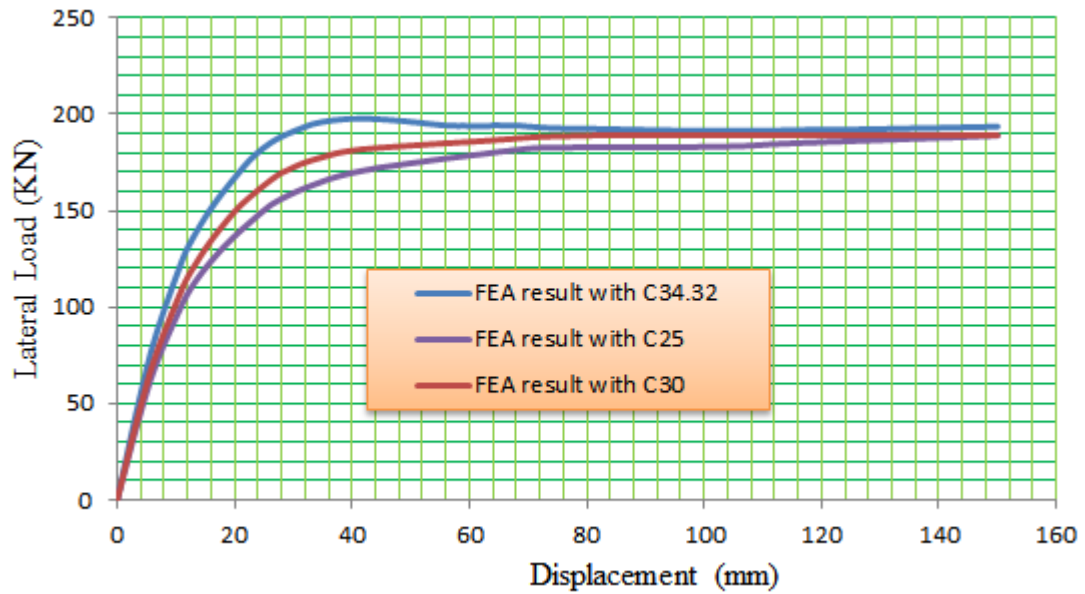
Fig. 4.3.3.2 Influence of concrete compressive strength for exterior connection

4.3.3.2 Influence of joint aspect ratio (h_b/h_c)

The ratio of beam height to column depth (h_b/h_c) is used to examine whether the shape of the joint panel in-plane direction dimensions might affect the joint shear behavior. The column width and depth, and beam width fixed constant while beam depth changes. The data base ranges from 0.875 to 1.375 for both interior and exterior joints. At point B, the joint shear stresses strains were little influenced by joint panel geometries for interior joint. However, at point C, increase or decrease in joint aspect ratio will not affect the shear strength because it depends on the smooth path of shear transfer between column and beam. For $hb/hc = 1.0$, shear resistance cpacity reduced slowly at phase of initiation of concrete crushing because there was smooth shear transfer between beam and column. Thus, ultimate shear resistance capacity of the joint was attained at early stage of concrete crushing. For exterior joint, at point B, inrease in joint aspect ratio results in increase in shear resistance capacity before yielding of reinforcement. Shear resistance capacity reduces slowly before concrete starts to crush. At point C, shear strength slowly increases. Thus, ultimate shear resistance capacity of the joint was attained at yielding of reinforcement

59
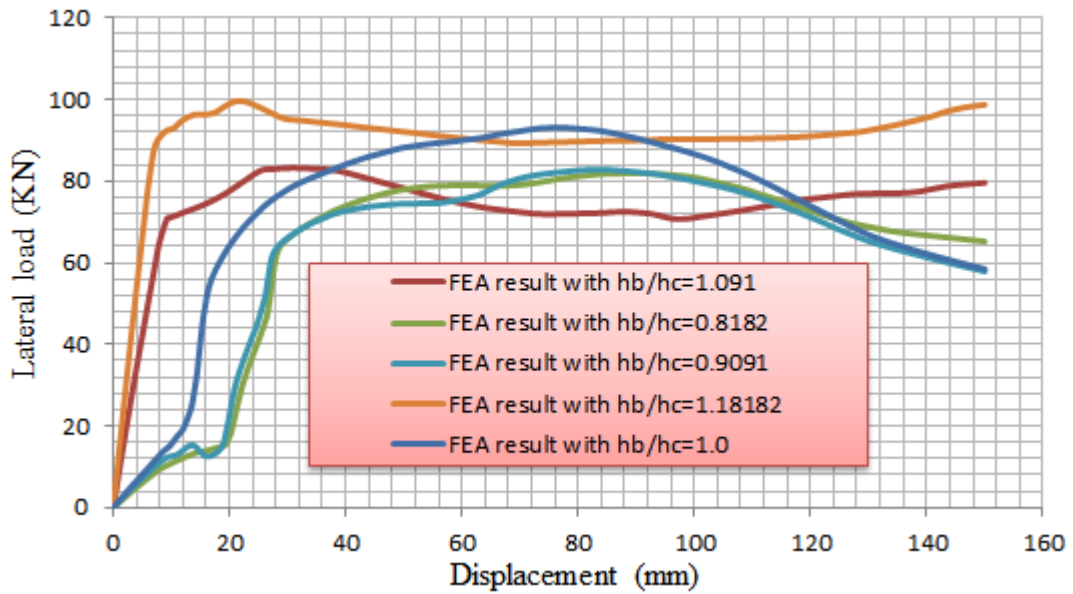
Fig.4.3.3.3 Influence of joint aspect ratio (h_b/h_c) for exterior connection
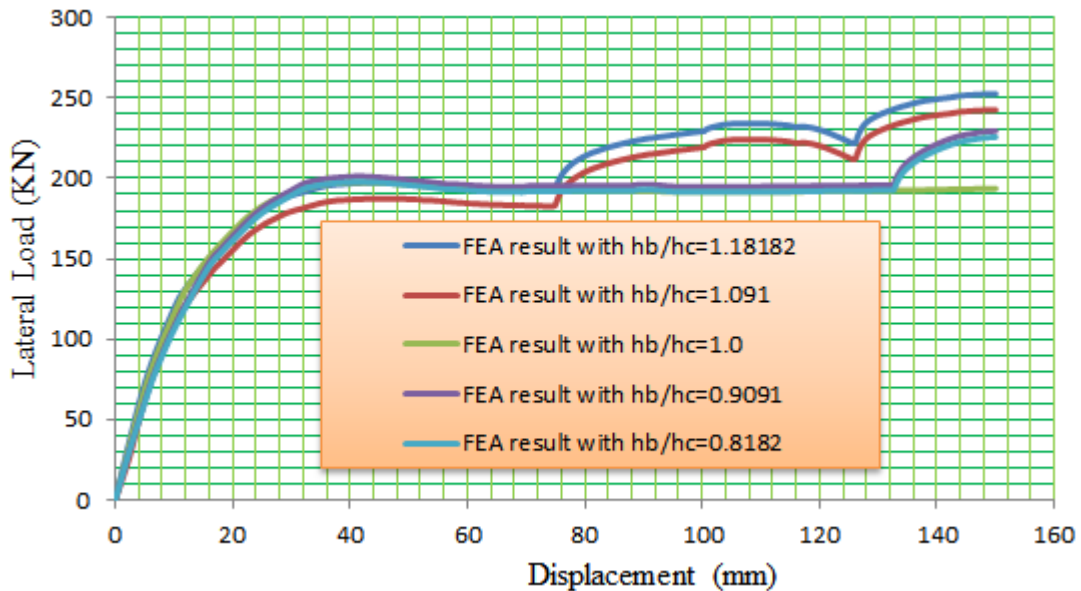
Fig.4.3.3.4 Influence of joint aspect ratio (h_b/h_c) for interior connection

4.3.3.3 Influence of Column axial load

The effect of column axial load on the seismic response of exterior and interior conventional beam column joints is that shear strength and stiffness of unreinforced interior and interior joints is not significantly affected by compressive column axial load. The shear strength and overall joint shear failure of interior and exterior beam column connections is not significantly affected for increase the compressive column axial load up to $7.6\%(f'_cAg)$. Many previous experimental data bases for beam column joints without joint transverse reinforcement showed that shear strength of joints would not be affected for axial load less than $20\%(f'_cAg)$,and after which

increase in column axial load reduces the stiifness and strength. Therefore, column axial load is not a key influencing parameter of shear strength of RC beam column connections subjected lateral cyclic loading.
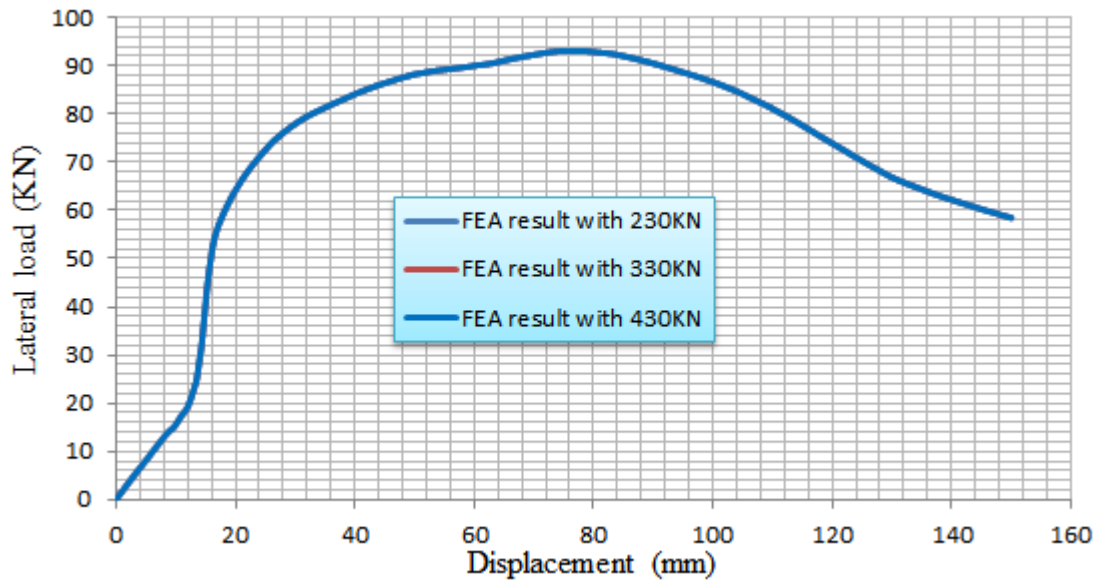
Fig.4.3.3.5 Influence of column axial load for exterior connection
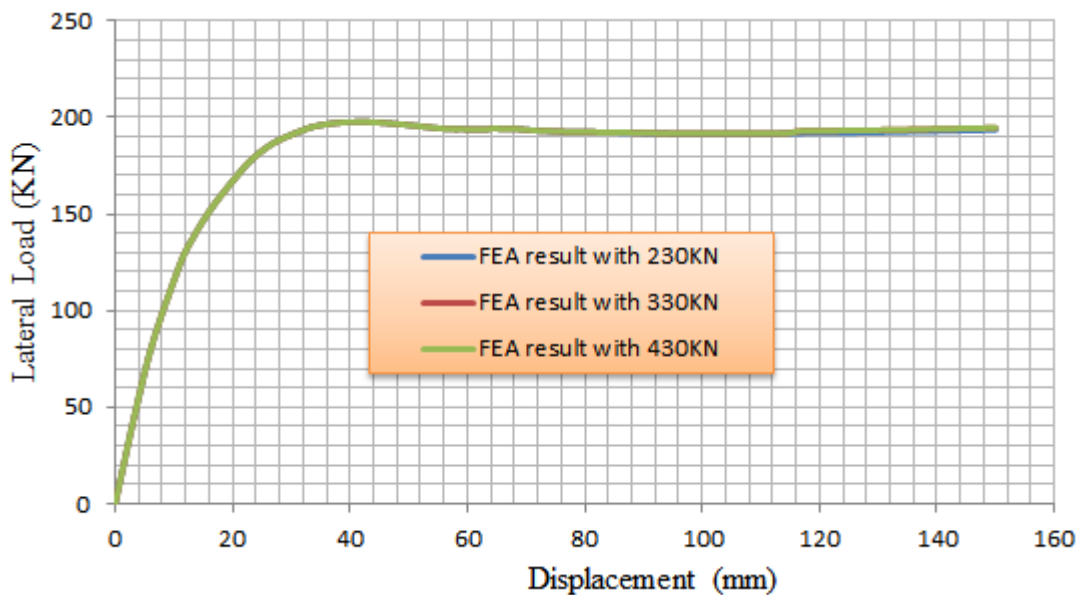
Fig.4.3.3.6 Influence of Column axial load for interior connection

4.3.3.4 Influence of beam longitudinal reinforcement ratio

Joint shear strength is affected by the amount of longitudinal reinforcement provided in flexural beam for joints without joint transverse reinforcement. The increase of beam longitudinal reinforcement ratio leads to the increase of the horizontal joint shear force without yielding of beam longitudinal bars i.e. larger horizontal shear force is imposed with less deterioration of

bond resistance around the beam longitudinal bars in the joint region which produces a wider diagonal strut which can carry the larger horizontal joint shear force. Increasing the beam longitudinal reinforcement ratio changes the failure type from a ductile failure (beam flexural failure) to a brittle one (joint shear failure). It is shown that the beam longitudinal reinforcement ratio affects the shear strength for BJ (the failure occurs around joint face extending to longitudinal beam) failure only. Thus, beam longitudinal beam reinforcement ratio may not be an influencing parameter in predicting the shear strength of beam column joints.
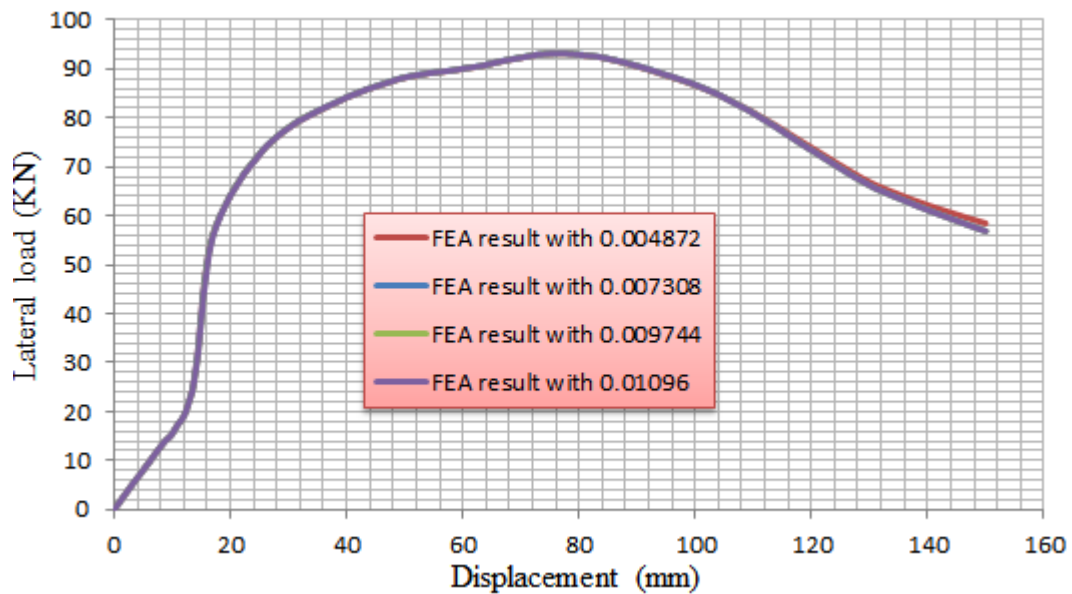
Fig.4.3.3.7 Influence of beam longitudinal reinforcement ratio for exterior connection
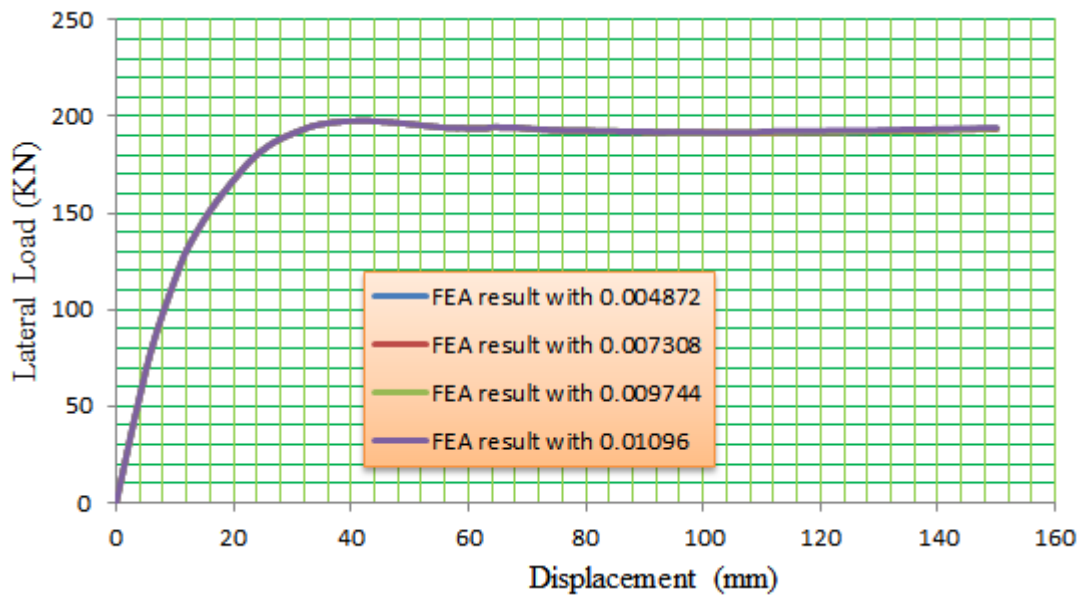
Fig.4.3.3.8 Influence of beam longitudinal reinforcement ratio for interior connection

4.4 Verification of Finite element model

To verify the Finite element model, the force-displacement curve obtained from finite element simulation is compared with the trace of the envelop behavior of the structure under cyclic loading reported by (Fadwa et al. (2014)).
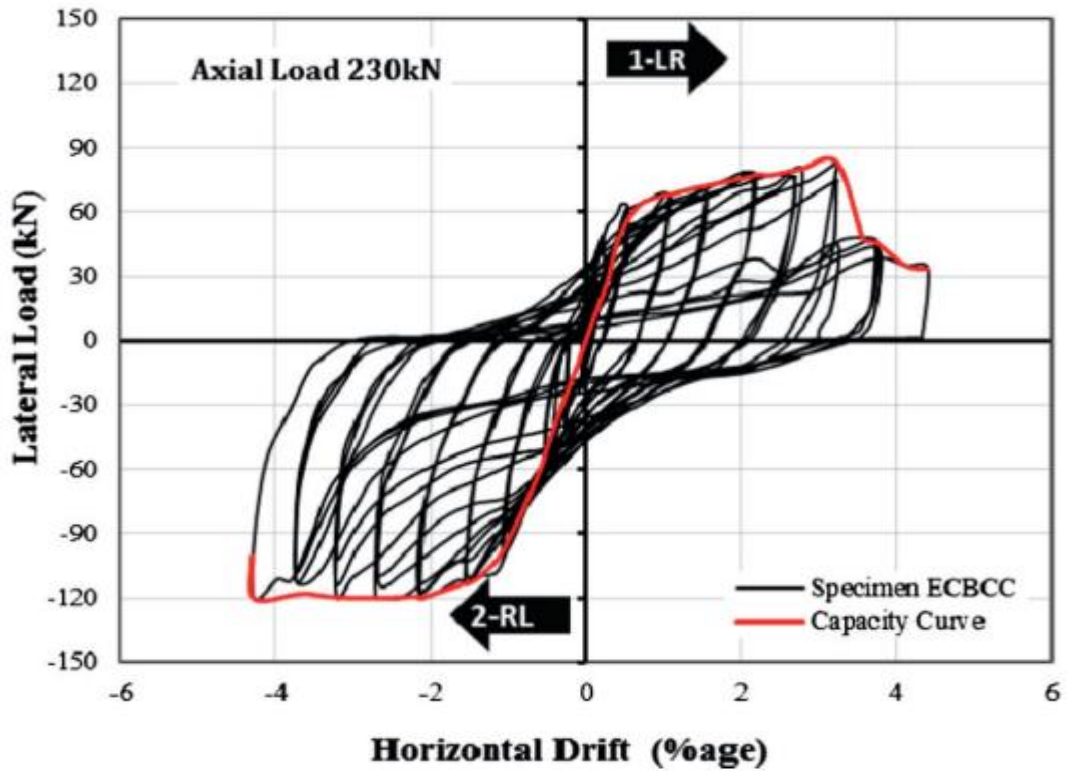
Fig.4.4.1 Experimental Load- displacement curve of exterior connection due to cyclic loading
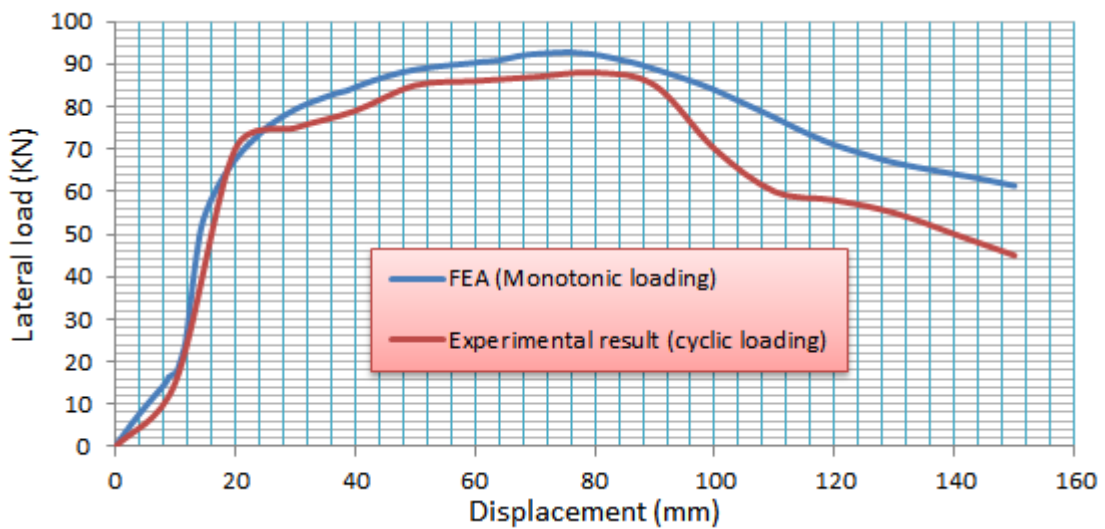
Fig.4.4.2 Exterior connection comparison of numerical and experimental results
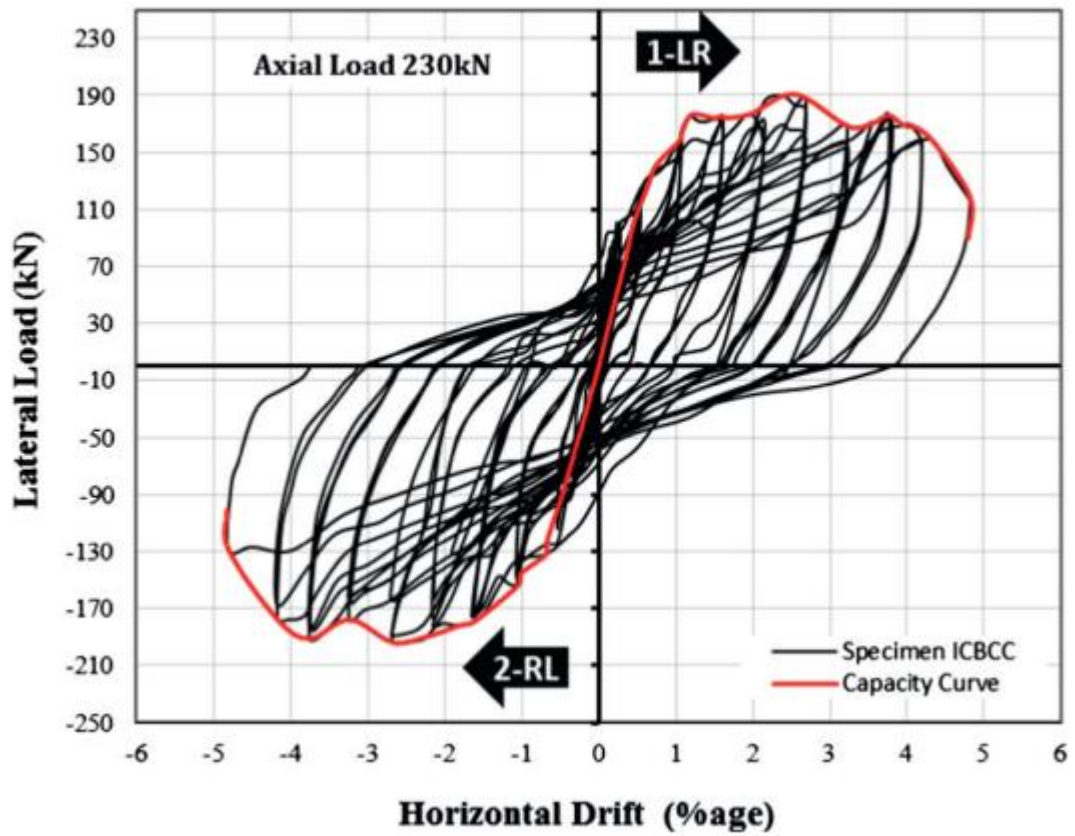
Fig.4.4.3 Experimental Load- displacement curve of Interior connection due to cyclic loading
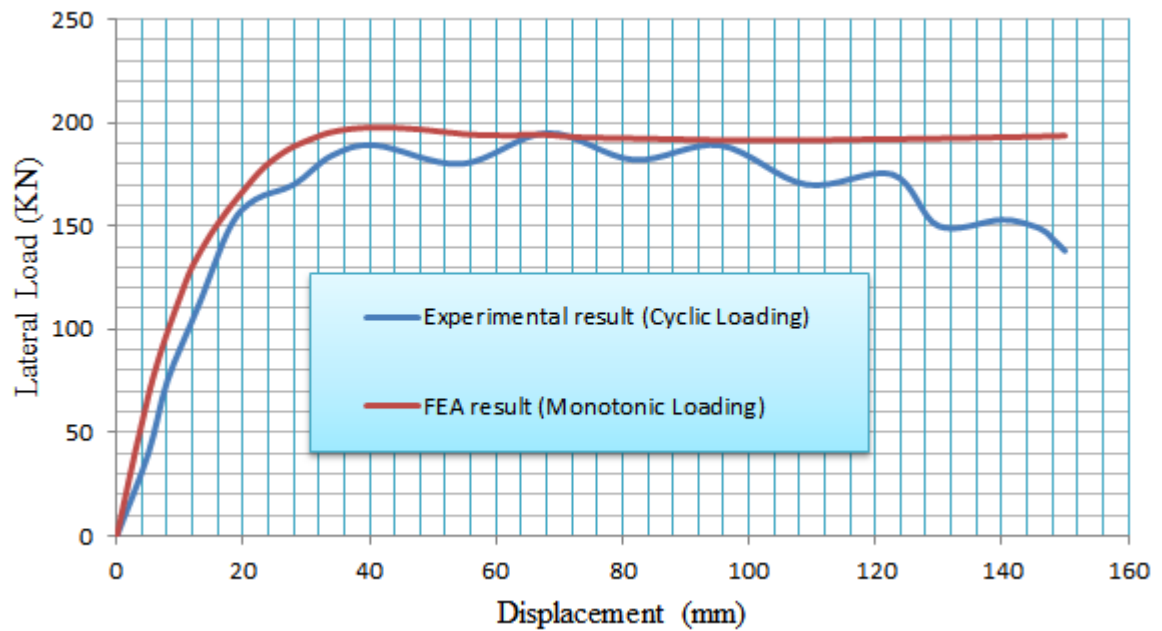
Fig.4.4.4 Interior connection comparison of numerical and experimental results

64
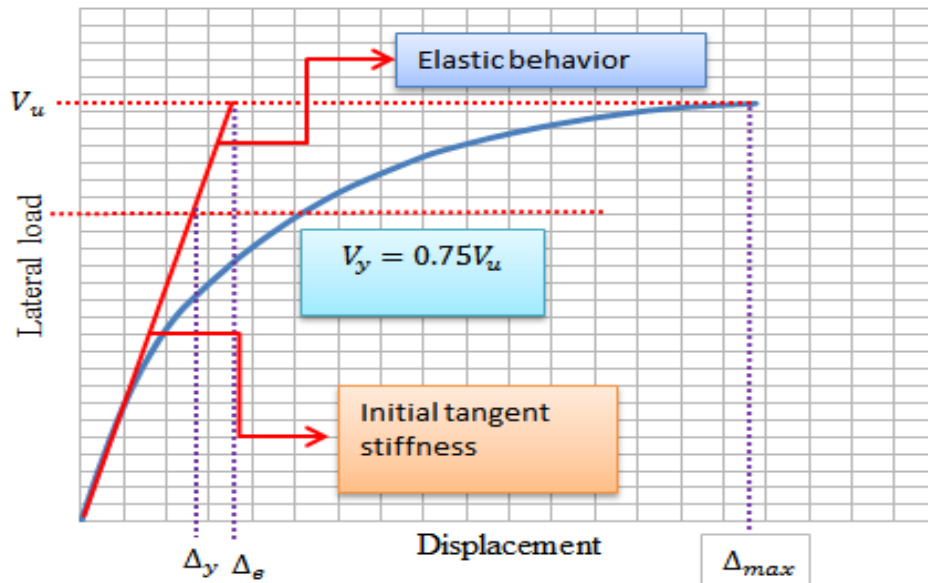
Fig.4.4.5 Estimation of yield displacement

The peak lateral load and displacement from the experiment and FEA is shown in table below.

Connection	Experimental results		FEA results		Difference (%)
	Peak lateral load (KN)	Peak lateral displacement (mm)	Peak lateral load (KN)	Peak lateral displacement (mm)	
Interior	189.71	95.45	197.66	45.2	4
Exterior	83.22	74.5	91.602	78.1	9.15

Table 4.1 Peak lateral load and displacement of FEA and Experiments

The force-displacement graph obtained from the Finite element simulation and experimental result reported by (Fadwa et al. (2014)) shows good agreement which verifies accuracy of finite element model. It can be understood from the two graphs that finite model prediction in elastic domain is a little lower than experimental test. It is shown that the difference in peak load in FEA and experimental test in interior beam column connection is 4%, whereas for exterior beam column connection is 9.15%. As illustrated in figure, the lateral force displacement curve predicted by the FEA follows most of the experimental curve closely.

4.5 Effect of mesh size on finite element analysis results

When the material exhibits softening, finite element size influences significantly the entire model behavior due to localization since the dissipated energy decreases upon mesh refinement.
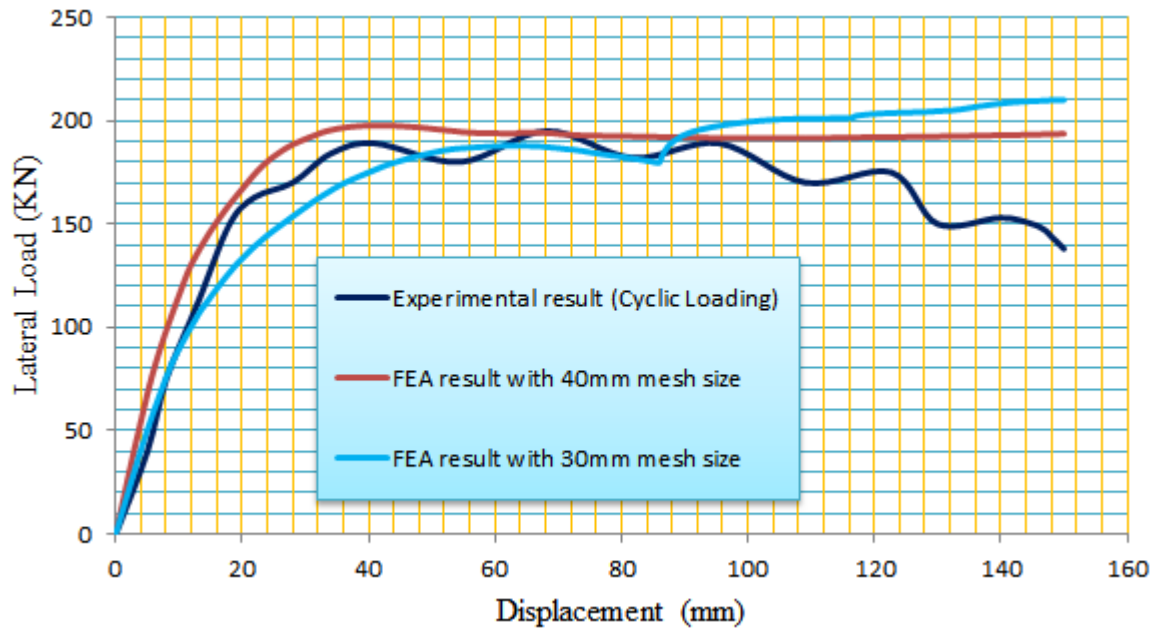
Fig.4.5.1 Load-displacement response of Interior connection for 30mm and 40mm mesh sizes
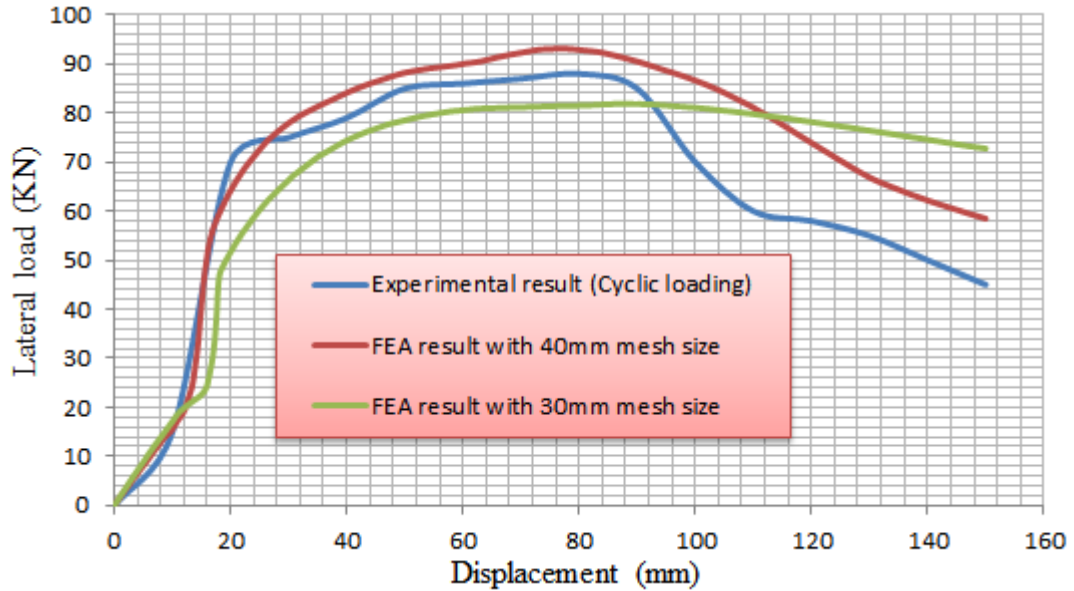
Fig.4.5.2 Load-displacement response of Exterior connection for 30mm and 40mm mesh sizes

CHAPTER 5

CONCLUSIONS AND RECOMMENDATIONS

5.1 Conclusion

The most influential parameters on joint shear behavior at identified distinct stiffness change due to initiation of diagonal cracking (point A), second distinct stiffness change due to yielding of reinforcement (point B) and maximum response and initiation of concrete crushing (Point C) have been analyzed using conventional interior and exterior RC beam column connections exhibiting joint shear failure. The data base for both RC beam column connections did not include the joint transverse reinforcement and out-of plane members such as transverse beams and slabs. Based on the assessement of influence parameters on joint shear failure, the most important results can be summerized as follows.

- For initiation of diagonal cracking (at point A) for both interior and exterior connections, the joint shear stress and strain can directly calculated by using stress/strain coordinate transformation based on principal stress and strain. The principal tensile stresses and tensile strains were assumed to be the stress and strain corresponding to concrete tensile strength.

- At yielding of reinforcement (at point B) and initiation of concrete crushing (point C), the concrete compressive strength was the most influential parameter of the overall joint shear stress and strain behavior. Joint shear resistance capacity of interior beam column connection at point B is more than that of exterior beam column connection under the same conditions of the concrete compressive strength and joint shear failure mode.

- The shear strength and overall joint shear failure of interior and exterior beam column connections is not significantly affected for increase the compressive column axial load up to $7.6\%(f'_c A_g)$. Many previous experimental data bases for beam column joints without joint transverse reinforcement had showed that shear strength of joints would not be affected for axial load less than $20\%(f'_c A_g)$,and after which increase in column axial load reduces the stiffness and strength.

- For the same amount of longitudinal reinforcement, constant beam width and column width, the increase in joint aspect ratio impoved the shear strength wich results in reduction of early iniatiation of diagonal cracking (at point A) for exterior beam column joint. After yielding of reinforcement is reached, the shear strength slowly reduces before concrete crushing and the shear resistance capacity is more improved than the joint with

lower joint aspect ratio. However, in interior beam column joint the increase in joint aspect ratio results in decrease in shear strength before yielding of reinforcement. For $hb/hc = 1.0$, shear strength reduced slowly at initiation phase of concrete crushing. At point C, increase or decrease in joint aspect ratio will not affect the shear strength because it depends on the smooth path of shear transfer between column and beam.

- The increase of beam longitudinal tension reinforcement ratio didn't show a significant change in shear strength for addition of small amount of tensile reinforcement. However, the cracking pattern slightly changed from the edge of the beam to the column edge. It has also improved shear resistance capacity at the crushing stage of concrete. Thus, beam longitudinal beam reinforcement ratio may not be an influencing parameter in predicting the shear strength of beam column joints. It is shown that the beam longitudinal reinforcement ratio affects the shear strength for BJ (the failure occurs around joint face extending to longitudinal beam) failure only.

In this study, finite element analysis results confirmed the capability of the developed finite element model to predict the RC beam column connections subjected to joint shear behavior.

5.2 Recommendations

1. Various conventional and wide RC beam column connections subjected lateral loading can be analyzed as geometric categories are a fuction of out-of- plane geometry such as presence of transverse beam(s) and/or slab(s).

2. The model can be used as powerful and applicable tool for further investigations of key influence parameters such as presence/absence joint tansverse reinforcement in joint panel zone, joint eccentricity, effect of column size,and longitudinal reinforcement anchorage ratio can be carried out and identified.

3. Corner (Knee) RC beam column connection can be investigated for the key influence parameters as joint shear failure is the governing shear failure mode.

4. The assesment of key influence parameters with respect to shear strength, deformation capacity and crack pattern can be done when joint shear failure is accompanied by beam flexural failure for ductile joints.

REFERENCES

1**.** ABAQUS Analysis user's manual 6.14-EF (2014). *Dassault Systems Simulia Corp. Providence*, RI, USA.

2. American Concrete Institute (ACI). "Building code requirement for structural concrete and commentary".Farmington Hills, Michigan. *ACI 318-95*. 1995.

3. ACI 352R-02. (2002). Recommendations for Design of Beam-Column Connections in Monolithic Reinforced Concrete Structures, Reported by Joint *ACI-ASCE Committee 352*.

4. Behnam, H.,Kuang,J.S, Bijan, S. (2018). Parametric finite element analysis of RC wide beam column connections, *Computers and structures 205*:28-44.

5. Etemadi E, Fallahnezhad K,. (2017). Behavior of reinforced concrete interior wide beam-column connections under lateral loading: A finite element study. *International Journal of Engineering and Technology 9*: 2559-2570.

6. Fadwa I, Ali TA, Nazih E, Sara M. (2014). Reinforced concrete wide and conventional beam–column connections subjected to lateral load. *Engineering Structures 76*:34–48.

7. Genikomsou, A.S., Polak, M.A. (2015). Finite element analysis of punching shear of concrete slabs using damaged plasticity model in ABAQUS*, Engineering Structures* 98: 38–48.

8. Guo-Lin Wang, Jian-Guo Dai, Teng, J.G. (2012). Shear strength model for RC beam–column joints under seismic loading, Engineering Structures 40: 350–360

9. Jankowiak, T., Lodygowski, T. (2005). Identification of parameters of concrete damage plasticity constitutive model. *Foundation of Civil and Environmental Engineering 6*:54-69.

10. Kim, J., LaFave, J.M. (2007). Key influence parameters for the joint shear behavior of reinforced concrete (RC) beam–column connections, *Engineering Structures 29*: 2523–2539.

11. Kim J, LaFave JM, Song J. (2009). Joint shear behavior of reinforced concrete beam–column connections. *Mag Concrete Research 61(2):*119–32.

12. Kim, J., LaFave, J.M. (2009). Joint Shear Behavior of Reinforced Concrete Beam Column Connections subjected to Seismic Lateral Loading. *NSEL Report Series.*

13. LaFave, J.M. and Wight, J.K. (2001). Reinforced concrete wide beam-column connections vs. conventional construction: Resistance to lateral earthquake loads. *Earthquake Spectra* **17**:479-505.

14. Lubliner J, Oliver J, Oller S, Onate E. (1989). A plastic-damage model for concrete. *International Journal of solids and Structures 25*:299–326.

15. Lee JY, Kim HJ, Chang MS. (2006). Ductile capacity of RC beam–column assembles subjected to reversed cyclic loading. *First European conference on earthquake engineering and seismology*: 45–54.

16. Masi A, Santarsiero G, Mossucca A, Nigro D. (2014). Influence of axial load on the seismic behavior of RC beam-column joints with wide beam. *Applied Mechanics of Materials*; Trans Tech Publications 508:208–214.

17. Masi, A., Santarsiero, G., Lignola, G.P., Verderame, G.M. (2013). Study of the seismic behavior of external RC beam–column joints through experimental tests and numerical simulations, Engineering Structures 52: 207–219.

18. Niroomandi, A., Najafgholipour, M.A., Ronagh, H.R. (2014). Numerical investigation of the affecting parameters on the shear failure of Non-ductile RC exterior joints, *Engineering Failure Analysis 46*: 62-75

19. NZS 3101. (2006). The design of concrete structures. Wellington, New Zealand; *Standards Association of New Zealand*.

20. Park, S., and Mosalam, K. M., (2012). Parameters for shear strength Prediction of exterior beam-column joints without transverse Reinforcement. *Engineering Structures 36*: 198–209.

21. Ravi, Kiran, and Giovacchino Genesio. (2014). A case study on pre 1970s constructed concrete exterior beam-column joints. *Case Studies in Structural Engineering 1*:20-25.

22. Shayanfar, J., Akbarzadeh Bengar, H., Niroomandi, A. (2016). A proposed model for predicting nonlinear behavior of RC joints under seismic loads, *Materials and Design 95*: 563–579

23. Shin M, LaFave JM. (2004). Modeling of cyclic joint shear deformation contributions in RC beam–column connections to overall frame behavior. *Structural Engineering and Mechanics 18(5):*645–669.

24. Uma SR, Prasad AM. (2004). Seismic evaluation of R/C moment resisting frame structures considering joint flexibility.*13th World conference on earthquake engineering conference proceedings*.

25. Wong HF, Kuang JS. (2008). Effects of beam–column depth ratio on joint seismic behavior. *Structures and Building 161(SB2):*91–101.

26. Zahran R, Benavent-Climent A., and Cahís X. (2009). Exterior wide beam-column connections in existing RC frames subjected to lateral earthquake loads. *Engineering Structures 31(7)*:1414-1424.

APPENDIX

Appendix A: Modeling of material properties

Material		Density (tonn/mm3)	Youngs modulus of elasticity (Mpa)	Poisson's ratio
Concrete		2.54e-9	31848	0.2
Steel	Rebar	7.85e-9	202405	0.3
	Stirrup	7.85e-9	195733	0.3

Concrete compressive uniaxial stress-strain behavior

Compression behavior	
Yield stress	Inelastic strain
12.837924	0
22.617245	0.000150766
29.407914	0.000368223
33.277769	0.000677529
34.32	0.001015435
34.292609	0.001076616
32.516269	0.001563476
28.010699	0.00213616
20.836026	0.002792779
19.792773	0.002877586

Concrete tensile uniaxial stress-strain behavior

Tensile behavior	
Yield stress	Displacement
2.65447422	0
2.24570071	0.01
1.8369272	0.02
1.42815369	0.03
1.01938018	0.04
0.61060667	0.05
0.53089484	0.051950024
0.51032849	0.06
0.48478014	0.07
0.4592318	0.08
0.43368346	0.09
0.40813511	0.1
0.38258677	0.11
0.35703842	0.12
0.33149008	0.13
0.30594173	0.14
0.28039339	0.15
0.25484505	0.16
0.2292967	0.17
0.20374836	0.18
0.17820001	0.19
0.15265167	0.2
0.12710332	0.21
0.10155498	0.22
0.07600663	0.23
0.05045829	0.24
0.02490995	0.25

Uniaxial tensile stress-crack width relationship for concrete

w	f
0	1.983447
0.01	1.75522
0.02	1.526993
0.03	1.298766
0.04	1.070539
0.05	0.842312
0.069525	0.396689
0.07	0.396012
0.08	0.381748
0.09	0.367484
0.1	0.35322
0.11	0.338956
0.12	0.324692
0.13	0.310427
0.14	0.296163
0.15	0.281899
0.16	0.267635
0.17	0.253371
0.18	0.239106
0.19	0.224842
0.2	0.210578
0.21	0.196314
0.22	0.18205
0.23	0.167786
0.24	0.153521
0.25	0.139257

Steel uniaxial stress-strain behavior

Yield stress	Plastic strain
300	0
320	0.1
460	0.235
730	0.51

Concrete damage plasticity (CDP) input parameters

Plasticity parameter	Dilation angle	Eccentricity	Stress ratio	Shape factor	Viscosity Parameter
Value used in the model	38	1	1.12	0.6667	0.01

Compression damage (d_c)   **Tensile damage (d_t)**

Compression damage	
Damage parameter	Inelastic strain
0	0
0	2.72917E-05
0	0.000150766
0	0.000368223
0	0.000677529
0	0.001015435
0.000798117	0.001076616
0.052556258	0.001563476
0.18383744	0.00213616
0.392889673	0.002792779
0.423287502	0.002877586

Tensile damage	
Damage parameter	Displacement
0	0
0.153994153	0.01
0.307988307	0.02
0.46198246	0.03
0.615976613	0.04
0.769970766	0.05
0.8	0.051950024
0.807747807	0.06
0.817372442	0.07
0.826997077	0.08
0.836621711	0.09
0.846246346	0.1
0.85587098	0.11
0.865495615	0.12

0.87512025	0.13
0.884744884	0.14
0.894369519	0.15
0.903994153	0.16
0.913618788	0.17
0.923243422	0.18
0.932868057	0.19
0.942492692	0.2
0.952117326	0.21
0.961741961	0.22
0.971366595	0.23
0.98099123	0.24
0.990615864	0.25

Appendix B: Numerical results of FEA and Experimental results
 Exterior connection numerical and experimental results

0	0	16.93493	56135.82	74.84753	93054.44
0.585938	1033.001	17.60311	58291.44	78.1022	93094.09
1.171875	1987.587	18.60536	60984.15	82.98418	92494
2.050781	3458.643	20.10875	64419.83	84.81493	92082.22
3.369141	5607.79	22.36384	68658.92	87.56104	91316.4
5.34668	8696.054	25.74646	73588.98	91.68022	89912.31
8.312988	13424.24	27.01495	75070.43	97.85899	87559.33
9.054565	14357.15	28.91768	77006.07	100.176	86566.34
9.796143	15230.02	31.77177	79359.48	103.6516	84891.24
10.90851	17344.47	36.0529	81944.23	108.8649	81841.39
12.02087	19308.99	37.65833	82810.51	110.8199	80562.58
13.13324	23299.87	40.06647	84159.06	113.7524	78543.37
13.55038	25305.26	43.67868	85868.14	118.1512	75275.77
14.17608	30634.87	49.09699	87953.28	124.7493	70484.74
14.41072	33020.42	51.12886	88483.12	127.2236	68729.79
14.76268	37736.23	54.17666	89095.6	130.935	66345.73
15.11464	42480.4	58.74836	89762.27	136.5022	63697.76
15.4666	46463.24	60.46275	90122.7	138.5899	62786.46
15.99454	51113.66	63.03433	90534.76	141.7214	61526.38
16.19252	52550.36	66.8917	91602.95	146.4187	59749.93
16.48948	54260.18	72.67776	92849.5	150	58476

0	0		60	86000		110	60000
10	15000		70	87000		120	58000
20	70000		80	88000		130	55000
30	75000		90	85000		140	50000
40	79000		100	70000		150	45000
50	85000						

Interior connection of numerical and experimental results
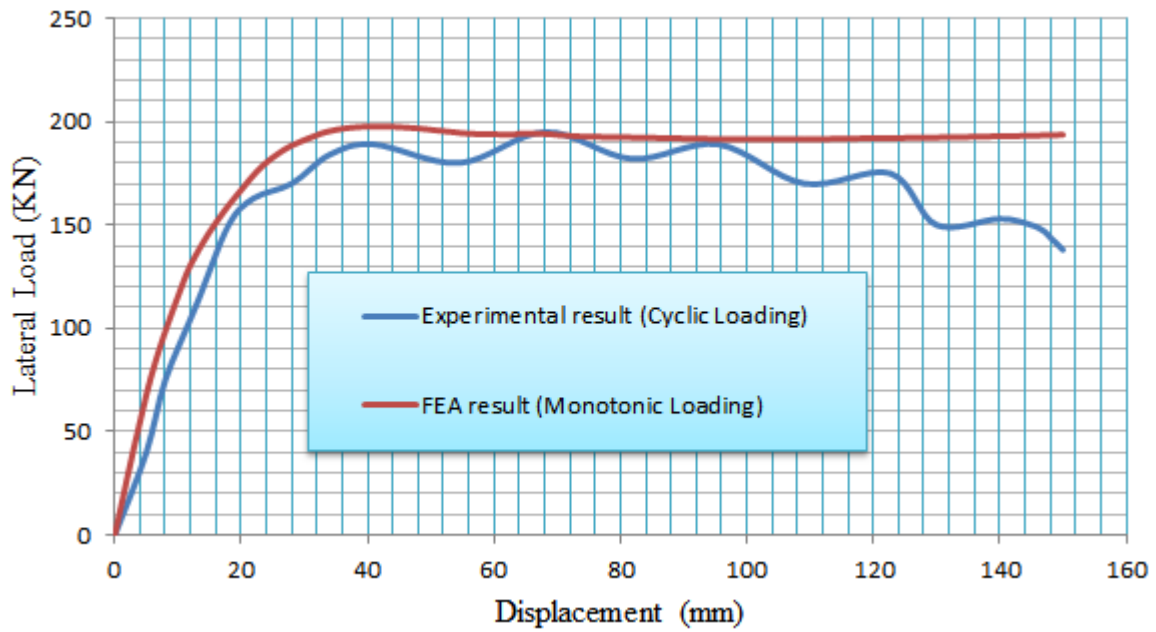
0	0		95.45455	189
5	40		109.0909	170
8	72		122.7273	175
13	112		130	150
18	162		140	153
22	163		145	150
28	170		147	147
34	184		148	144
40.90909	189		149	141
54.54546	180		150	138
68.18182	195			
81.81818	182			

75

0	0	55.16507	194373.8
2.34375	32927.2	55.25548	194352.1
2.929688	40970.55	55.39109	194321.4
3.515625	48630.7	55.59451	194278.8
4.394531	60088.38	55.89963	194220.2
5.712891	76372.3	56.01405	194197.7
7.69043	95890.8	56.18568	194164.8
10.65674	120942.5	56.44313	194118.6
11.39832	126803	56.53967	194101
12.13989	131629.9	56.68449	194075.7
13.25226	137794.3	56.90171	194040.5
14.92081	146273.3	56.98317	194027.1
17.42363	157233.8	57.10536	194007.8
21.17786	171371.5	57.28864	193981
22.5857	176220.4	57.35737	193970.7
24.69746	181994.4	57.46046	193956.3
27.86509	188235.1	57.61511	193938.1
32.61655	194204	57.6731	193931
33.80441	195240.8	57.76009	193921.9
34.99227	196029	57.89057	193914.4
36.77407	196883.4	57.9395	193911.1
39.44676	197568	58.01289	193907.4
42.11945	197663.2	58.04042	193906
44.79214	197373.4	58.0817	193904.3
48.80118	196490.2	58.14363	193903.4
49.80344	196156.5	58.16685	193903.2
50.8057	195803.5	58.20168	193905.7
52.30909	195317.2	58.25394	193911.2
52.87286	195127.5	58.33231	193918.1
53.71852	194871.9	58.44988	193980.1
54.03564	194751	58.62622	194006.1
54.15456	194698.3	58.69236	194006.7
54.33294	194630.3	58.79155	194005.7
54.39983	194602.8	58.94035	193998.2
54.50017	194566.9	59.16353	193986.3
54.65068	194519.2	59.49832	193955.8
54.70712	194501	60.0005	193903.2
54.79178	194476	60.75376	193828.9
54.91877	194440.6	61.88366	193745.8
54.9664	194427.5	61.98959	193737.3
55.03783	194408.2	62.14848	193724.8
55.06462	194400.8	62.20807	193719.6
55.1048	194390	62.29744	193712.4

65.11207	194188.9	62.43151	193703.4	113.61	191753.2
65.9073	194162.1	62.48178	193699.7	114.1008	191769
67.10013	194165.2	62.55719	193693.4	114.837	191781.8
68.88938	193929.3	62.58547	193690.2	115.9413	191804.4
71.57326	193263.3	62.62789	193685.8	117.5977	191845.5
75.59908	192660.1	62.69152	193682.7	118.2189	191858.3
79.62489	192490	62.71538	193681.4	119.1506	191878.9
83.6507	192234.4	62.75117	193681.8	119.5	191886.1
87.67652	192004.8	62.80486	193684.5	120.0241	191898
91.70234	191762.6	62.82499	193685.2	120.8103	191919.1
95.72816	191529.4	62.85519	193686.1	121.9895	191957.7
99.75397	191412.4	62.90049	193687.5	123.7584	192027.8
105.7927	191442.3	62.96844	193691.1	126.4117	192148.1
106.3588	191423.2	63.07035	193698.4	130.3916	192343.4
106.925	191412	63.10858	193700.6	136.3615	192708.1
107.4911	191397.5	63.1659	193703.1	138.6002	192845.3
107.7034	191391.8	63.1874	193703.8	141.9583	193048.2
108.0218	191389.1	63.21965	193704.6	146.9954	193382.1
108.1413	191387.4	63.26803	193706.1	150	193602.8
108.3204	191387.3	63.27256	193706.1		
108.3876	191387	63.27937	193706.3		
108.4883	191387.5	63.28957	193707		
108.6395	191390.4	63.30487	193710.1		
108.6961	191391.6	63.31061	193711.5		
108.7811	191394.9	63.31922	193714.1		
108.813	191396.1	63.33213	193719.8		
108.8608	191398.7	63.35151	193735.1		
108.8788	191399.6	63.37088	193755.8		
108.9057	191401.4	63.39025	193779.5		
108.946	191405.2	63.4193	193815.3		
109.0065	191410.8	63.4302	193828		
109.0973	191418.5	63.44654	193847.3		
109.1314	191421.3	63.47106	193876.5		
109.1824	191426.3	63.50784	193923.2		
109.259	191436	63.563	193985		
109.3739	191452	63.58368	194005.6		
109.5463	191472.1	63.61471	194033.7		
109.8048	191488.5	63.66125	194069.9		
110.1926	191505.5	63.73107	194112		
110.7743	191517.2	63.83579	194153.7		
111.6468	191532.9	63.99287	194186.6		
112.9556	191556.2	64.22849	194204.3		
113.2828	191715.1	64.58192	194204		

Appendix C: Shear stress-Shear strain relationship
Exterior shear stress-shear strain relationship for C34.32

0	0	0.000593	63.26246	0.027369	101.2651
0	1.395136	0.000766	65.55231	0.029268	101.2258
0	2.687594	0.001042	68.41632	0.032166	100.4995
0	4.6758	0.001491	72.07497	0.033258	100.0365
0	7.578218	0.00223	76.59353	0.034907	99.1986
0	11.74193	0.003454	81.84647	0.037392	97.70033
0	17.97133	0.003927	83.42358	0.041138	95.27393
0	19.16214	0.004663	85.47972	0.042547	94.26691
0	20.24754	0.005818	87.96766	0.044667	92.58421
0	22.57269	0.007638	90.66558	0.047885	89.52415
3.95E-06	24.6722	0.008332	91.56306	0.0491	88.23605
2.89E-05	28.89843	0.009401	92.95171	0.05094	86.18682
4.31E-05	31.01783	0.011062	94.68359	0.053747	82.82913
8.57E-05	36.63222	0.01367	96.73227	0.058058	77.81242
0.000105	39.13005	0.014663	97.22793	0.059689	75.96071
0.000147	44.03152	0.01618	97.76788	0.062163	73.41605
0.000199	48.93916	0.018515	98.29935	0.065937	70.46239
0.000262	53.0735	0.019402	98.61961	0.067362	69.42712
0.000372	57.95282	0.020754	98.96147	0.069525	67.95232
0.000416	59.46573	0.022848	99.96005	0.072822	65.80433
0.000484	61.27358	0.026124	101.1077	0.075371	64.226

Interior shear stress-shear strain relationship for C34.32

0	0	0.033391	235.8065	0.037755	234.5883	0.043971	234.1482
0	40.19769	0.033531	235.7362	0.037862	234.5694	0.044053	234.1447
0	50.01717	0.033742	235.6443	0.038021	234.547	0.044084	234.1434
0	59.38356	0.033821	235.6075	0.038081	234.5381	0.04413	234.1439
0	73.3642	0.033939	235.5587	0.038171	234.5259	0.044199	234.1475
0	93.22015	0.034118	235.4934	0.038205	234.5212	0.044225	234.1484
0	117.0216	0.034184	235.4686	0.038256	234.5146	0.044264	234.1497
0	147.494	0.034285	235.4343	0.038332	234.506	0.044322	234.1524
2.52E-06	154.5952	0.034436	235.3857	0.03836	234.5027	0.044409	234.1571
1.07E-05	160.314	0.034492	235.3677	0.038403	234.4992	0.044541	234.1655
4.47E-05	167.7509	0.034577	235.342	0.038467	234.4958	0.04459	234.1676
0.000181	178.1394	0.034609	235.3322	0.038563	234.4926	0.044664	234.1699
0.000685	191.4225	0.034657	235.3184	0.038708	234.5186	0.044692	234.1705
0.002218	208.5316	0.034729	235.2987	0.038925	234.5498	0.044734	234.1714
0.00291	214.3862	0.034836	235.2718	0.039007	234.5528	0.044797	234.1789
0.004173	221.2589	0.034998	235.2303	0.039129	234.5555	0.044802	234.1797
0.006478	228.7005	0.035241	235.1676	0.039313	234.5538	0.044811	234.1806
0.010597	235.7555	0.035607	235.0751	0.039589	234.5415	0.044824	234.1831
0.011664	236.9682	0.035745	235.0395	0.040005	234.5102	0.044844	234.1892
0.012764	237.8791	0.035951	234.9874	0.040632	234.4486	0.044852	234.1915
0.014479	238.843	0.036262	234.9127	0.04158	234.3512	0.044863	234.1957
0.017169	239.5618	0.036378	234.8844	0.043019	234.2318	0.04488	234.2032
0.019963	239.5365	0.036553	234.8429	0.043154	234.2195	0.044905	234.2203
0.022847	239.0578	0.036817	234.7835	0.043357	234.2013	0.04493	234.2442
0.027346	238.0688	0.036915	234.761	0.043433	234.1939	0.044955	234.2705
0.028481	237.6493	0.037064	234.7282	0.043548	234.1835	0.044993	234.31
0.029626	237.2085	0.037287	234.6814	0.043719	234.1697	0.045007	234.3241
0.031368	236.5738	0.03737	234.6635	0.043784	234.1642	0.045028	234.3447
0.032025	236.3196	0.037496	234.6377	0.043881	234.1564	0.04506	234.375
0.033018	235.9695	0.037685	234.6018	0.043917	234.153	0.045108	234.4199

0.045108	234.4199	0.114584	231.6381	0.124031	231.7806
0.04518	234.4809	0.115149	231.6222	0.124628	231.9657
0.045207	234.5019	0.115362	231.6155	0.125226	232.0054
0.045247	234.5307	0.11568	231.6082	0.126125	232.0158
0.045308	234.5677	0.1158	231.6052	0.127478	232.019
0.045399	234.6116	0.115979	231.6016	0.129517	232.0218
0.045537	234.6568	0.116248	231.5985	0.132597	232.0283
0.045743	234.6963	0.116349	231.5974	0.133754	232.028
0.046053	234.7232	0.116501	231.5974	0.135497	232.0277
0.046521	234.7345	0.116558	231.5972	0.136152	232.0269
0.047225	234.7333	0.116643	231.5979	0.137135	232.0263
0.048291	234.7235	0.116675	231.5981	0.138615	232.0258
0.049908	234.7397	0.116723	231.5989	0.140844	232.0253
0.052375	234.745	0.116795	231.6015	0.144207	232.0238
0.056161	234.7076	0.116903	231.6073	0.14929	232.0315
0.062012	234.602	0.117065	231.6169	0.156983	232.0785
0.068035	234.304	0.117126	231.6205	0.168588	232.2516
0.074223	233.8032	0.117218	231.627	0.172945	232.3462
0.080577	233.2545	0.117354	231.6384	0.17948	232.546
0.087096	232.7283	0.11756	231.6561	0.189316	232.9023
0.09378	232.3325	0.117868	231.6785	0.19521	233.153
0.100623	232.0349	0.118331	231.7041		
0.11121	231.7782	0.119027	231.7287		
0.112206	231.73	0.120074	231.7504		
0.113205	231.6934	0.121651	231.7671		
0.114208	231.6532				